U.PORTO

FEUP FACULDADE DE ENGENHARIA
UNIVERSIDADE DO PORTO

NUMERICAL MODELLING OF THE DYNAMIC BEHAVIOUR OF A SOIL IN TRUE TRIAXIAL TESTS WITH BENDER ELEMENTS

ANA RITA DIAS DE SOUSA E SILVA

Dissertação submetida para satisfação parcial dos requisitos do grau de

MESTRE EM ENGENHARIA CIVIL — ESPECIALIZAÇÃO EM GEOTECNIA

Orientador: Professora Doutora Cristiana Maria da Fonseca Ferreira

---

Coorientador: Professor Doutor João Filipe Meneses Espinheira Rio

JULHO DE 2014

MESTRADO INTEGRADO EM ENGENHARIA CIVIL 2013/2014

DEPARTAMENTO DE ENGENHARIA CIVIL

Tel. +351-22-508 1901

Fax +351-22-508 1446

✉ miec@fe.up.pt

Editado por

FACULDADE DE ENGENHARIA DA UNIVERSIDADE DO PORTO

Rua Dr. Roberto Frias

4200-465 PORTO

Portugal

Tel. +351-22-508 1400

Fax +351-22-508 1440

✉ feup@fe.up.pt

🌍 http://www.fe.up.pt

To my love

“All you have to decide is what to do with the time that is given to you.”

J. R. R. Tolkien

ACKNOWLEDGEMENTS

First and foremost, I wanted to thank my supervisor, Professor Cristiana Ferreira for her incredible support, not only because she had a special interest in the theme, but also due to her kindness towards me throughout the development of this dissertation. Also, for her confidence in me and my capabilities and for always being available to help me with this study.

To my co-supervisor, Professor João Rio, who helped me understand the features of the computer software *FLAC*^{3D}, for his availability and ultimately for his major support in the numerical modelling of the true triaxial apparatus.

To Professor Quintanilha Menezes, for his kindness and collaboration in providing me the opportunity to use the software *FLAC*^{3D}.

To Professor José Miguel Castro, for showing availability to help me in whatever I needed and to Professor José Couto Marques, for his kindness in helping me with the background of numerical modelling.

To Cláudio Pereira, who provided me the chance to learn more about the frequency domain and even the opportunity to include a study regarding it, in this dissertation.

À Bárbara, à Catarina e à Lígia pela amizade e por me apoiarem e compreenderem durante todo o desenvolvimento da tese.

À Mariana, ao Luís e à Diana pela companhia durante o estudo e por serem simplesmente meus amigos.

Ao Tiago Ivo por ser meu amigo e por não se importar de rever o meu inglês.

À minha mãe e ao meu pai, pelo apoio emocional e compreensão.

E finalmente ao meu namorado, Tiago, por estar sempre lá quando eu precisei e por todo o apoio e carinho que me deu sem eu precisar pedir.

Thank you all.

Muito obrigada a todos.

ABSTRACT

The dynamic behaviour of the soil depends of its inherent properties, namely stiffness, void ratio, stress state, anisotropy, heterogeneity, natural structure, fabric, saturation conditions, among others.

It is precisely the study of this type of behaviour that is the main goal of this dissertation, for the case of a residual soil from Porto granite, a geotechnical material that possess a complex mechanic behaviour. To that end, a detailed experimental research was developed, in true triaxial conditions, considering the measurement of seismic wave velocities through bender elements. Moreover, it was also taken into consideration previous studies associated either to the geomechanical characterization of these soils, or the particulate nature of soil in general.

To complement those investigations and in the scope of this study, the objective was to produce a three-dimensional numerical model that could characterize the behaviour of this particular residual soil, specifically a finite difference program, named *FLAC*^{3D}, through a model inspired in the true triaxial apparatus, previously utilized. Its main advantages reside in its simplicity, versatility and the possibility of directly measuring seismic wave velocities, not only in the three principal directions, but also in inclined directions.

This study requires the implementation of bender elements in the platens of the true triaxial apparatus, in order to assess the influence of its cubical geometry and boundary conditions (rigid or flexible platens, or even reflective and absorbent), as well as the validation of stiffness parameters attained from the measurement of seismic waves.

For this purpose, a series of parametric and sensitivity studies were developed, considering the linear elastic constitutive model, with isotropic loading, in the previously mentioned software, to particularly evaluate the influence of each parameter in the numerical modelling of the true triaxial apparatus, and which values are better suited for its correct representation. These parameters are: time step, amplitude, frequency, damping, Poisson's ratio and finally, boundary conditions and a cross-anisotropic constitutive model. With these studies completed, a comparison and validation between the numerical results attained and the laboratory results previously done by Ferreira (2009), regarding residual soil specimens from Porto granite was in order. Due to time limitations, only the dry specimens ($w \approx 0\%$), namely, R8D-TT and R4D-K_0TT were used in this comparative study.

KEYWORDS: numerical modelling, dynamic behaviour, seismic waves, bender elements, true triaxial testing.

RESUMO

O comportamento dinâmico de um solo depende das suas propriedades inerentes, nomeadamente rigidez, índice de vazios, estado de tensão, anisotropia, heterogeneidade, estrutura natural, fábrica, condições de saturação, entre outras.

É precisamente este comportamento que se pretende estudar para o caso do solo residual de granito do Porto, um material geotécnico com um comportamento mecânico complexo. Para esse fim, foi efetuada uma investigação experimental detalhada, em condições verdadeiramente triaxiais com medição das velocidades das ondas sísmicas por meio de *bender elements* e tendo em consideração trabalhos anteriores relacionados com a caracterização geomecânica destes solos, bem como a natureza particulada dos solos em geral.

Em complemento a essa investigação e no âmbito deste trabalho, procedeu-se à modelação numérica do comportamento desse solo, em condições tridimensionais, num programa de diferenças finitas, nomeadamente o *FLAC*^{3D}, através de um modelo inspirado no equipamento verdadeiramente triaxial, anteriormente utilizado, cujas vantagens principais residem na sua simplicidade, versatilidade e possibilidade de medição direta das velocidades das ondas sísmicas, não apenas nas três direções principais, mas também em direções inclinadas.

Este estudo implica o estabelecimento e definição do modelo numérico do equipamento, bem como a implementação de *bender elements* nas suas faces, de modo a avaliar a influência da geometria cúbica, das condições fronteira (paredes rígidas versus flexíveis) e do estado de tensão tridimensional na medição e interpretação das ondas sísmicas, com vista à validação dos parâmetros de rigidez obtidos experimentalmente.

Para este fim, foi efetuada uma série de estudos paramétricos e de sensibilidade, considerando o modelo constitutivo elástico linear, com carregamento isotrópico, no programa previamente mencionado, de modo a avaliar a influência de cada parâmetro na modelação do equipamento verdadeiramente triaxial, bem como os valores mais adequados para a sua correcta validação. Estes parâmetros são: time step, amplitude, freqência, amortecimento, coeficiente de Poisson e, finalmente, condições-fronteira e o modelo constitutivo transversalmente isotrópico ou anisotrópico (de anisotropia cruzada). Finalizados estes estudos, procedeu-se à comparação e validação dos resultados numéricos com os resultados laboratoriais previamente obtidos por Ferreira (2009), relativamente a amostras de solos residuais de granito do Porto. Por restrições de tempo, apenas houve possibilidade de estudar as amostras secas (w $\approx$ 0%), nomeadamente, R8D-TT e R4D-K_0TT.

PALAVRAS-CHAVE: modelação numérica, comportamento dinâmico, ondas sísmicas, *bender elements*, equipamento verdadeiramente triaxial.

TABLE OF CONTENTS

ACKNOWLEDGEMENTS v

ABSTRACT vii

RESUMO ix

1 INTRODUCTION 1

1.1 SCOPE AND OBJECTIVES 1

1.2 DISSERTATION LAYOUT 2

2 STATE OF THE ART 3

2.1 SEISMIC WAVES 3

2.1.1 GENERAL CONSIDERATIONS 3

2.1.2 VOLUMETRIC VERSUS SURFACE WAVES 3

2.1.3 DAMPING 6

2.1.3.1 Undamped Free Vibration 7

2.1.3.2 Damped Free Vibration 8

2.2 DYNAMIC BEHAVIOUR OF SOILS 9

2.2.1 GENERAL CONSIDERATIONS 9

2.2.2 NON-LINEAR CHARACTER OF SOILS 10

2.2.3 STRAIN LEVEL VERSUS STRAIN RATE 13

2.3 SEISMIC WAVE TESTING METHODS 15

2.3.1 IN SITU METHODS 15

2.3.1.1 Cross-hole seismic test (CH or CHT) 16

2.3.1.2 Down-hole test (DH) or Down-hole seismic test (DHT) 17

2.3.2 LABORATORY METHODS 18

2.3.2.1 Ultrasounds 18

2.3.2.2 Bender elements and other piezoelectric transducers 19

2.3.2.3 Resonant column 31

2.3.2.4 Hollow cylinder 32

2.3.2.5 True Triaxial Apparatus 33

3 NUMERICAL MODELLING 35

3.1 INTRODUCTION 35

3.2 FINITE ELEMENT METHOD VERSUS FINITE DIFFERENCE METHOD 36

3.3 PROGRAM *FLAC^{3D}* 38

3.3.1 BACKGROUND ... 38
3.3.2 OTHER USES OF THE PROGRAM *FLAC*^{3D} ... 41
4 PARAMETRIC AND SENSITIVITY STUDIES ... 43
4.1 INTRODUCTION ... 43
4.2 PREVIOUS LABORATORY TESTING ... 43
4.3 DESCRIPTION OF THE MODEL SIMULATION PROGRAM ... 45
4.3.1 MESH GENERATION ... 45
4.3.2 CONSTITUTIVE MODELS AND PROPERTIES ... 48
4.4 SIMULATION STUDIES ... 52
4.4.1 FILTER OF THE SIGNAL ... 52
4.4.2 TIME STEP ... 53
4.4.3 AMPLITUDE AND FREQUENCY ... 54
4.4.4 DAMPING ... 60
4.4.5 POISSON'S RATIO ... 63
4.4.6 BOUNDARY CONDITIONS ... 65
4.4.7 ANISOTROPY ... 68
4.5 KEY FINDINGS ... 71
5 RESULTS AND DISCUSSION ... 73
5.1 INTRODUCTION ... 73
5.2 SIMULATION MODEL ... 73
5.3 PRELIMINARY COMPARISONS ... 74
5.3.1 DAMPING ... 74
5.3.2 BOUNDARY CONDITIONS ... 75
5.3.3 ANISOTROPY ... 76
5.4 COMPARISON WITH LABORATORY TESTS ... 77
5.4.1 R8D-TT ... 78
5.4.2 R4D-K_0TT ... 80
6 CONCLUSIONS ... 83
6.1 KEY FINDINGS ... 83
6.2 FURTHER WORKS ... 84

REFERENCES ... 88

LIST OF FIGURES

Figure 1 – Schematics of seismic waves: a) P-wave; b) S-wave (Bolt 1976) 4

Figure 2 –Seismic waves schematics: a) Rayleigh wave; b) Love wave (Bolt 1976) 6

Figure 3 – Schematics for the equation of motion 7

Figure 4 – Schematics of the damping coefficient: a) over-damped system; b) critically damped system; c) underdamped system (Braja 1993) 9

Figure 5 – Non-linear characteristic stiffness-strain behaviour of soil with standard strain ranges (after Atkinson and Salfors, 1991 and Mair, 1993) 10

Figure 6 –Stress-strain and stiffness-strain curves of a non-linear soil (Atkinson, 2000) 13

Figure 7 – Measurement of soil stiffness with respect to strain level (Atkinson, 2000) 14

Figure 8 – Strain rate effects on soil stiffness (Teachavorasinskun *et al.* 1991) 14

Figure 9 – Schematics of a cross-hole seismic test (Matos Fernandes, 2011, after GATTEL/LNEC, 1993a) 16

Figure 10 – Schematics of a down-hole seismic test (Matos Fernandes, 2011) 17

Figure 11 – Ultrasonic transducers of: a) compression; b) shear 19

Figure 12 – Range of ultrasonic waves 19

Figure 13 –Schematic of piezoelectric transducers and associated electronics used during traixial testing (Brignoli *et al.* 1996) 20

Figure 14 – Types of piezoelectric transducers (Piezo systems) 21

Figure 15 – Bender element: a) model (Stokoe and Santamarina 2000); b) operating schematics (Ferreira 2003) 21

Figure 16 – Bender element: Directivity of both P and S-waves generation (Santamarina *et al.* 2001) 23

Figure 17 – Pressure versus distance for near and far-field effects (Santamarina *et al.* 2001) 24

Figure 18 – Bender element measurement in the frequency of 8 kHz: a) Presence of cross-talk in the output signal; b) No presence of cross-talk in the output signal; c) Comparison between a) and b) 26

Figure 19 – Definition of travel distance: a) direct arrival for a triaxial cylindrical specimen; b) direct and inclined waves for a true triaxial specimen (Ferreira 2009) 29

Figure 20 – Schematics of the determination of the travel time of an S wave, regarding the first direct arrival of the output signal 30

Figure 21 –Resonant-column: a) schematic of a fixed-free, torsional resonant-column (Stokoe and Santamarina 2000); b) example of an apparatus (from GDS Instruments) 31

Figure 22 – Hollow cylinder: a) Schematic of a hollow cylinder model; b) Small-strain hollow cylinder apparatus (from GDS Instruments) 32

Figure 23 – Arrangement of rigid platens of the true triaxial apparatus: a) Schematics of the Cambridge true triaxial apparatus; b) Photograph of the true triaxial apparatus at the University of Bristol (Sadek 2006) 33

Figure 24 – Flexible boundary true triaxial apparatus: a) Frame view; b) Example of a flexible boundary true triaxial apparatus at the University of Bristol 34

Figure 25 – Major outlines of a numerical model 36

Figure 26 – General solution analysis 40

Figure 27 – True triaxial apparatus: a) Nomenclature for the platens and shape of the bender elements (Ferreira, 2009); b) FEUP true triaxial apparatus; c) T-shaped pair of bender elements 44

Figure 28 – Brick shaped mesh (Itasca 2002a) 45

Figure 29 – Radially graded mesh around brick (Itasca 2002a) 45

Figure 30 – Dimensions of the bender elements 46

Figure 31 – Brick and radbrick mesh, representing the soil and a vertical bender element, respectively 47

Figure 32 – Upper half of the true triaxial apparatus, with both vertical and horizontal bender elements 47

Figure 33 – Full representation of the true triaxial apparatus with embedded bender elements 48

Figure 34 – Simple schematics of the true triaxial apparatus model 52

Figure 35 – Example of a sine wave without and with a filter in the output signal 53

Figure 36 – Time step variation 54

Figure 37 – Linear amplitude variation 55

Figure 38 – Variation of input frequency, considering local damping: a) 0.4 kHz; b) 2.5 kHz; c) 4.0 kHz; d) 8.0 kHz 56

Figure 39 – Variation of frequency, considering Rayleigh damping 58

Figure 40 – Frequency spectra for different frequency values, with indication of the central frequency 59

Figure 41 – Local damping, considering several fractions of critical damping 61

Figure 42 – Rayleigh damping, considering a certain fraction of critical damping, namely 0.05, to several frequency values 61

Figure 43 – Local damping (L) regarding a fraction of the critical damping of 0.05 62

Figure 44 – Rayleigh damping (R), regarding a fraction of critical damping of 0.05 and a frequency of 10 kHz 62

Figure 45 – Variation of Poisson's ratio and the first arrival of both P and S waves in: a) Face C; b) Middle point between face A and C 64

Figure 46 – Two dimensional plane model 66

Figure 47 –Reflective (R) and absorbent (A) boundary conditions 67

Figure 48 – Displacements, from face A to C, considering an anisotropic constitutive model: a) X-displacement (horizontal); b) Z-displacement (vertical) 69

Figure 49 – Polarization of the model: a) Vertical; b) Horizontal 70

Figure 50 – Anisotropic and Isotropic behaviour from face A to C and B to D 70

Figure 51 – Output signal response of the complex model..... 73

Figure 52 – Example of a typical damped signal on specimen R2W-TT 75

Figure 53 – Example of a reflective boundary of the specimen R8D-TT 76

Figure 54 – Displacements for both isotropic and anisotropic constitutive models 77

Figure 55 – Three-dimensional view of the strains measured in the experimental test for isotropic loading 78

Figure 56 – Three-dimensional view of the strains associated with each isotropic stress stage..... 79

Figure 57 – Simulations of seismic wave propagation for several stress values..... 80

Figure 58 –Horizontal and vertical displacements, correspondent to horizontal and vertical stresses of: a) 35 kPa and 100 kPa; b) 70 kPa and 200 kPa..... 81

Figure 59 – Signal variation, considering a horizontal stress of 175 kPa and 500 kPa..... 82

LIST OF TABLES

Table 1 – Wave phenomena: complexity and richness * (Stokoe and Santamarina 2000) 15

Table 2 – Input wave shapes by different authors 28

Table 3 – Elastic properties of the residual soil from Porto granite and the bender elements 49

Table 4 – Transversely isotropic elastic properties of the residual soil from Porto granite 51

Table 5 –Comparison between the time step inputted and that of the model 53

Table 6 – Variation of P and S wave velocities with Poisson's ratio 65

Table 7 – Horizontal and vertical displacements of both isotropic and anisotropic models 69

Table 8 – Physical properties of the reconstituted specimens tested in the true triaxial apparatus 74

Table 9 – Anisotropy ratios, α_G, considering residual soil specimens from Porto granite 76

Table 10 – Anisotropy ratios, α_G for numerical results and comparison to experimental results 77

Table 11 – Vertical displacements, considering several stress values 78

Table 12 –Horizontal and vertical displacements of a horizontal stress of 35 kPa and a vertical stress of 100 kPa 81

Table 13 – Horizontal and vertical displacements of a horizontal stress of 70 kPa and a vertical stress of 200 kPa 81

LIST OF ABBREVIATIONS AND SYMBOLS

Abbreviations

BE, B/EE	Bender elements, Bender/extender elements
BT, BR	Bender element transmitter; Bender element receiver
CC	Cubical cell apparatus
CH	Cross-hole test
CP	Cone pressuremeter test
CPT(U)	Cone penetration test (Piezocone)
DH	Down-hole test
DMT	Marchetti's flat plate dilatometer test
FD	Frequency domain
ISO	Isotropic
LDT	Local deformation transducer
LVDT	Linearly variable differential transformer
OCR	Over consolidation ratio
OED	Oedometer
P	Compression wave
PLT	Plate loading test
PMT	Menard's pressuremeter test
PT	Potentiometer
RC	Resonant column apparatus
S	Shear wave
SASW	Spectral analysis of surface waves
SBPT	Self-boring pressuremeter test
SCPT	Seismic cone penetration test
SP	Stress-path cell
SPT	Standard penetration test
SQD	Specimen quality designation
TD	Time domain
TT	True triaxial apparatus
TX	Standard triaxial apparatus

Symbols

A	Amplitude
a	Acceleration
[C]	Stiffness matrix / coefficients relating stresses to strains
C_{ij}	Generic coefficient relating stresses to strains; independent elastic constant
D	Diameter, damping ratio
d	Travel distance of a seismic wave
D_{50}	Mean grain size
$e\ e_{min}\ e_{max}$	Void ratio, minimum and maximum void ratio
E	Young's modulus
$E_s\ E_t$	Secant and tangent Young's moduli
$E_V\ E_H$	Young's modulus in the vertical and horizontal directions
F	Force
f	Frequency
F_S	Factor of safety, Far-field component of the shear wave
f_T	Resonance frequency for torsional motion (in the resonant-column)
g	Acceleration of gravity
G	Shear modulus
G'_{ij}	Shear modulus from wave propagation in the *i* direction and polarisation in the *j* direction
H	Height
h	Horizontal direction
K	Bulk modulus
L	Length, travel length (in BE testing)
l_{BE}	Protrusion of the bender elements
m	Mass
M	Constrained modulus
n	Generic exponent; porosity
N_P	Near-field component travelling at a compression-wave velocity
N_S	Near-field component travelling at a shear-wave velocity
$n_v\ n_h\ n_{ij}$	Empirical vertical and horizontal stress exponents, generic exponent
p'	Mean effective stress

p_a	Atmospheric pressure (reference pressure)
R	Laboratory reconstituted specimen
R_d	Number of wavelengths, similar to N
S_{hv} S_{hh}	Horizontally propagated and vertically / horizontally polarised shear wave
S_{ij}	Non-dimensional constant reflecting fabric and structure of a soil
S_{vh}	Vertically propagated and horizontally polarised shear wave
t	Time, travel time
t_S, t_P	Travel time of a shear wave and of a compression wave
V	Volume
V_P	Compression wave velocity
V_S	Shear wave velocity
V_R V_{Phase}	Rayleigh wave velocity
W	Weight
w	Water content
$x\ y\ z$ $X\ Y\ Z$	Horizontal (x and y) and vertical (z) axes and directions
α	Anisotropy ratio, generic angle
Δ	Increment, difference
ε_a	Axial strain
ε_s	Shear strain
σ'_v σ'_h	Vertical and horizontal effective stresses
σ'_X σ'_Y σ'_Z	Effective stresses in the X, Y and Z directions
ν	Poisson's ratio
ρ	Mass density

1 INTRODUCTION

1.1 SCOPE AND OBJECTIVES

The understanding of the characteristics and dynamic properties of soils is an important aspect from which many engineering problems depend, especially due to the high non-linearity present in the response of practically all soils and soft rocks, given its particulate nature and heterogeneity. Residual soil is a good example, since it is formed when the chemical decomposition and physical disintegration associated with the weathering process develops more quickly than the erosion, transport and sedimentation of the resulting grain degradation. This type of soil is more frequent in regions with seasoned or tropical climate and abundant vegetation.

The discovery of the non-linear behaviour led to the development of several methods to better comprehend and evaluate the dynamic response and the particulate nature of soils, for which the measurement of seismic waves is particularly appropriate, since it enables to study its nature without affecting neither the structural equilibrium, fabric or inherent mechanical properties (Fam and Santamarina 1995). This method is a practical, non-destructive, cost-effective and usually non-invasive means of determining small-strain stiffness of soils and can be influenced by many parameters, such as stress state, void ratio, inherent and induced anisotropy, natural structure and saturation conditions. Shear and compression wave velocities can be measured both in situ (with down-hole tests (DHT), cross-hole tests (CHT), suspension logging, seismic refraction and reflection and spectral analysis of surface waves (SASW)) and in the laboratory, with the resonant-column, hollow cylinder, triaxial and true triaxial testing apparatuses equipped with piezoelectric transducers, among others. Piezoelectric transducers are used in triaxial test chambers in different forms namely: bender elements, compression transducers, shear plates and, more recently, bender-extender elements. However, bender elements are the most widely used, because of their capacity to allow standard mechanical, static and cyclic tests, simultaneously with seismic wave dynamic tests. These transducers enable the transmission and reception of shear or/and compression waves, for different applications and purposes, such as the assessment of structure and anisotropy, process monitoring or sampling quality (Ferreira 2009).

These seismic wave measurements are also possible in a true triaxial apparatus with embedded bender elements in the center of each platen, providing different propagation and/or polarization directions, that is, not only in two directions as usual in a standard triaxial chamber, but in all directions, from the orthogonal to the inclined ones, where the different factors mentioned above can be investigated. It is also possible to independently vary the principal stresses. Nonetheless, due to its simplicity regarding the uniformity of imposed deformations or stresses that are inexistent in other testing devices, such as the hollow cylinder apparatus and directional shear cells, controlled gradual rotation of principal axes of stress and strain is not permitted (Airey and Wood 1988). However, it serves as a guide to the generation of realistic constitutive relations for soils, making it a redundant but relevant, versatile and

robust test, providing a reliable characterization, with minimal necessity of calibration. Therefore, despite being a complex testing equipment with limits to the practical stress and strain ranges (Ferreira 2009), the advantages of using the true triaxial apparatus are much more important to the understanding of the stress-strain response, as well as the stiffness to stress and strain relationships and hence to the advancement of geotechnical engineering.

Well, it is precisely the study involving a validation of the elastic, small strain stiffness parameters from seismic wave measurements on a residual soil from Porto granite in a true triaxial apparatus the main goal of this dissertation, through a numerical modelling in a finite differences software named *FLAC*^{3D}. The selection of a three-dimensional numerical model to simulate this apparatus was made simply to overcome some limitations of more standard devices and to better understand wave propagation phenomena and the influence of several non-linearity aspects in the results in a more explicit way. Last, but not least, the use of this program is also important to evaluate the influence of the cubical geometry and boundary conditions of the equipment in the dynamic behaviour of this soil.

1.2 DISSERTATION LAYOUT

The work presented in this dissertation has been divided in six chapters.

Following this chapter, which provides a framework of the main objectives of this particular study, Chapter 2 presents the state of the art. Basically it consists in an overview of the basic notions of seismic waves, dynamic behavior focusing the non-linear behavior of the soil and the seismic wave measurements, both in situ and in the laboratory, with mention of the bender elements, as well as the true triaxial apparatus.

On the other hand, Chapter 3 describes numerical modelling in general, including the major outlines of any numerical model, along with the differences between finite element method and finite difference program, which was the one chosen. Additionally, a brief explanation of the advantages and disadvantages of program *FLAC*^{3D} is taken into account, also mentioning previous and successful uses of the same software.

Chapter 4 consists in the description of the simulation program, i.e. all the steps taken in order to achieve the desired mesh to simulate the true triaxial apparatus and the embedded bender elements. However, the parametric and sensitivity studies developed in this chapter consider a simpler version of this mesh, namely a simple brick-shaped mesh, with the application of a velocity in the lateral boundaries of the model, in order to achieve more realistic results. These studies include the assessment of the time step, amplitude, frequency, damping, Poisson's ratio, boundary conditions and a cross-anisotropic constitutive model. Moreover, these studies allowed to understand the influence of each of these parameters and which ones would be better suited for this particular dissertation.

Chapter 5 include the main objective of this dissertation, which is to compare the numerical results developed in Chapter 4 with the laboratory results previously undertaken by Ferreira (2009), regarding the dry ($w \approx 0\%$) residual soil specimens from Porto granite, validating and analyzing the results.

Finally, Chapter 6 discusses and analyses the results, summarizing the key findings and the further developments that could be made to improve this pioneer research.

2
STATE OF THE ART

2.1 SEISMIC WAVES

2.1.1 GENERAL CONSIDERATIONS

The Earth trembles, abruptly and unexpectedly, around a million times per year, but fortunately, only some earthquakes are strong enough to produce catastrophic consequences. Earthquakes are caused by unexpected impacts, like an explosion or abrupt and rough movements, most times due to a sudden release of energy in unstable zones of the Earth's interior, such as a local slip in tectonic fracture zones. This way, the equilibrium is disturbed and replaced by movement, since the applied load is not instantaneously transmitted to all parts of the medium.

This type of movement is known as mechanical waves, which are small disturbances that go through a particulate medium, varying both in space and time, and can do so without causing any permanent effects or modifying on-going processes. They can be generated from a particular point in an elastic medium with finite propagation velocities. The complexity of the wave field will depend upon the characteristics of the disturbance and the uniformity of the medium.

Considering an array of points sufficiently far from the disturbance centre, these seismic waves can be named planar or body waves, where the wave properties are considered independent from the nature of the source (Rio 2006) or even internal or volumetric waves, since they include all the medium volume in their movement. Consequently, in relation to the way they propagate, the waves are dilatational or distortional.

There are also surface waves which involve movements essentially confined to a narrow surface layer (Timoshenko and Goodier 1971) and are characterized by an exponential decrease in amplitude the greater the distance from the surface. These waves can be described as Rayleigh or Love waves and are capable of causing more damage than volumetric ones, due to the possible transmission of the resulting vibrations to buildings and other man-made works. Besides, they may exceed the plasticity limit of the involved materials, causing significantly more damages or even total destruction.

2.1.2 VOLUMETRIC VERSUS SURFACE WAVES

Regarding volumetric waves, there can be considered two very distinct types of particle movement: dilatational and distortional.

Dilatational or longitudinal waves are characterized by the parallel particle vibration in relation to the direction of propagation and their velocity of propagation is substantially higher than all other wave types. Wave propagation takes place by a series of alternating pulses of compression and extension of

the entire mass, in a single direction and without any kind of resulting rotations. These type of waves are also known by compression or P (primary) waves and can be represented by a potential function, ϕ. Besides, these waves are able to propagate in solid, liquid or gas media. An example of this type of wave is a sound wave in air.

On the other hand, the particle oscillation in the other type of volumetric waves, known as distortional, shear or S (secondary) waves, is perpendicular to the direction of wave propagation and can be distinguished by two independent movements according to its polarization direction: SH waves (horizontally polarized) and SV (vertically polarized). Considering this fact, it can be assumed that these S-waves have two degrees of freedom instead of a single degree of freedom, as do the P-waves, but in turn can only propagate through solid matter. These waves can cause changes in the shape of the material in which these propagate and are represented by a potential function, ψ.

In Figure 1 both wave propagation modes can be observed.

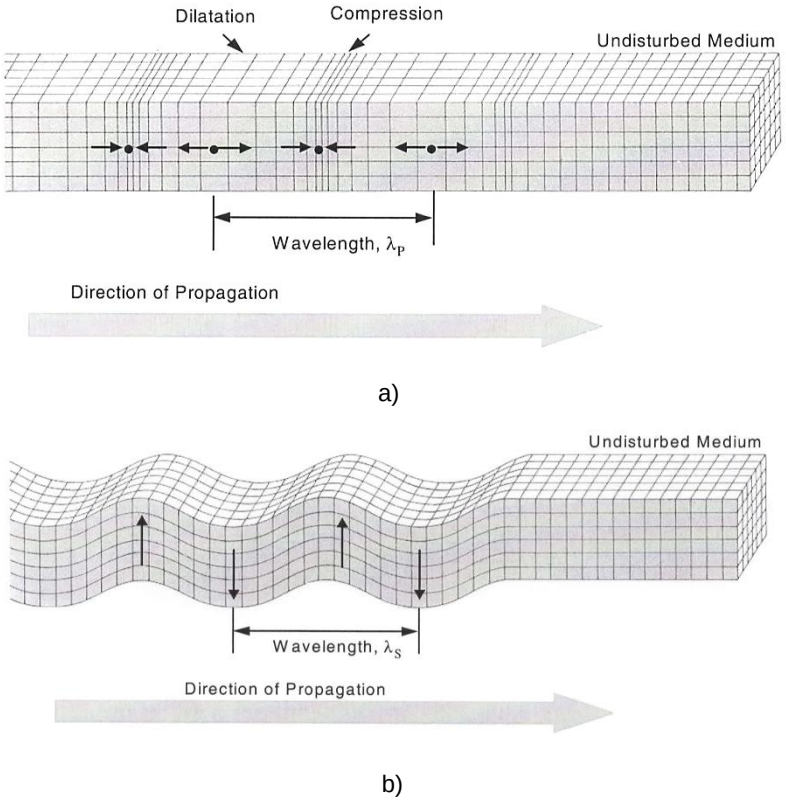

Figure 1 – Schematics of seismic waves: a) P-wave; b) S-wave (Bolt 1976)

Both P and S wave velocities, V_P and V_S respectively, are directly affected by the properties of the materials in which these propagate, and therefore enable to infer changes in the characteristics of those materials through variations in the wave propagation velocities. Moreover, the propagation velocities are directly proportional to the stiffness of the material. The expressions deduced from the equations of movement, reflect the dependence of these waves in the medium and allow an evaluation of the elastic parameters of the medium, assumed to be infinite, elastic and homogeneous.

$$V_P = \sqrt{\frac{E}{\rho} \times \frac{(1-\nu)}{(1+\nu)\times(1-2\nu)}} = \sqrt{\frac{M}{\rho}} \tag{2.1}$$

$$V_S = \sqrt{\frac{E}{2\rho} \times \frac{1}{(1+\nu)}} = \sqrt{\frac{G}{\rho}} \tag{2.2}$$

Where,

- E is Young's modulus;
- ρ is the density of the material;
- ν is Poisson's ratio;
- M is the confined modulus;
- G is the shear modulus.

Poisson's ratio can also be determined from both known V_P and V_S, by the combination of the equations (2.1) and (2.2), as shown in (2.3). Young's modulus can be easily determined by either one of the equations (2.1) or (2.2).

$$\nu = \frac{\left(\frac{V_P}{V_S}\right)^2 - 2}{2\times\left(\frac{V_P}{V_S}\right)^2 - 2} \tag{2.3}$$

On the other hand, surface waves can be described as either Rayleigh or Love waves and are a result of the interference caused by both P and S waves, despite being relatively slower than S waves.

Rayleigh waves were first theoretically predicted by Lord Rayleigh in 1885. This type of wave is characterized by an elliptical motion in an elastic medium described by the particles in a parallel plane in relation to the direction of propagation, causing a particular movement similar to sea waves. The resulting velocity is attained through a combination of both V_P and V_S, along with Poisson's ratio, ν and have relatively high amplitudes.

Love waves were named after Augustus E. H. Love in 1911 and model particle vibration as solely horizontal, making a 90º angle in relation to the propagation direction. These waves can only propagate in a medium limited in its upper part by the soil-air discontinuity and in its bottom by a medium where the velocity of the S wave is higher than the former (Ferreira 2003). Furthermore, since the decay of Love waves is rather slow, these waves are the most destructive outside the surrounding area of the focus, making them the waves that people most feel during an earthquake.

Both wave propagation modes can be observed in Figure 2.

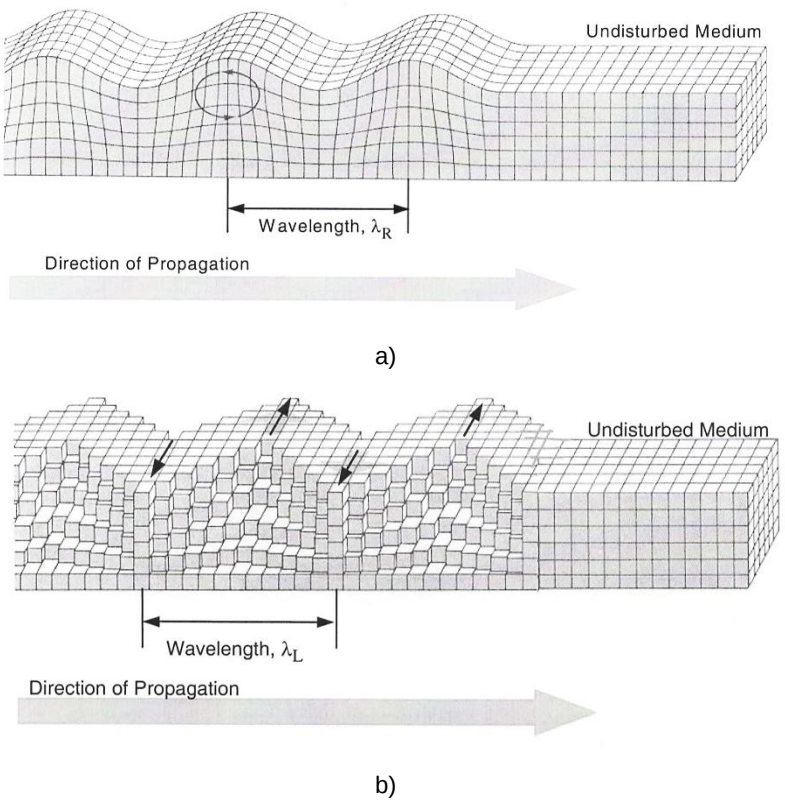

Figure 2 –Seismic waves schematics: a) Rayleigh wave; b) Love wave (Bolt 1976)

Seismic events are an important means of characterizing the Earth's interior as well as its material properties, thus being a great example of dynamic phenomena, making seismology an ever increasing force to the development of general dynamic theory.

2.1.3 DAMPING

Damping consists in the dissipation of mechanical energy from a system, through mechanisms such as internal particle friction, plasticity and viscosity phenomena and can also be referred to as attenuation in the study of wave propagation.

The most common models of damping can be associated to mechanical viscous damping, for simple systems and hysteretic damping, a more realistic model of damping, which is amplitude dependent and refers to the actual properties of the system. However, for simplicity purposes, the model used in this study is the mechanical viscous damping. This type of damping is only frequency-dependent, due to the induced dissipation forces, proportional to the velocity of the oscillating particles (Muscolino *et al.* 2005) besides being considered a property of the medium and a function of the particle oscillation theory.

Viscous damping is also important because of its part in the equation of motion, namely f_a, which is the starting point to characterize vibration behaviour of simple dynamic systems (Rio 2006). The equation of motion, adequate for single degree of freedom (SDOF) systems, requires the following terms to maintain equilibrium, as can also be verified by its schematics, in Figure 3:

$$p(t) - f_{in}(t) - f_a(t) - f_e(t) = 0 \Leftrightarrow m\ddot{u}(t) + c\dot{u}(t) + ku(t) = p(t) \tag{2.4}$$

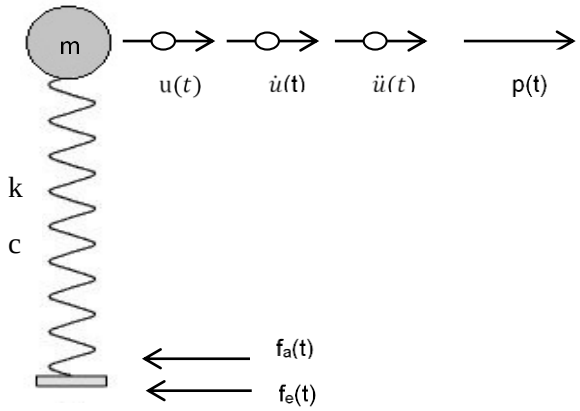

Figure 3 – Schematics for the equation of motion

The term *p(t)* represents an external force applied to the body; $f_{in}(t)$ represents the internal force; $f_a(t)$ represents the damping force; $f_e(t)$ is the inertial force; *m* is the body mass; *c* is the damping of the system and *k* is the stiffness of the spring. On the other hand, *u* represents the position of the body or displacement and naturally $\dot{u}$ and $\ddot{u}$ are its first and second derivatives, in other words, velocity and acceleration, respectively.

The most common types of damped vibration will be explained next, in a simple and straightforward way.

2.1.3.1 Undamped Free Vibration

Undamped free vibration occurs when there is no damping and no external force applied to the system. The damping force disappears, once the damping coefficient is made equal to zero (c=0) and the vibration starts whether by an initial displacement or by an initial velocity and the equation of motion is as follows:

$$m\ddot{u}(t) + ku(t) = 0 \tag{2 5}$$

Due to the necessity of a response by this equation for any instant, *t*, the natural angular frequency, ω, expressed by radians per second, which represents the frequency responsible for the vibration of any given system, is obtained:

$$\omega_n = \sqrt{\frac{k}{m}} \tag{2 6}$$

2.1.3.2 Damped Free Vibration

When a mechanical system is damped, i.e., the value of the damping coefficient is higher than zero (c>0), the equation of motion has all terms. There are three cases of damped free vibration: the critically damped, the over-critically damped and the under-critically damped cases.

The critically damped case represents the situation where the damping coefficient, *c*, is so high that the system becomes no longer capable of oscillating, in other words, the equilibrium position is reached without the need for the system to oscillate. A new coefficient is therefore in order, the critical damping coefficient, c_c, which is also a property of the system and can be characterized as:

$$c_c = 2 \times m \times \omega_n \tag{2.7}$$

Similarly, the over-critically damped case, where $c>c_c$, is similar to the critically damped case, however it takes longer to reach the equilibrium position.

On the other hand, the under-critically damped case, where $c<c_c$, some oscillation does occur. This type of damping is the most common in fields like Civil Engineering and is characterized by a damped free-vibration frequency, ω_D, given by:

$$\omega_D = \omega\sqrt{1-\xi^2} \tag{2.8}$$

and a damping ratio (observed in Figure 4), *D*, by:

$$D = \frac{c}{c_c} \tag{2.9}$$

In current cases, the damping coefficient varies between 2% and 20%. If for example, D=0.20:

$$\omega_D = \omega\sqrt{1-D^2} = 0.98\omega \Rightarrow \omega_D \cong \omega \tag{2.10}$$

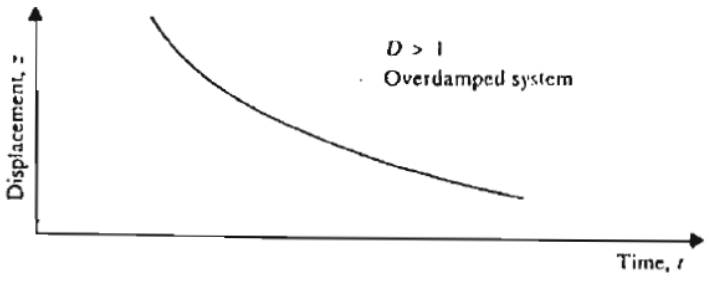

a)

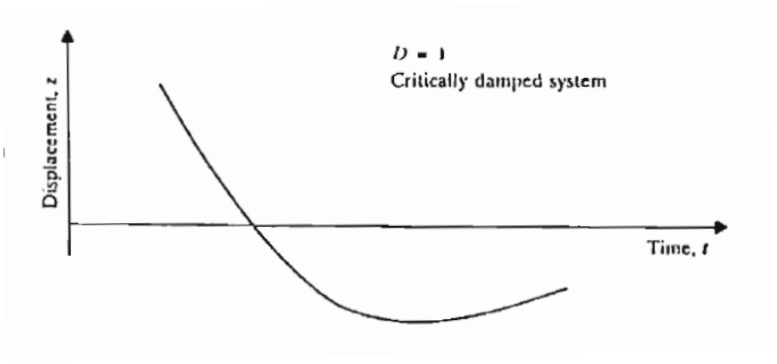

b)

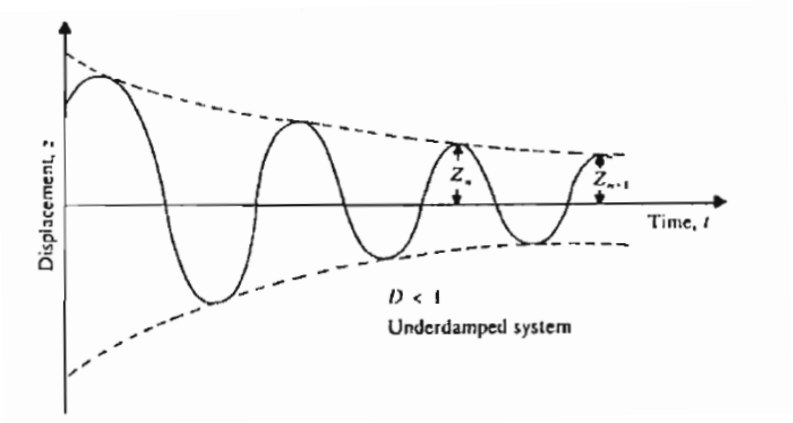

c)

Figure 4 – Schematics of the damping coefficient: a) over-damped system; b) critically damped system; c) underdamped system (Braja 1993)

2.2 DYNAMIC BEHAVIOUR OF SOILS

2.2.1 GENERAL CONSIDERATIONS

To better understand the behaviour of soils, it is necessary to comprehend that, contrary to the general belief for a long time, the soil is highly non-linear. This fact has a great influence on the selection of design parameters for general geotechnical calculations, as well for calculations of ground and structure movements, and although soil parameters or properties are variable, these vary in a very consistent and predictable way. The development of complete and consistent constitutive relationships regarding the modelling of the behaviour of soil appeared for the first time in 1963, in Cambridge, England, when J. B. Burland worked under the supervision of K. H. Roscoe (Burland 1989).

The need to understand the principal features of the soil stiffness related to various aspects of non-linearity, along with new demands in civil engineering led to the development of new dynamic methods that incorporated this new discovery. Besides, the discrepancies regarding the values of the stiffness properties and the stress-strain relationship achieved both in situ or laboratory methods, also requested more sophisticated methods with samples of much higher quality and with the aid of numerical analysis. For example, previous dynamic measurements of the shear modulus, *G*, or Young's modulus, *E*, until recently, leaned towards results significantly higher than pseudo-static values obtained in the laboratory. More recently, the search for more accurate measurement of small strains, by the development of more

efficient laboratory testing methods and procedures, has successfully been closing the void among the static and dynamic measurement of ground stiffness.

In fact, it is only at the very small strain range that the correlation between stress and strain is actually linear, as can be seen in Figure 5. This figure translates one of the most brilliant results of the studies made over the years, consisting in the prospect of the stiffness of soils for a vast array of strain levels, also called the stiffness degradation curve. As can be observed, the shear stiffness, G_0 or G_{max}, reaches its maximum value for very small strains, whereas for large strains its value is significantly lower. This decay shows a clear dependence between the stiffness of the soil and the strain level, which are indispensable parameters when interpreting the values obtained from measurements both in situ and in the laboratory, proving unequivocally the non-linearity of soils.

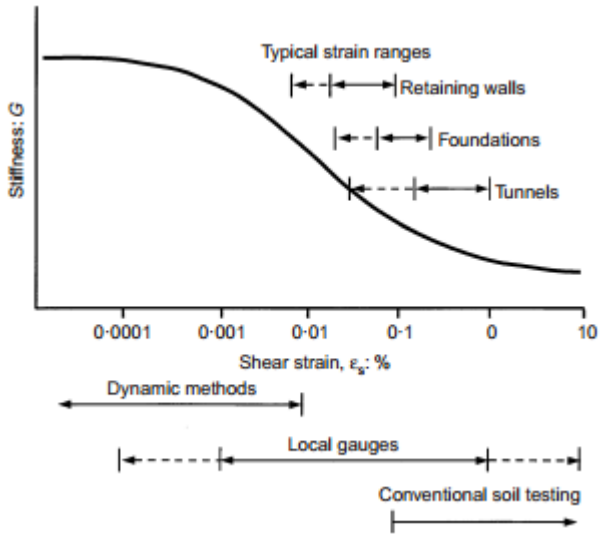

Figure 5 – Non-linear characteristic stiffness-strain behaviour of soil with standard strain ranges (after Atkinson and Salfors, 1991 and Mair, 1993)

In 1989, Burland stated "Small is beautiful" (Burland 1989). This statement might sound strange when seen for the first time, but it is completely true as far as strains are concerned, since although soils are highly non-linear, they also have an elastic region. Both Burland (1989) and Atkinson (2000) researched the non-linearity of the soil and its stiffness, concentrating in the small-strain behaviour. Their research ended up corroborating the work of Jardine *et al.* (1985), who showed the significant effects on different aspects, such as the interaction between the soil and the surrounding structure, stress distributions in the soil mass and displacement profiles around loaded areas and excavations concerning the non-linearity of stress-strain response (Burland 1989). As stated by Lings (2001), "beyond the elastic region, soil behaviour is often markedly non-linear, but moduli at very small strain are important anchor points when characterising the degree of non-linearity involved" (Lings, 2001, after Atkinson, 2000). The fact is that without the concept of non-linearity included in the dynamic methods used, the interpretation of field measurements and in situ tests may be confusing, thus leading to wrongful conclusions.

2.2.2 NON-LINEAR CHARACTER OF SOILS

The improvement of geophysical measurements and its worldwide application, namely regarding the determination of in situ stiffness properties, enabled a better comprehension of wave propagation and

dynamic soil-structure interaction studies, as well as damping, strain level and strain rate effects (Burland 1989).

The non-linear behaviour of soils can be characterized by the rigidity and degree of non-linearity, which can consequently be determined from very small strain stiffness, failure strain and peak strength (Atkinson 2000). Soil stiffness at very small strains can be determined through direct measurements of seismic wave velocities, either in situ (detailed in section 2.3.1) or in the laboratory (in section 2.3.2).

It is also of significant value, to distinguish the different stiffness parameters, which depend on the stress and strain relationships. The general three-dimensional form of Hooke's law relates stresses and strains according to the theory of elasticity, by a compliance matrix [C] encompassing 36 coefficients C_{ij}, which characterize the properties of a material, in the following form:

$$\begin{bmatrix} \varepsilon_{xx} \\ \varepsilon_{yy} \\ \varepsilon_{zz} \\ \gamma_{yz} \\ \gamma_{zx} \\ \gamma_{xy} \end{bmatrix} = \begin{bmatrix} C_{11} & C_{12} & C_{13} & C_{14} & C_{15} & C_{16} \\ C_{21} & C_{22} & C_{23} & C_{24} & C_{25} & C_{26} \\ C_{31} & C_{32} & C_{33} & C_{34} & C_{35} & C_{36} \\ C_{41} & C_{42} & C_{43} & C_{44} & C_{45} & C_{46} \\ C_{51} & C_{52} & C_{53} & C_{54} & C_{55} & C_{56} \\ C_{61} & C_{62} & C_{63} & C_{64} & C_{65} & C_{66} \end{bmatrix} \begin{bmatrix} \sigma_{xx} \\ \sigma_{yy} \\ \sigma_{zz} \\ \tau_{yz} \\ \tau_{zx} \\ \tau_{xy} \end{bmatrix} \tag{2.11}$$

Nonetheless, it is important to comprehend that while some parameters, such as the critical state friction angle, ϕ_c, depends solely on the nature of grains, the very small strain shear modulus, as well as the non-linear behaviour and the soil stiffness are always associated with the current state of the soil, the most common being isotropic and anisotropic stresses. The major difference between them lies in the fact that while isotropy is the property that characterizes the materials which possess the same physical properties, regardless of the direction considered, in other words, uniformity in all directions; anisotropy implies variations with the direction considered and can be separated into (structural) inherent and (stress) induced anisotropy. Structural inherent anisotropy is related to over-consolidated, aged, structured and compacted soils, and refers to a preferential orientation taken by the particles, on account of the geological stress history, namely successive strata loading, whereas induced anisotropy regards more recent soils, and is characterized by a random disposition of particles.

For these reasons, in 1927, Love determined that a symmetry should exist in the compliance matrices for anisotropic materials, in other words, $C_{ij} = C_{ji}$, which led to the reduction of the number of coefficients from 36 to 21. Yet, given that most natural materials show some kind of this symmetrical behaviour, the coefficients can suffer an even greater reduction. There are several types of anisotropic symmetry systems, first presented in 1981 by Crampin, with the most common including: completely anisotropic (21 independent elastic constants); monocyclic (13 independent elastic constants); orthorhombic (9 independent elastic constants); tetragonal (6 or 7 independent elastic constants); trigonal (6 independent elastic constants); hexagonal or cross-anisotropic (5 independent elastic constants); cubic (3 independent elastic constants) and last but not least, isotropic (2 elastic constants), namely Young's modulus and Poisson's ratio.

Nevertheless, in the numerical model used in this study, the objective regarding the state of the soil is related to cross-anisotropy or transverse isotropy. This type of state occurs when the soil properties are considered identical in any horizontal direction, corresponding to a hexagonal anisotropy state.

Therefore, the relationship for cross-anisotropic materials in terms of stress and strain increments can be described through the following matrix (Lings 2001):

$$\begin{bmatrix} \Delta\varepsilon_{xx} \\ \Delta\varepsilon_{yy} \\ \Delta\varepsilon_{zz} \\ \Delta\gamma_{yz} \\ \Delta\gamma_{zx} \\ \Delta\gamma_{xy} \end{bmatrix} = \begin{bmatrix} \frac{1}{E'_h} & -\frac{\nu'_{hh}}{E'_h} & -\frac{\nu'_{vh}}{E'_v} & . & . & . \\ -\frac{\nu'_{hh}}{E'_h} & \frac{1}{E'_h} & -\frac{\nu'_{vh}}{E'_v} & . & . & . \\ -\frac{\nu'_{hv}}{E'_h} & -\frac{\nu'_{hv}}{E'_h} & \frac{1}{E'_v} & . & . & . \\ . & . & . & \frac{1}{G'_{hv}} & . & . \\ . & . & . & . & \frac{1}{G'_{hv}} & . \\ . & . & . & . & . & \frac{1}{G'_{hh}} \end{bmatrix} \begin{bmatrix} \Delta\sigma'_{xx} \\ \Delta\sigma'_{yy} \\ \Delta\sigma'_{zz} \\ \Delta\tau_{yz} \\ \Delta\tau_{zx} \\ \Delta\tau_{xy} \end{bmatrix} \tag{2.12}$$

Where:

E'_v is Young's modulus in the vertical plane;

E'_h is Young's modulus in the horizontal plane;

ν'_{vh} is Poisson's ratio for horizontal strain given the vertical strain;

ν'_{hv} is Poisson's ratio for vertical strain given the horizontal strain;

ν'_{hh} is Poisson's ratio for horizontal strain given the horizontal strain at the right angle;

G'_{hv} is the shear modulus in the vertical plane;

G'_{hh} is the shear modulus in the horizontal plane.

However, as stated above, the coefficients or elastic constants can be further reduced. This was the case for the five independent elastic constants comprised in the cross-anisotropic model. Due to the following equations, the seven parameters included in the matrix above, resulted in the five elastic constants that are associated to this particular model.

$$G'_{hh} = \frac{E'_h}{2(1+\nu'_{hh})} \tag{2.13}$$

as well as

$$\frac{\nu'_{hv}}{E'_h} = \frac{\nu'_{vh}}{E'_v} \tag{2.14}$$

The small-strain shear stiffness depends exclusively of shear solicitations and it is a reference parameter, in other words, a key parameter in geotechnical design (Atkinson 2000). Nonetheless, the shear modulus is not only relevant to small strains and the prediction of soil and soil-structure interaction behaviour due to earthquakes, traffic and machine vibration, explosions, wind and wave loading, but also to large strains, since it is likewise one of the reference parameters whenever the non-linear behaviour of soil is considered.

In truth, there are essentially three regions that characterize the typical behaviour of soils. As observed in Figure 6, they are: the very small-strain region, corresponding to the elastic response, where stiffness reaches an approximately constant value, where E_t (tangent modulus) ≈ E_s (secant modulus) ≈ E_0 or E_{max} (highest value of the Young's modulus), which is limited by a certain strain, namely ε_0; the small-strain region, characterized by a significant decrease in the stiffness value and limited by the previous value, ε_0 to about 0.1% or 10^{-3}; and the large-strain region, represented by a softer decrease of the variation of the stiffness with strain and where stiffness can reach its lowest value.

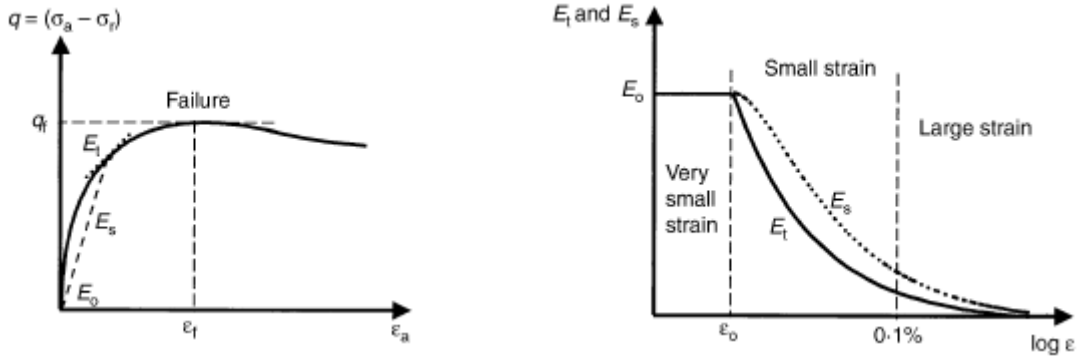

a) b)

Figure 6 –Stress-strain and stiffness-strain curves of a non-linear soil (Atkinson, 2000)

As mentioned above, "small is beautiful" and most of the times, it is the smallest measurement that provides a greater amount of information. From this viewpoint, it is expected that these new developments of both in situ and laboratory techniques, the major problems previously stated of the past thirty years, will be completely overcome.

2.2.3 STRAIN LEVEL VERSUS STRAIN RATE

The most common value of strain level for working conditions of the soil involved in the majority of geotechnical structures is 0.1% (Burland 1989). Therefore, it proves what was mentioned above, regarding the importance of the study of higher stiffness present in smaller strains. It is then possible to assume that soil stiffness is strain level dependent, excepting very low and low strains, of course (Atkinson 2000), as these are regions characterized by an elastic behaviour, though eventually influenced by the viscous behaviour of soil.

Unfortunately, traditional in situ testing methods are not sufficiently accurate in order to be able to measure the lower strain levels of soil stiffness. Advanced laboratory equipment such as local strain gauges have capacity and precision to measure strains above approximately 0.001%, which is the limit value for which the maximum stiffness can be attained, and only the dynamic methods can measure the

very small strain region, as shown in Figure 7. A perfect example of a dynamic testing equipment are bender elements (Jovicic and Coop 1998).

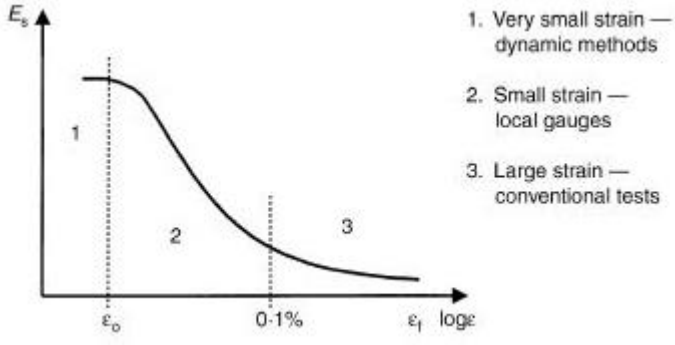

Figure 7 – Measurement of soil stiffness with respect to strain level (Atkinson, 2000)

Another important aspect in the stress-strain behaviour of a soil is its strain rate dependency. Soil stiffness may be affected by the strain rate, or loading frequency, often distinguished in terms of static and dynamic stiffness moduli. In fact, rate-dependent and irreversible stress-strain behaviour (i.e., inelastic behaviour) of a soil can be observed at small strain levels, generally above 0.001% (Teachavorasinskun *et al.* 1991). Figure 8 illustrates the dependency of stiffness on strain rate. This means that the elastic deformation characteristics can be evaluated for different strain rates, not only in dynamic tests but also in static tests. Therefore, within the small strain range, it is more adequate to refer to static and dynamic measurements of stiffness moduli. Hirakawa *et al.* (2003) showed that the strain range in which the stress-strain behaviour is essentially elastic decreases with a decrease in the strain rate, while the secant stiffness approaches an upper bound (i.e., the elastic modulus) with an increase in the strain rate.

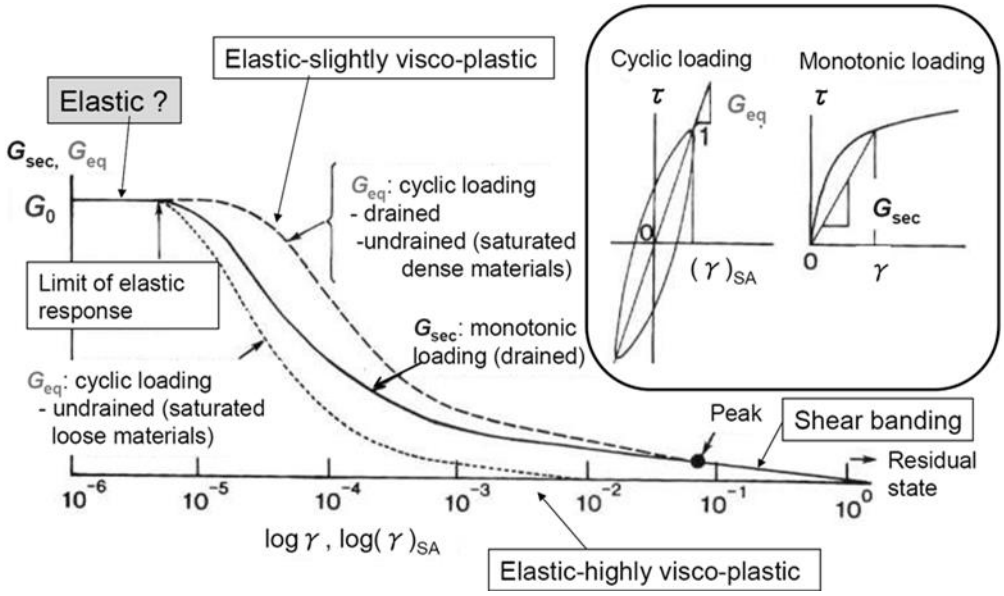

Figure 8 – Strain rate effects on soil stiffness (Teachavorasinskun *et al.* 1991)

In the present study, the focus is on the dynamic behaviour of a soil and therefore elasticity can be assumed.

2.3 SEISMIC WAVE TESTING METHODS

Wave-based methods add complexity to the field and laboratory tests interpretation, but play a very important role in near surface characterization. Table 1, below, shows a summary of the most inherent characteristics in wave phenomena, shared by both elastic and electromagnetic waves.

Table 1 – Wave phenomena: complexity and richness * (Stokoe and Santamarina 2000)

Assumption	Consequences
Infinite medium	P-waves (requires a material: fluid or solid) *
	S-waves (requires shear stiffness)
Finite medium	
Propagation modes	R-waves, L-waves, S-waves *
	Rod waves, Tube waves *
Interfaces	Reflection, transmission and refraction
	Mode conversion
Heterogeneous	
Gradual	Curved rays and deformed wavefronts (Fermat)
Anomalies	Diffraction, cattering (Huygens)
Lossy	Attenuation and dispersion
	Relaxation
Anisotropic	Quasi-propagation *
	S-wave splitting and birefringence
Non-Linear	Shock waves *
Discrete	Dispersion
	Low-pass filtering
Multiphase medium	Slow and fast P-waves *
Coda	A signal tail captures information about boundaries and heterogeneity

* Examples are specific to elastic waves

2.3.1 IN SITU METHODS

In order to comprehend the soil in geological and geotechnical terms, one must understand its dynamic behaviour. For this purpose, both intrusive (when boreholes or penetrometers are used) and non-intrusive (when all the instrumentation used is assembled at the surface) in situ methods have been created to identify, for example, the sequence of layers or strata that are part of the terrain, to characterize its boundary conditions and to analyse the physical, mechanical and hydraulic conditions of the soils that compose the layers or strata which behaviour may affect the future structure to be built. The methods presented in the following sections are only the ones relevant for this particular study.

2.3.1.1 Cross-hole seismic test (CH or CHT)

The cross-hole test consists of the artificial generation of shear (S waves) and compression (P waves) waves at a specific depth, by means of an impact inside a borehole and in the registration of the wave arrival in one or more receivers placed at the same depth, in order to assure immediate detection of the waves, yet with a certain distance from the initial disturbance, as can be seen in Figure 9. By knowing the distance between boreholes, it is possible to measure the travel time and consequently, calculate the shear and compression wave velocities, V_S and V_P, respectively, simply by dividing one factor by another. Additionally, due to the relative distance between boreholes, and their depth, the medium is considered to be non-dispersive.

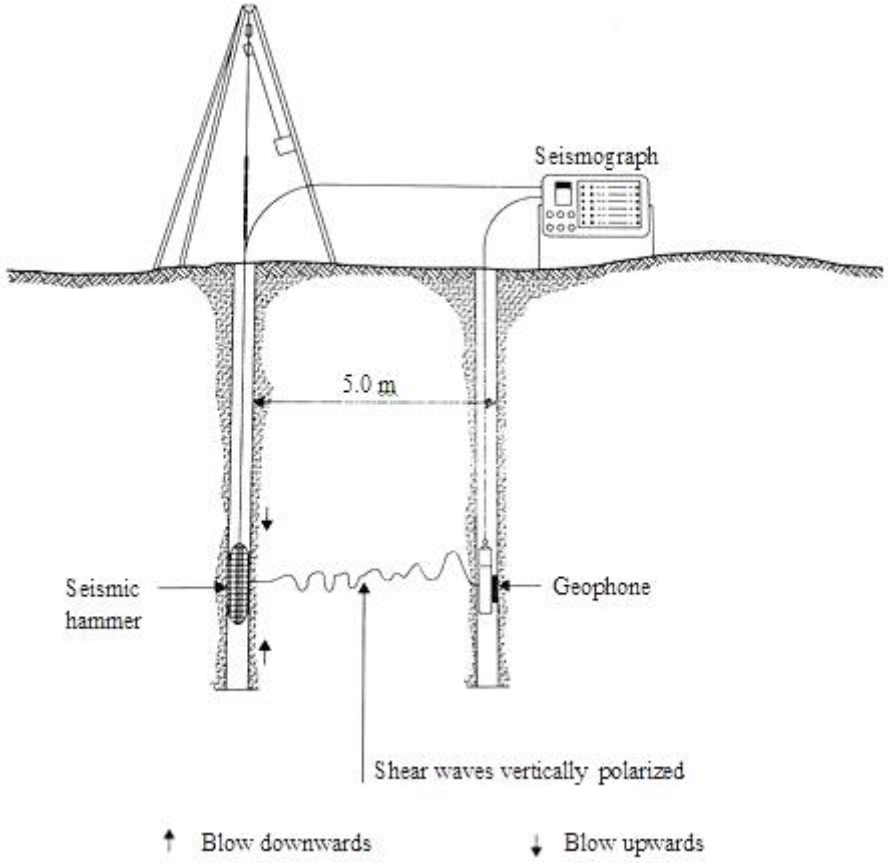

Figure 9 – Schematics of a cross-hole seismic test (Matos Fernandes, 2011, after GATTEL/LNEC, 1993a)

The basic equipment required to perform this test method includes: a *seismograph*, to register, record and keep the results for eventual posterior treatment, and its features include the wave travel-time measurement between the source of energy and the receiver; a *seismic hammer* manually controlled from the surface by means of a cable, capable of applying an impact to the backstop, either downward or upward, enabling the reversal of the shear waves direction (this fact significantly facilitates their identification on a seismograph); and finally a *receiver*, usually geophones or hydrophones, placed inside the boreholes at the same depth as the source, fixed to the borehole coating and oriented in the vertical direction, since it is the direction of the shear load transmitted from the source to the ground.

Although the cross-hole test is an intrusive method and therefore destructive, its advantages overcome the disadvantages, since it encompasses virtually unlimited depth, it is applicable to any soil, from the

softest to the more resistant or stiff, and since it involves the small strain field, it is possible to reliably determine the elastic shear and compression modulus.

2.3.1.2 Down-hole test (DH) or Down-hole seismic test (DHT)

The down-hole test is a less expensive alternative to the cross-hole test, though also an intrusive one, where an impact is applied at the surface, therefore only one borehole is needed. Inside the borehole is placed a receiver, successively at different depths, while the source of energy remains on the surface, close to the borehole. Seismic waves are generated by horizontal impacts from a hammer at the surface in a wood or metal plate vertically pressured against the ground, as shown in Figure 10.

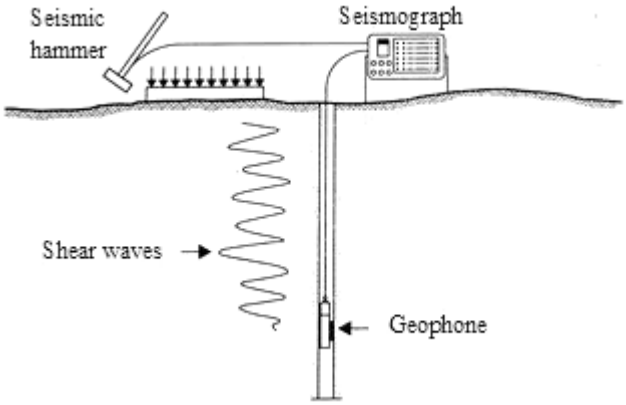

Figure 10 – Schematics of a down-hole seismic test (Matos Fernandes, 2011)

The equipment and the means of registration of the propagation of these planar waves is, as well as the travel time measurement and the resulting velocities, V_S and V_P, the same used in the cross-hole test, although the travel distances are usually based on the assumption of straight ray paths between the source and the receivers. However, this method has a disadvantage that the latter does not have, which is that as the depth increases, the wave energy is forced to travel increasingly larger distances, thus increasing its attenuation.

Both tests are fundamental in the study of the inherent anisotropy of the soil, the at rest stress state and its effects on the elastic properties as well as in the comparison with laboratory testing, since these are the only field testing methods that can be applied to all soil types. It should be noted that these tests are considered intrusive but only where the boreholes are made, since the characterized zone involves a much larger area.

Other field testing methodologies correspond to geophysical methods adapted from classical mechanical methods, like the cone-penetration test (CPT) and the dilatometer test (DMT). Geophysical methods present unique opportunities to characterize sites, materials and processes, or to infer engineering design parameters, due to the strong theoretical bases upon which they are founded, the complementary physical principles that support numerous in situ tests and the ability to perform the same basic measurement both in the field or in the laboratory. The most widely used examples are the seismic cone penetration test (SCPT) and the seismic dilatometer Marchetti test (SDMT). The SCPT or SCPTU (seismic piezocone) is a modification of the CPT, with the cone tip endowed with a receiver, which

enables the measurement of seismic waves in a down-hole testing arrangement (Campanella *et al.* 1986). After testing at a certain depth, the test is repeated by penetrating the cone further into the soil. One of its advantages is the combination of seismic data with the cone resistance values, leading to a more accurate knowledge of soil type, stiffness, strength and layering. On the other hand, the SDMT is a combination of both the DMT (Dilatometer Marchetti Test) and a seismic module for measuring the shear wave velocity, V_S, placed on top of the DMT blade (Marchetti *et al.* 2008). It is therefore similar to the SCPT.

2.3.2 LABORATORY METHODS

The most important aspects to always have in consideration when in the laboratory are to correctly preserve the structural integrity of the specimen from the site in order to accurately reproduce environmental conditions, such as the stress state, initial fabric, pore fluid chemistry, among others, and consequently accurately characterize the soils and particulate materials, in this case, with waves. The preserved specimens represent a single point in the soil mass, yet it is enough to capture internal spatial and temporal scales if these are compatible with its size. In other words, it is possible to assume that the obtained results from the study of the specimen can correctly reproduce the dynamic behaviour of the entire medium. Since the main objective is to analyse the soil skeleton, which is generally in saturated conditions, shear waves are the most relevant to measure.

The presented methods are dynamic methods, employing high frequencies and inducing very small to moderate strains, which use seismic waves to determine the elastic properties of soils, such as ultrasounds, bender elements, resonant column, hollow cylinder and true triaxial apparatus.

2.3.2.1 Ultrasounds

Ultrasounds were first mentioned in 1893, when Sir Francis Galton constructed a whistle that produced that sound level. Combined with the discovery of the piezoelectric effect, in 1880, by both Pierre and Jacques Curie, it was possible to create new ultrasonic transducers to generate and detect ultrasonic waves in water or air. Consequently, the first ultrasonic testing method created by Dr. Floyd Firestone was patented in 1942.This method is non-destructive and consists of the transmission of very short ultrasonic pulse-waves for characterization of materials and even detect possible internal flaws and measure the thickness of objects. The normal ultrasonic frequencies are around 0.1 to 15 MHz and sometimes up to 50 MHz (humans can only ear until approximately 20 kHz). Examples of these transducers for compression and shear waves are depicted in Figure 11. The range of ultrasonic waves can be observed in Figure 12.

Among the advantages are its high penetrating power and high sensitivity, increasing the ability to detect flaws deeper in the medium; great accuracy and equipment portability. Yet, the ultrasonic testing method has its disadvantages, especially regarding the requirement of experienced technicians in handling the equipment and interpretation, calibration and inspection procedures.

a) b)

Figure 11 – Ultrasonic transducers of: a) compression; b) shear

The method itself involves a set of ultrasound transducers connected to an oscilloscope or signal processing device that receives and displays the wave propagation signals on the object being inspected. There exist two methods of receiving an ultrasound wave, namely attenuation and reflection. Attenuation mode consists in the transmission of an ultrasound wave through the surface and its detection in a separate receiver. On the other hand, the reflection mode is related to the ability of the transducers to both transmit and receive pulse waves, in other words, the wave is reflected back to the transducer. Ultrasounds are also used as a form of guidance and detection of prey by certain animals, such as bats (called echolocation) and whales (called bio sonar), as well as a basis for medical sonography (diagnostic medical imaging technique to visualize tendons, muscles and other internal organs by means of real time tomographic images).

Figure 12 – Range of ultrasonic waves

2.3.2.2 Bender elements and other piezoelectric transducers

The piezoelectric effect was first demonstrated in 1880 by physicists Pierre and Jacque Curie, when combining their knowledge in macroscopic piezoelectricity phenomena with crystal structures. The result was achieved by measuring surface surcharges on crystals especially prepared and subjected to mechanical stresses. However, they were not responsible for the discovery of the converse piezoelectric effect. This discovery was due to Lippmann in 1881, by mathematically deducing this property from fundamental thermodynamic principles, which was later confirmed by the Curie brothers.

Piezoelectricity refers to the ability of converting electrical energy into mechanical energy or vice-versa, generating an electric potential during either deformation, therefore allowing the transducers to be reversible in their functions, that is, these can act as sensors, actuators or both. This electric charge can

be found in certain crystals in nature, crystals that possess polar axes, like lithium, tourmaline, berlinite, quartz, topaz, among others and even in biological matter, like bone, wood and silk. It can also be reproduced artificially, by means of polycrystalline ceramic materials, in other words, by the polarization of some ceramic materials, like titanates, depending on their shape, application field, polarization direction and composition (Brignoli *et al.* 1996).

Piezoelectric transducers can be of two types, whether constituted by a single or double-layer thin piezoceramic plate. When a single piezoceramic plate is excited, it can produce compression-extension movements in all three orthogonal directions, by suffering longitudinal deformation in the same directions. Whereas two combined piezoceramic plates can produce not only compression-extension, but also bending movements (Piezo Systems 1994). These transducers can then be designed and mounted in mechanical testing apparatuses to generate and detect both compression and shear waves (see Figure 13). Also, it is important to perceive that installations based on piezoelectric transducers allow for accurate travel time determinations (Stokoe and Santamarina 2000).

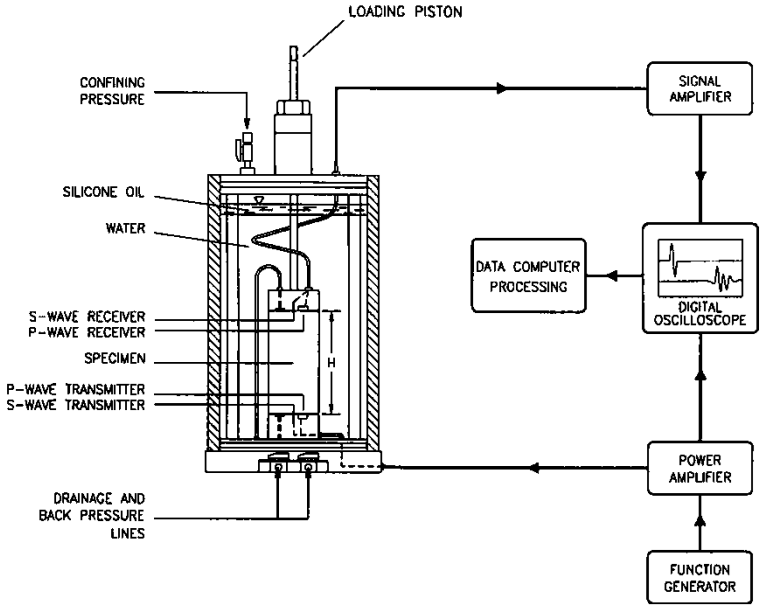

Figure 13 –Schematic of piezoelectric transducers and associated electronics used during traixial testing (Brignoli *et al.* 1996)

Besides the bender elements, which are the most widely used, specially due to its development and widespread dissemination, there are other piezoelectric transducers such as shear plates (consisting of a single piezoceramic element, with a prismatic shape, polarized in the longitudinal direction and similar to bender elements producing shear waves), compression transducers (consisting of a single cylindrical piezoceramic element, protected superficially by an epoxy resin and polarized in the direction of its thickness, enabling the propagation of compression waves) and extender elements (similar to bender elements, but wired to generate deformation in extension-compression, hence also propagating compression waves), as Figure 14 shows. All these transducers allow performing static, cyclic or standard mechanical tests at the same time as the seismic wave dynamic tests; its analysis is not relevant to this study, therefore this brief synopsis will be the only reference.

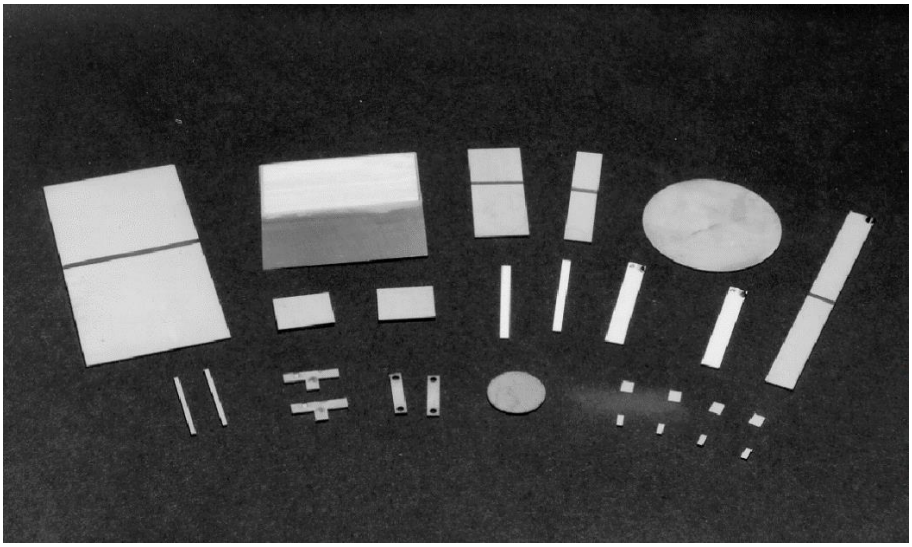

Figure 14 – Types of piezoelectric transducers (Piezo systems)

Bender elements (BE) function much like a cantilever beam and consist of two piezoceramic transducers composed of two piezoceramic plates rigidly attached to an intermediate metallic shim and electrodes on its exterior surfaces. The piezoceramic plates are very thin, which enable the production and detection of transversal motion, not from a shear wave deformation (shear wave transducers), but rather from a bending deformation, thus the name, bender elements. Since the piezoceramic plates are very fragile, they are protected by a rigid epoxy resin coating (which electrically isolates and avoids direct contact with soil and water) and the metallic shim behaves as a reinforcement. Figure 15 shows its composition and operating schematics.

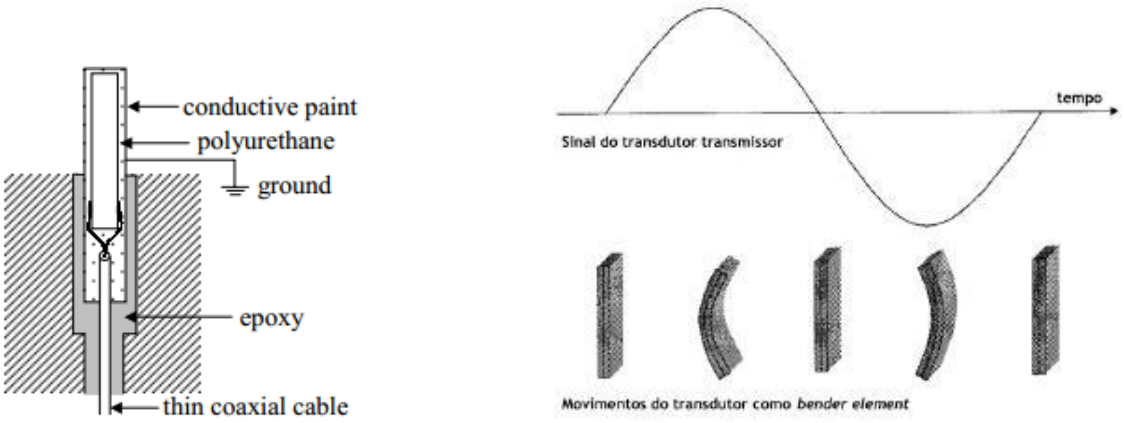

a) b)

Figure 15 – Bender element: a) model (Stokoe and Santamarina 2000); b) operating schematics (Ferreira 2003)

These transducers use piezoelectricity and can be electrically connected in two different ways: parallel-connected, when the plates are polarized in the same direction and series-connected, when the plates are polarized in different directions, enabling the transmission of waves to obtain distinct values of the shear stiffness of the soil. The fact that the electrical connection between plates is made taking into account the polarization direction of both of them is very important to ensure an accurate flexural movement, in

order to propagate shear waves during its deformation. However, like with other piezoelectric elements, a gradual depolarization happens with aging (Santamarina *et al.* 2001). Both electrical connections can function as transmitter or receiver, yet the plates connected in series produce twice the energy as the ones connected in parallel, at the same time undergoing only half the deformation regarding the same given input. For these reasons, the series-connected elements have a better performance when acting as the receiver element and the parallel-connected elements as the transmitter element (Dyvik and Madshus 1985). It is their apparent simplicity that is so attractive, provided that their results are simple to read off an oscilloscope, allowing the direct determination of the travel time and thus the shear wave velocity, which is a characteristic of the medium, by simply comparing the input and output waves. Then, it is possible to obtain the shear stiffness of the medium (Redwood 1960) as can be observed in the following expression:

$$G_0 = \rho \times v_S^{\,2} \tag{2.15}$$

In order to achieve accurate results in the laboratory, the bender elements geometry is a needed aspect to consider. The BE model can be a single transducer or a T-shaped pair of transducers and although its size can vary due to new testing challenges, such as the need to observe vertical and horizontal homogeneity in triaxial specimens and consequently evaluate anisotropy, the approximate size is about 12 mm long, 8 mm wide and 0.6 mm thick, presuming that the particles diameter is around 1 mm (Santamarina *et al.* 2001). Also, these transducers are usually embedded in the top and bottom plates of a triaxial or oedometer cell and can penetrate about 3 mm into the sample (Atkinson 2000). The first detailed model of bender elements was done in 1985 (Dyvik and Madshus 1985), which could be inserted in practically any soil testing equipment.

One of the reasons why this method is adequate for this study is centred in the fact that it can be used in the small strain domain, hence for elastic properties, because the maximum distortion produced in the surrounding "neighbourhood" of the transmitting element is around 10^{-6} (Atkinson 2000). However, these transducers also have the capacity to significantly develop large deformations for a very low electrical excitation, making them a fairly versatile instrument of study. Besides, the installation of bender elements is quite quick and although the specific electronics equipment, including an oscilloscope and a function generator, require some investment, truth is, the results largely compensate the costs, since all laboratory users can run different tests in the same laboratory. Other advantages include their portability, the facility in interpreting the results, the versatility regarding small-strain testing of wet or dry soils in a variety of cells and load conditions (Dyvik and Madshus 1985; Hryciw and Thomann 1993; Fam and Santamarina 1995; Viggiani and Atkinson 1995) and the lower cost in comparison with stress-path tests using local gauges. Besides, bender elements can also be used to measure shear wave velocities in unconfined samples instantly after their recovery from in situ testing sites (Atkinson 2000).

The first known application of bender elements in soils, where shear waves were both transmitted and received was due to Shirley and Hampton, 1978, and these BE were originally developed to measure shear wave velocities in soft soils. However, in 1992, Viggiani found a way to modify them to be able for testing in stiff soils and soft rocks (Atkinson 2000). Nowadays, some applications of bender elements focus on the definition of the elastic stiffness, assessment of sampling quality, anisotropy and

liquefaction potential, identification of destructuration, suction control, comparison of dynamic and static stiffness moduli, as well as for monitoring processes like consolidation, curing and cementation, among others.

Nevertheless, like all devices, some marginal errors should be taken into account, associated to the seismic wave propagation that can overlap the original input wave and of course its shape and the various phenomena that can affect the bender elements performance. The near-field effects, cross-talk, environmental noise are but a few of them.

a) Near-field effects

Much of the subjectivity and uncertainty of bender element testing is quickly associated with the near-field effects, which though common in laboratory testing results, is not very accurate, since there could be a number of different reasons for it. In geotechnical engineering, the concept of near-field effects was first introduced by Sanchez-Salinero *et al.* (1986). In their work a sinusoidal pulse is considered in an infinite isotropic elastic medium, assuming theoretical records from two receivers placed at different distances. This knowledge led to the solutions for the equations of motion for both shear and compression waves, represented as:

$$\Gamma = \Gamma_1 + \Gamma_2 - \Gamma_3 = F_S + N_P - N_S \tag{2.16}$$

The three wave components represent shear movements, yet propagating at different velocities, with F_S and N_P representing the far-field and near-field components of the shear wave, therefore propagating at the shear wave velocity, V_S, and compression wave, therefore compression wave velocity, V_P, respectively, and N_S the near-field effect of the shear wave, hence shear wave velocity. Figure 16 shows such propagation.

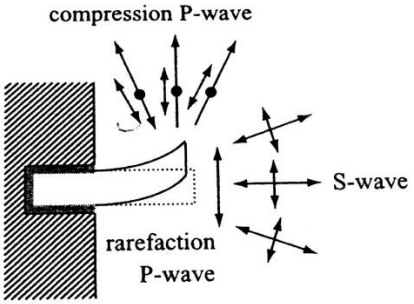

Figure 16 – Bender element: Directivity of both P and S-waves generation (Santamarina *et al.* 2001)

The significance of the terms near and far-field effects is related to the different attenuations experienced with distance. The near-field effect attenuates much faster and can have twice the amplitude and velocity of the far-field effect, despite being a relevant component in the lower frequencies and short distances domain, regarding the source. The far-field components are, on the other hand, non-dispersive, that is, these can propagate with a constant velocity, no matter the distance or the frequency from the source signal, as can be observed in Figure 17.

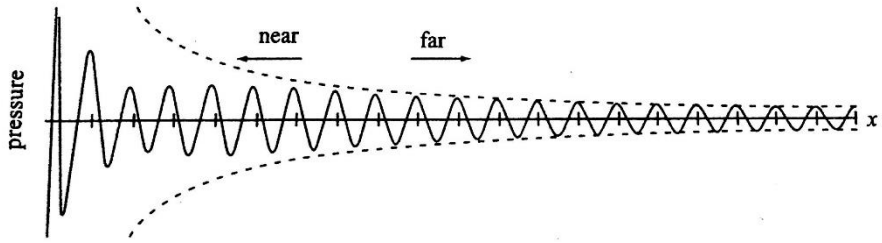

Figure 17 – Pressure versus distance for near and far-field effects (Santamarina *et al.* 2001)

It is important to control and evaluate both the input wave configuration and the attenuation level that occurs during the propagation. This is achieved through the parameter R_d or N, which represent the ratio between distance and wavelength.

$$R_d = \frac{d}{\lambda} = \frac{d \times f}{V_S} = N \tag{2.17}$$

Where:

- d is the travel distance;
- λ is the wavelength;
- f is the transmitted frequency;
- V_S is the shear wave velocity.

However, when discussing the best approach for bender elements testing, the conclusion generally is to select high input frequencies, rather than to alter the distance between transmitter and receiver, in order to minimize the near-field effects and work in far-field conditions. Some investigators, like Brignoli *et al.* (1996), Jovicic *et al.* (1996) and Arulnathan *et al.* (1998) applied these relative limits regarding the distance between transmitter and receiver transmitters in their bender elements tests, showing proof for small relative distances of near-field effects, usually for N lower than 2. This effect decreases significantly with the increase of the input wave frequency, in other words, as the N value increases, making the distinction among the shear and compression waves clearer, thus facilitating the interpretation process. Having these ideas in mind, it is important to realize that these processes of interpretation are significantly reinforced and eased by the independent measurement and record of both waves, through the use of the piezoelectric transducers associated to each wave (Brignoli *et al.* 1996).

b) Cross-talk

The phenomena of cross-talk occurs when there is a signal "leakage" from the transmitted to the received signals, essentially contaminating the latter. Generally, this kind of noise is not random in nature and both the input and the output signal present comparable magnitudes, almost mirroring the transmitted signal, except for a slightly different amplitude and shift in phase, which may result in a considerable source of error. The presence of cross-talk can be enhanced in the case of a low voltage of the actual

shear wave signal, which corresponds to a very low signal-to-noise ratio. In order to enable the complete dissipation of this noise it is necessary to use high enough frequencies before the arrival of the shear wave. In practical terms, the signal of the input frequency should finish at least half the travel time, which normally corresponds to two wavelengths traveling in the length of the specimen. Assuming that the user understands these facts and is capable of knowing the difference from the actual wave, the interpretation of the signals and the first arrival are unaffected. However, this is what happens in the time domain. In the frequency domain, the existence of cross-talk can also result in a substantial source of error.

Nonetheless, the presence of cross-talk can also be related to other sources from other points in the circuit (Rio 2006), such as the lack of grounding of the testing apparatus and the plugs proximity to the electronics equipment. In these cases, a better insulation of the equipment should be in order. Yet, the most usual cause of the cross-talk phenomena is the electromagnetic coupling between transmitter and receiver associated with bender elements testing (Santamarina *et al.* 2001), predominant in a conductive medium, namely saturated soils. The solutions, in this case, would be a better grounding of the bender elements and the use of a parallel/series bender elements combination.

In Figure 18 can be observed a real measurement of bender elements with a frequency of 8 kHz, done in the laboratory. While in a) the presence of cross-talk is evident, given the clear contamination of the output signal, probably enhanced by the low voltage of the actual shear wave; in b) there is no evidence of cross-talk, since the output signal is approximately constant, which is probably due to adequate insulation and grounding. Thereby, the fact that there is no presence of cross-talk results on a high signal-to-noise ratio, facilitating the interpretation of the output signal.

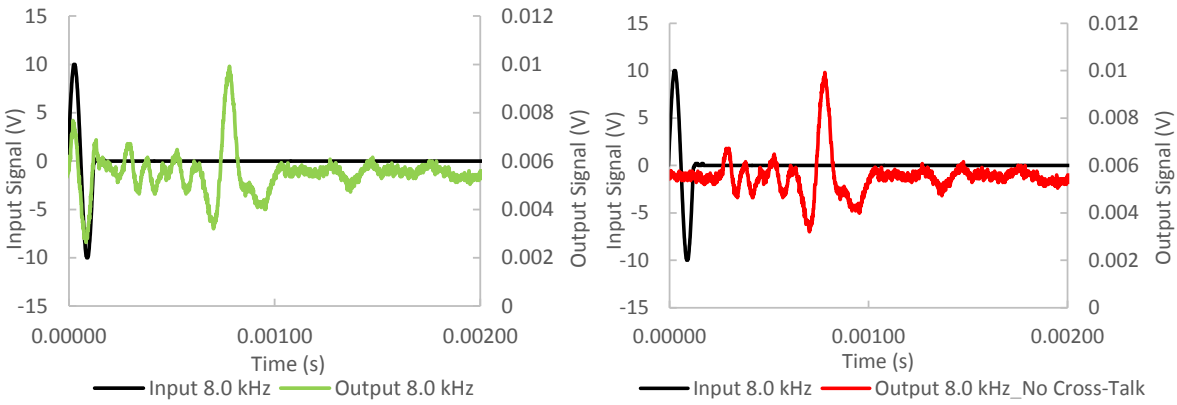

a) b)

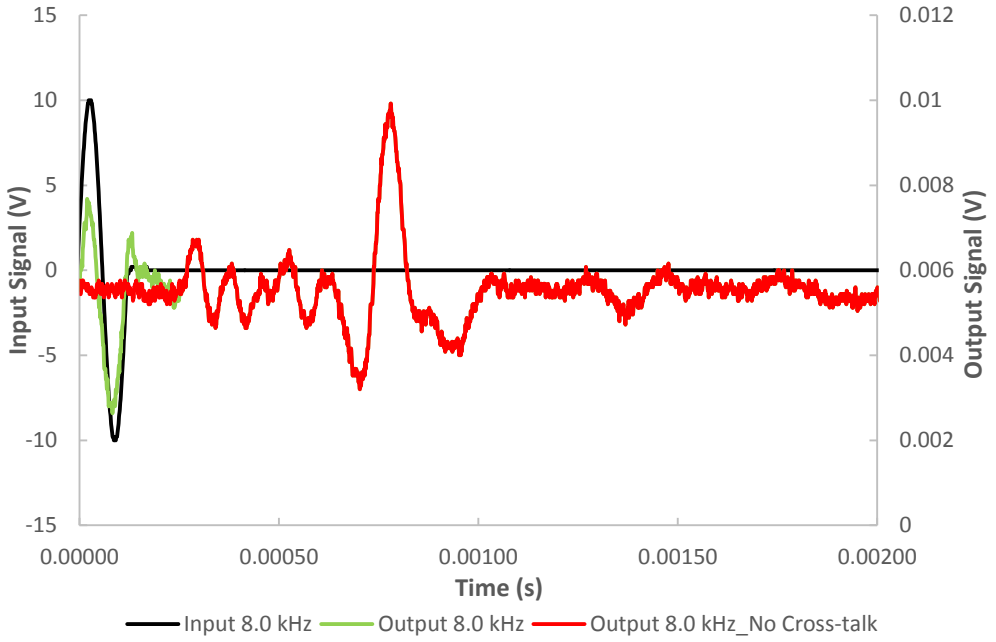

c)

Figure 18 – Bender element measurement in the frequency of 8 kHz: a) Presence of cross-talk in the output signal; b) No presence of cross-talk in the output signal; c) Comparison between a) and b)

[Note: The polarity of the output signals is inverted, in relation to the input signals]

Altogether, despite the possible considerably decrease of this effect, it may sometimes be nearly impossible to eliminate it completely.

a) Environment noise

To optimise the bender elements measurement, one of the technical requirements is a noise-free environment. However, in most laboratories it is near impossible to remove all background noise from electromagnetic noise and mains supply. The lower the quality of the test signal, the more visible the noise level becomes. Though random in nature, environment noise affects mainly the output signal, especially due to the transducers uptake capacity and a usual low frequency of approximately 50 Hz which can be seen in the oscilloscope. To minimize this effect there is a need for doubling the isolation of the equipment and apparatus, a careful choice and assembly of the cables and, if necessary, post-processing analytical filters.

The interpretation process must always have in consideration the factors that can eventually prejudice the results.

Moreover, most authors have difficulties in the interpretation of bender element results, especially due to their apparent subjectivity, which requires some degree of judgement on part of the interpreter and until now, there is still not a single ideal method of interpretation agreed by the majority of authors. To aid in this interpretation, the configuration of the input signal, especially regarding its frequency and

shape, is determinant in the configuration of the output signal, with implications in practical terms concerning the levels of intelligibility and ease of interpretation. In relation to the seismic velocities, there are two measurements that can be made, namely the travel length and the travel time, which is influenced by frequency, the input signal configuration and dispersion. All these parameters are going to be explained below.

b) Frequency

The ideal excitation frequency depends on several factors, such as the stiffness and structure of the soil, the confined pressure, the travel length, among others. On the other hand, parameters like the near-field effect strongly depends on the chosen input frequency. Since there is not a single correct frequency *per se*, the only possibility is to suggest procedures based on experience and analysis. Actually, the best way to observe a clearer signal and therefore to correctly interpret the results is to use different frequency values with various methods of interpretation and to posteriorly observe the different responses obtained when testing (Arulnathan *et al.* 1998). These initial tests can provide estimates of the final shear wave velocity, V_S.

As observed above, to reduce the near-field effects, Sanchez-Salinero *et al.* (1986) established a minimum value of N, equal to 2, which would mean that it is necessary to ensure that at least two wavelengths exist continuously travelling along the specimen. This conclusion was corroborated by many of their peers, being possible to observe that, in these conditions, the near-field effect can be easily recognized, whether by manual filtration or simply by being visually ignored (Ferreira 2003). The equation presented next was rewritten to N>2 and enables the definition of a starting frequency, after arbitrating a realistic value for the shear wave velocity:

$$f > \frac{2 \times V_s}{d} \tag{2.18}$$

However, for bender elements, this limit may actually be higher, given its mechanical response to the given frequency and considering the friction between the soil and a transducer. This friction effect is more prominent in case of the presence of more rigid and/or coarse soils, leading to the necessity of applying higher frequencies, although more limited. This could be minimized by choosing a frequency that could induce resonance on the receiver or by changing the input wave configuration. The mechanical response of the transducers is able to handle excitations of approximately 30 kHz (Jovicic *et al.* 1996). Some researchers were also able to verify that the damping during the propagation of the higher frequencies signals is stronger and quicker than in the lower frequencies.

c) Input signal configuration

In bender elements testing, different kinds of configurations of the input signal have been used. The input signal configuration refers to the shape of the generated electric signal, which is directly conducted to the transmitter bender element. The response of a certain system can be determined when there is an excitation with input signals, both in time and in frequency domain. The most common configurations of the input signal can be characterized by an impulse of square or step signal, or a sinusoid, a wavelet or wave packet and even random noise. An impulse, by definition, is known for including a broad range of frequencies, since it starts and finishes at a rest position, so its response can fully characterize the system (Santamarina *et al.* 2001). Square or step signals were used in the first bender elements tests;

however, by including a large frequency range, these could generate unwanted near-field effects, compromising the arrival time of the output wave. Furthermore, apart from a very well-defined start, no other noticeable features and problems are arisen concerning its sharp initial start. The random noise is also known to be broad-banded and it is characterized by the presence of all frequencies simultaneously, spreading the energy in the selected frequency band, hence facilitating low strain measurements (Cascante and Santamarina 1997). On the other hand, wavelets or wave packets have a characteristic frequency of their own, while a pure sinusoidal signal, which is the most usual way of excitation nowadays, contains energy in a single frequency, enabling more reliable time measurements, mainly because the frequency components are reduced, therefore minimizing velocity dispersion (Blewett *et al.* 2000). The typical input signals can be seen in Table 2.

Table 2 – Input wave shapes by different authors

Time	Frequency	References
Square or Step 	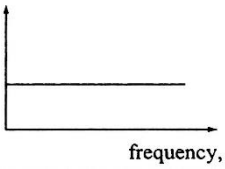	Dyvik and Madshus (1985) Fam and Santamarina (1995)
Impulse 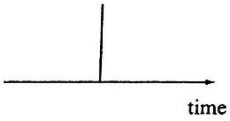	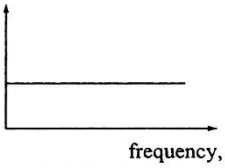	Lee and Santamarina (2005)
Sinusoid 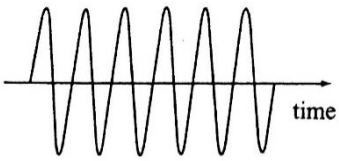	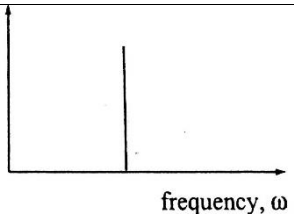	Viggiani and Atkinson (1995) Brignoli *et al.* (1996)
Wavelet or Wave Packets 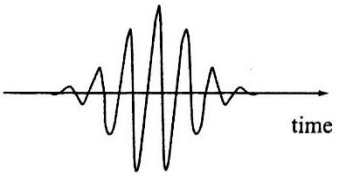	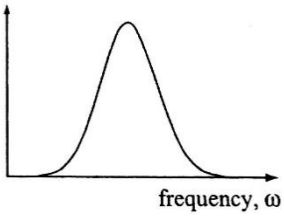	Kumar and Foufoula-Georgiou (1997)
Random Noise 	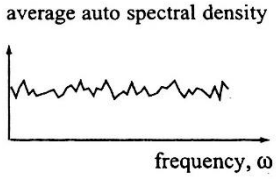	Roesler (1979) Santos *et al.* (2007)

d) Dispersion

When a wave is disintegrated into different frequencies, each with specific propagation velocities, the phenomena presented is dispersion. One example is referred in the work of Rayleigh and Lindsay (1945), who compared wave dispersion with a pool of still water and the propagation of the waves from a local disturbance. The most common causes of dispersion are usually waveguide dispersion and near-field effects. On one hand, the waveguide dispersion is caused by the wave components being reflected on the boundaries of the surrounding medium and on the other hand, the near-field effects, as opposed to the far-field effects, possess different amplitudes and propagating phase wave velocities. Also, although in this study the soil is considered homogeneous, in a more realistic view, the structure of the soil, heterogeneous in nature, is considered yet another cause of dispersion, leading to heterogeneous interactions among particles with wave propagation and possibly to anisotropic wave propagation.

Dispersion should be considered in dynamic test methods that involve wave propagation, especially to determine the elastic properties of the medium, like its elastic constants or damping characteristics (Rio 2006). Besides, regarding time and frequency domain, it is important to understand that the dispersion effect is more prejudicial in the time domain, since it is difficult to extract the travel time values, because it is scrambled with the signal. Nevertheless, in the frequency domain, it is possible to extract the needed information more efficiently, since it enables the comparison between cause and consequence.

e) Travel length

Considering the seismic waves travel length, the most accepted theory is that the distance effectively travelled through the sample corresponds to the distance between the transmitter and the receiver bender element at the time of wave propagation or tip-to-tip distance. Studies made by Dyvik and Madshus (1985), Viggiani and Atkinson (1995), Brignoli *et al.* (1996), Lee and Santamarina (2005), among others, supported this theory. In the case of triaxial tests, this distance corresponds to the height of the soil specimen at the time of the testing, minus the protrusion of each of the bender elements, depending on their dimensions and their setup in the apparatus. These corrections of the protrusions are only applicable to bender and extender elements and not to the other transducers. However, in a true triaxial apparatus, which is the apparatus used in this study, the more realistic measurements consist in the centre-to-centre distance, since the wave is generated by the movement of the whole transducer, as shown in Figure 19.

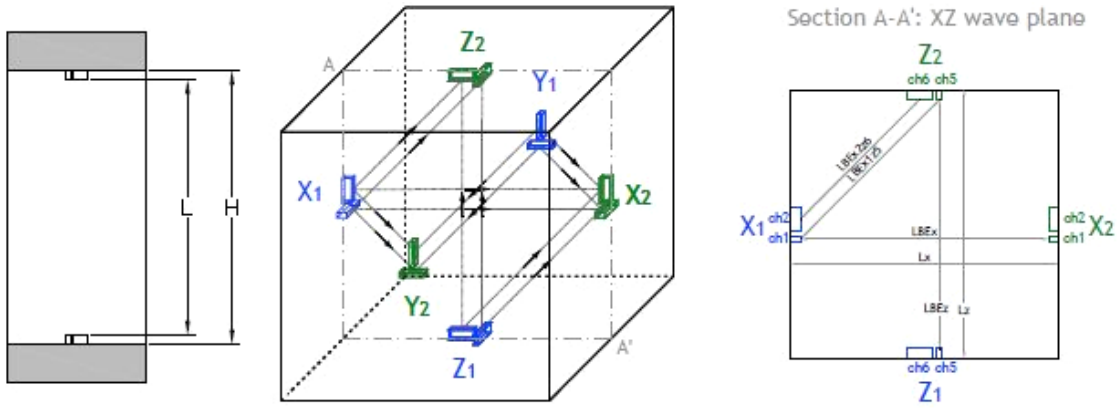

a) b)

Figure 19 – Definition of travel distance: a) direct arrival for a triaxial cylindrical specimen; b) direct and inclined waves for a true triaxial specimen (Ferreira 2009)

Of course, there is not always a unanimous theory, and in this case, the other theories regarding the travel length belong to Porovic (1995), who considered the effective travel length as the distance between the centres of the transducers, which consequently could provide an excellent agreement between the shear stiffness obtained from bender element measurements and resonant-column tests. On the other hand, Rio (2006) concluded that by carrying several bender elements tests on artificial polyurethane samples, the travel length could be measured among the centres of dynamic pressure exerted by the transducers on the surrounding soil, approximately one third of the embedded height. Yet, until now, the accepted theory has been the first one described above.

Therefore, since the wave velocity, as well as its corresponding modulus, is directly dependent of the travel length, its accurate determination is of extreme importance, especially given the relatively small dimensions of the laboratory specimens.

f) Travel time

The determination of the wave travel time, when measured directly between the input and output waves is a usual practice and, as in the geophysical methods, it is based on the identification of the first arrival time of the output wave, that is, the first inflection of the output wave (Figure 20). This method is immediate and with intuitive, yet often subjective, interpretation techniques, as many of the different users can select different arrival points, assuming plane wave-fronts and the absence of both reflected and/or refracted waves (Arulnathan *et al.* 1998).

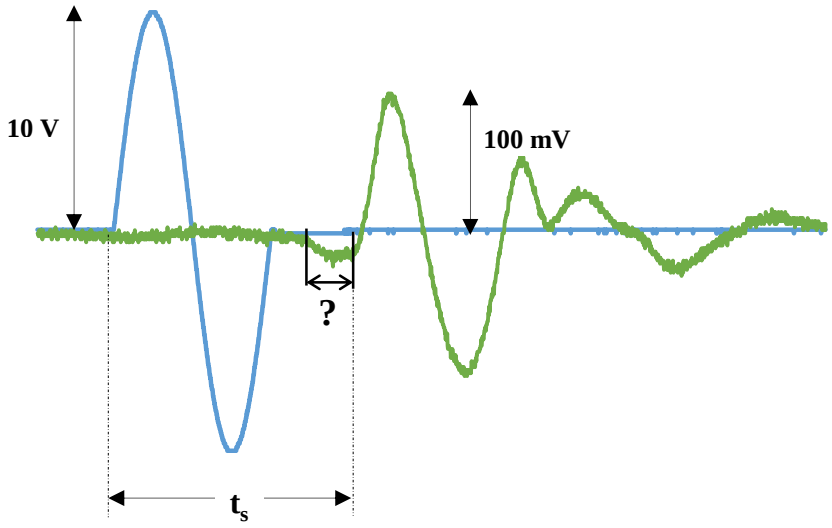

Figure 20 – Schematics of the determination of the travel time of an S wave, regarding the first direct arrival of the output signal

The travel time is considered independent of the input frequency, at least within the selected range of frequencies. Nevertheless, the quality of the measurement of the travel time depends on the shear wave, namely, its amplitude, frequency and form. Regarding the differences in the frequency values, it is also possible to observe in Figure 20, the strength of the input signal is fairly higher than the one of the output signal, which is described by a strong sinusoidal wave, followed by a series of smaller cycles. However, it is important to realize that the near-field effects, as well as other error factors have their polarization

reversed, since the evaluation of high propagation waves in such small routes is more sensitive to the previous mentioned factors.

The usual procedure most used nowadays is to use various input signals, and to observe the similarities of peaks, troughs and zeroes and only then determine the best estimate of the travel time. The response signals will have different shapes, as well as more or less cycles and amplitude, namely within 1 kHz and 10 kHz.

2.3.2.3 Resonant column

The resonant-column test is the most widely used laboratory device that studies the dynamic behaviour of soils, namely its shear stiffness (by first obtaining the shear velocity), *G*, and damping ratio, *D*, for a wide range of strains, from 10^{-6} to 10^{-4}. The first application of this technique is attributed to Ishimoto and Iida (1937). Moreover, by varying the previous parameters values while increasing strain magnitude, it was possible for engineers to better assess natural and engineered structures bound to cyclic and dynamic loadings, through non-linear and finite element analytical methods.

The resonant-column is usually used to induce a frequency vibration in the forms of a longitudinal or torsional excitation, which can vary according to the resonance (which serves as a magnification of the motion of the particles and facilitates experimental observations) of the system, to a solid or hollow cylindrical specimen, previously subjected to a stress state controlled in a triaxial chamber, as can be observed in Figure 21.

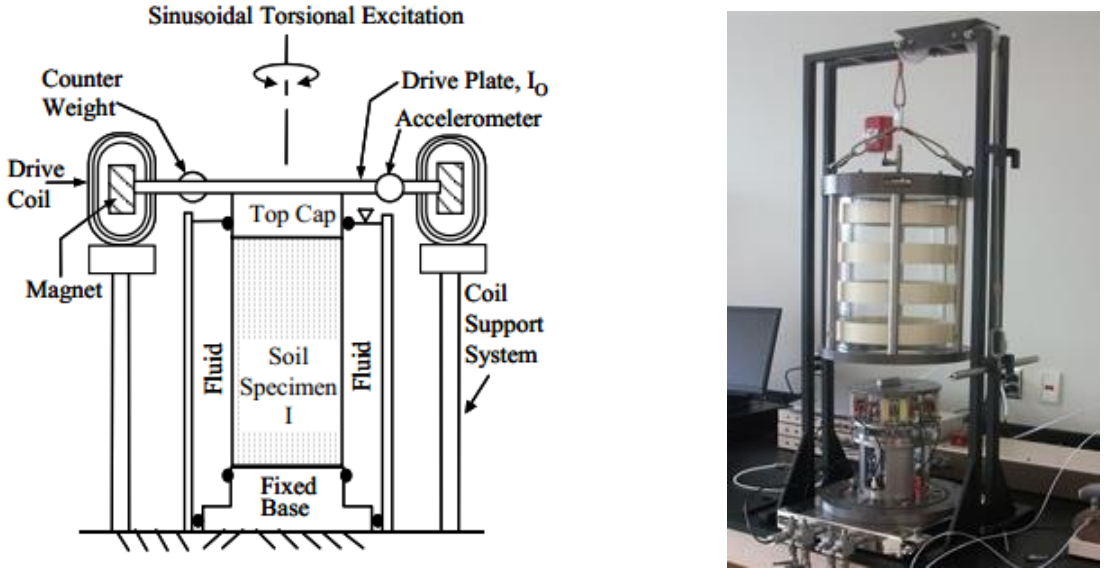

a) b)

Figure 21 –Resonant-column: a) schematic of a fixed-free, torsional resonant-column (Stokoe and Santamarina 2000); b) example of an apparatus (from GDS Instruments)

The vibration previously mentioned relates to the dynamic behaviour of soils by a response curve, which contains both the phase delay of the response and the amplitude given by each frequency variation. The boundary conditions considered are related to the fixity ends of the cylindrical device and can be fixed-free, where there is a restriction in mobility in one of its ends, or free-free, i.e., without restrictions. The

most used is the fixed-free resonant-column with a torsional mode of vibration, the only mode that is non-dispersive.

One of the most important advantages of the resonant column testing is that measurements can be done in the small strain range, as it is done in field testing (Stokoe and Santamarina 2000). Also, by having the ability to determine the shear stiffness of soils in a wide range of strains, it can relate to the bender elements, especially in the small strain domain. A preliminary comparative study between both devices was made in 1985, by Dyvik and Madshus and, more recently, by Ferreira (2007), evidencing good agreement in the results obtained by the two methods. Therefore, despite being a more expensive device than bender elements or other piezoelectric transducers, it is more sophisticated and reliable, since it takes into account the derived parameters, which are based in the wave propagation theory.

2.3.2.4 Hollow cylinder

Another widely used device, although less used than the piezoelectric transducers, is the hollow cylinder apparatus, for measuring the shear strength of soils. This device enables a stress path testing, whilst a rotational displacement and torque are applied in a soil specimen, allowing to evaluate the soil dynamic behaviour in which complex stress paths take place. This is possible by controlling the magnitude and direction of the principal stresses, which are axial stress, internal and external cell pressures and torque, as demonstrated in Figure 22. Furthermore, in the hollow cylinder, geometric proportions can and should be chosen carefully in order to minimize any unwelcome non-uniformities (Saada and Townsend 1981).

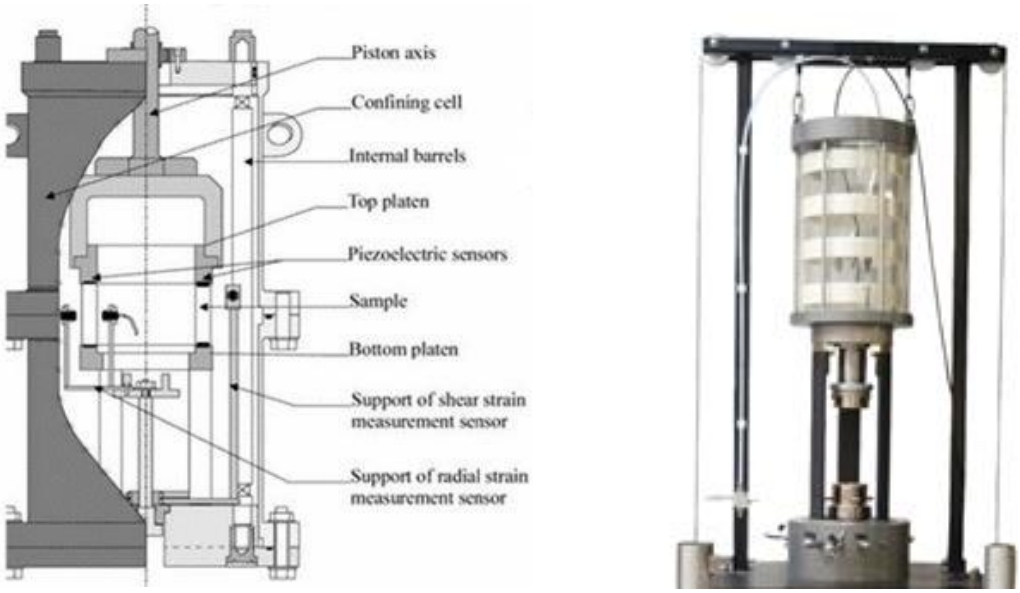

a) b)

Figure 22 – Hollow cylinder: a) Schematic of a hollow cylinder model; b) Small-strain hollow cylinder apparatus (from GDS Instruments)

Some of the studies made possible with this device focus on the effects of the rotation of the principal stresses and the anisotropy of soil specimens. Besides, there has been a recurrent approach to the use of the hollow cylinder apparatus with bender elements in soil characterization tests (Di Benedetto *et al.* 1999; Geoffroy *et al.* 2003).

The study regarding the characterization of the pre-failure deformation and large strains behaviour of sand by Ibraim (2011) is but one of the many examples of the hollow cylinder apparatus.

2.3.2.5 True Triaxial Apparatus

The cube shape design of the true triaxial apparatus was chosen due to the possibility of varying the principal stresses independently, and therefore providing one more degree of freedom than the conventional triaxial apparatus, an aspect required by the general models of failure and stress-state behaviour. The main categories of the possible models of true triaxial apparatuses are: strain-controlled rigid boundaries; stress-controlled flexible boundaries and mixed boundaries (Ferreira 2009). The true triaxial designs were pioneered by Hambly (1969) which can be observed in a) b)

Figure 23, Wood (1974), Matsuoka *et al.* (2002) and Sadek (2006), regarding the rigid boundaries, Ko and Scott (1967) and Lomize (1967) for the flexible boundaries and last but not least, Green (1972) and Lade and Duncan (1975) for the mixed boundaries. If on one hand, a rigid boundary cannot guarantee uniformity of applied stress, on another, a flexible boundary cannot guarantee uniformity of applied deformation (Airey and Wood 1988).

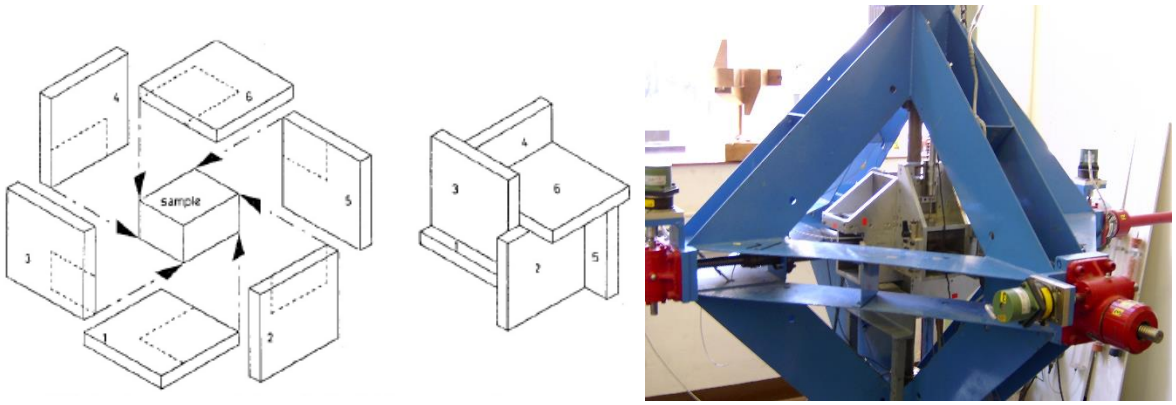

a) b)

Figure 23 – Arrangement of rigid platens of the true triaxial apparatus: a) Schematics of the Cambridge true triaxial apparatus; b) Photograph of the true triaxial apparatus at the University of Bristol (Sadek 2006)

An example of a rigid boundary is the device attained from the collaborative project between FEUP and the University of Western Australia which consists of six square platens assembled in a cubical frame made composed by anodized aluminum, which will be further detailed in the following chapters.

Another example of a true triaxial apparatus, now with flexible boundaries, also called a cubical cell (CC) apparatus, is illustrated in Figure 24. It contains six pressurized bags, similar to rubber cushions, which enclose the sample within a loading frame. Finally, the mixed boundaries apparatus is also widely used, consisting in a mixture of rigid and flexible boundaries, hence lacking the important aspect of symmetry, which consequently limits the regions of principal stress space that can be explored and essentially provides the development of preferential directions of failure.

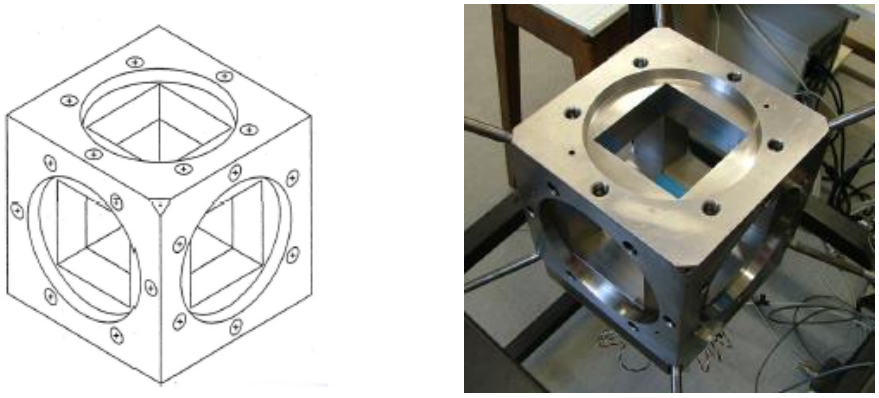

a) b)

Figure 24 – Flexible boundary true triaxial apparatus: a) Frame view; b) Example of a flexible boundary true triaxial apparatus at the University of Bristol

True triaxial devices are extremely versatile, as either effectively uniform shear stresses and normal stresses can be applied to its faces (Arthur 1988) and its simplicity and uniformity of imposed deformations or stresses allow controlled gradual rotations of the principal axes of stress and strain. Nevertheless, the simplicity of the design leads to a limitation regarding the corners, hence a lack of control of the stresses exerted on them. Yet, given the usual large size of the sample, this limitation is normally disregarded. However, this device can provide much information, usually inaccessible in standard triaxial testing, that can be applied to regions of stress and strain space, in order to guide the generation of realistic constitutive relations for soils (Airey and Wood 1988).

3
NUMERICAL MODELLING

3.1 INTRODUCTION

Since the beginning of times Man have tried to develop new ways to evolve. From the discovery of fire and new lands, to the wheel and the Industrial Revolution, Man have developed new methods to improve their quality of life and to understand more of the world they live in. The soil or rock behaviour is one of those things, providing the stability or instability of structures. Nevertheless, against major belief, the soil response is highly non-linear depending upon many factors, some of which are not yet fully understood, being therefore necessary the use of more advanced technology to take into account factors that are not included or cannot be extracted in situ and tested in the laboratory.

Traditionally, the modeling of geotechnical processes was made through simple and empirical analyses, however the introduction of less expensive but yet more sophisticated and relatively easy, computer software and hardware has allowed significant advances in this kind of analysis (Potts and Zdravkovic 1999). This way, there is no longer a necessity of great quantities of data, but simply little site specific data and an understanding of the dominant mechanisms of soil behaviour.

As a basis for a numerical analysis, a number of steps should be considered. First, after the main characteristics of the problem in study have been correctly understood, a definition of the objectives to be accomplished should be made and if, for any reason there are complicating features that have little influence in the results, then they can be omitted. Then, it is important to have an initial estimate of the expected behaviour according to the gathered conditions, much like a conceptual picture (Itasca 2002a). It is also essential and efficient but not obliged, to build a simple model input as a way to validate and better understand both the program and the data, before the detailed model creation. With its results, it may be necessary to review the former step in case, correcting the data with the new insights. In essence, it is a process of trial and error. Now, it is possible to progress to the actual detailed model, where many types of data will be needed, such as details of geometry, locations of geological structures, such as faults and joint sets, material behaviour, soil properties, initial conditions, boundary conditions and external loading. Furthermore, as in all kind of analysis, there is a need to consider the model calculations and the results interpretation. Also, it is important to know how much time is required to perform the model calculations and if the number of monitoring locations is enough to an accurate interpretation of the results and consequently of the model analysis, thus improving modelling efficiency. As more information is available, the more "richer" and reliable the model will be, depending on the correct incorporation of the data and provided that the complexity of the model does not become counterproductive.

Basically, when building a detailed model the major outlines in order should be as observed in Figure 25:

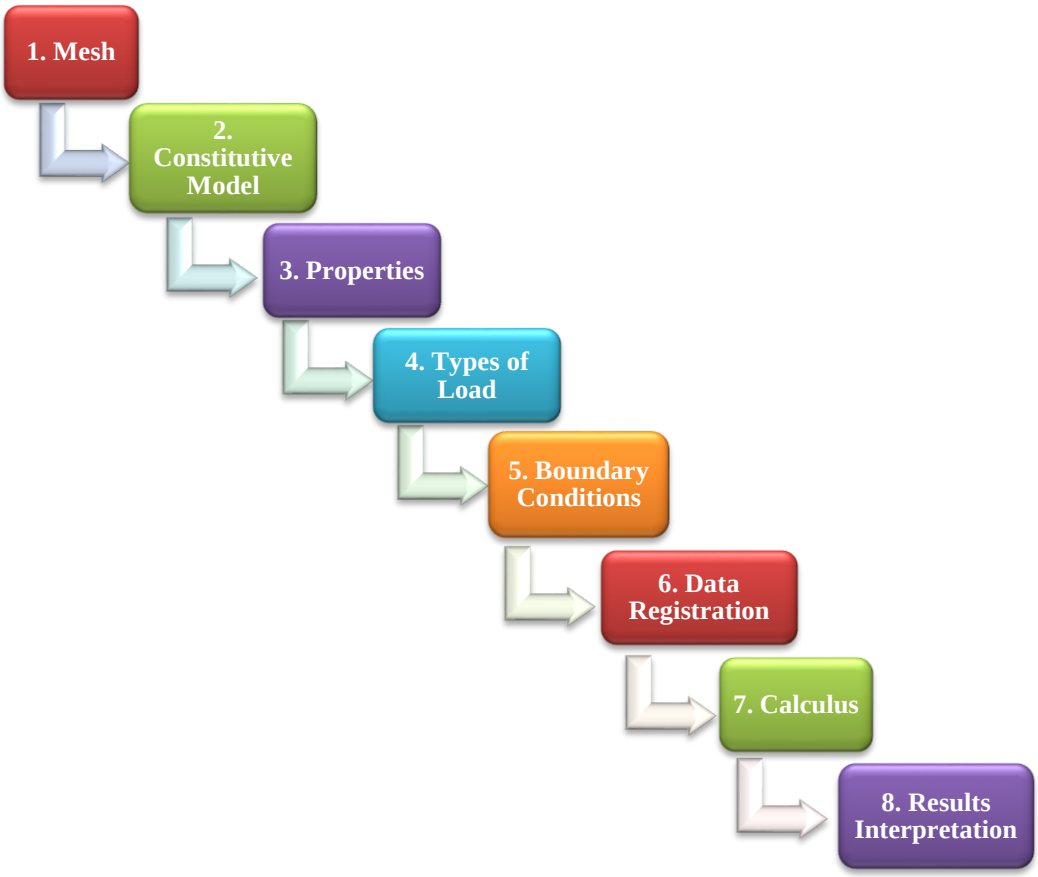

Figure 25 – Major outlines of a numerical model

A correct interpretation of the results does not depend solely in the acquired data, but also in the good sense of judgment of engineers, because though numerical analysis allowed engineers to solve a large array of problems which could not be dealt in any other way, the fact is that there is always a potential for error and misinformation, that can have disastrous consequences. A perfect example is the Nicoll Highway collapse in Singapore, where the temporary retaining wall for the deep excavation work failed, due to its lack of strength to handle the stress, causing the death of four people.

This way, makes perfect sense to use the numerical modelling to complement the previous study of the geomechanical characterization of residual soil from Porto granite in the laboratory by Ferreira (2009), regarding the use of the true triaxial apparatus with bender elements. In other words, there is a need to confirm if the achieved results are correct and if the errors encountered were due to equipment mistakes or material behaviour.

3.2 FINITE ELEMENT METHOD VERSUS FINITE DIFFERENCE METHOD

In most engineering problems, engineers have to deal with the non-linearity of equations and the irregularities of the Earth's behaviour, making almost impossible to find a solution with only analytical resorts. This led to the emergence of approximate methods, such as the finite difference method and the

finite element method, which are now among the most widely used. This type of methods started to develop more when the amazing improvement of computers over the last decades allowed solving complex issues till then with no answer, leading to new formulations and algorithms in order to resolve differential equations. Such solutions stopped relying only on simple differential equations and systems, to rely on algebraic, linear and non-linear equations and systems as well (Sá 2004)

These methods are competitive in some fields, therefore the selection of an appropriate numerical model is a key step to the correct resolution of a certain problem and its consequent application. There is not a perfect solution, since every method has its advantages and disadvantages for particular problems, but the more data acquired the better.

The finite difference method is probably the oldest numerical model and has applications in the achievement of approximate solutions of differential equations and partial derivatives. The approximate solution is obtained on a finite set of points through the domain discretization from an algebraic equations system (finite differences). These system equations are usually obtained by dividing the domain into a uniform grid, approximating the derivatives, initial conditions and boundary conditions in the differential equations through finite differences of values in the wanted function in different points of the grid (Sá 2004). However, there is no shape function, due to the assumption of a linear variation between two points. These approximations are often done in a time-stepping manner, in other words, this method can efficiently regenerate the differential equations at every step. On the other hand, the functions used in the finite element method are attained by local approximations in discrete regions of the previous mentioned domain, named finite elements (includes nodes on the vertexes, sides and in the interior of the domain – Gaussian Points), instead of the application of explicit predefined functions for the whole domain, as used for the previous method. To minimize an error function and procure a more stable solution, the formulation requires an adjustment of these parameters.

The subdivision of the domain into simpler parts in either one of the methods has many advantages, including an accurate representation of complex geometry, as well as an easy representation of the total solution, besides allowing the insertion of heterogeneous material properties and the capture of local effects. But, whereas the finite difference method can be very easy to implement, there are reasons to believe that the quality of the approximation between grid points of a mathematical foundation is poor, comparing to the finite element method, which is sounder. The latter method is the most favored and versatile nowadays, although the former one is more used in fields like fluid mechanics or even in association with the finite element method, regarding the integration on the time variable and large displacements.

The potentiality of both these methods prompted to its globalization and increasingly simplification and generalization, allowing its use not only to their creators and the wealthy but also to the everyday people, leading to a new technological world. Nonetheless, it is important to understand that in order to achieve a correct handling of the programs based on numerical modelling and interpretation of the acquired results, it is necessary that the engineer responsible has the required skills and knowledge (Potts and Zdravkovic 1999).

3.3 PROGRAM *FLAC^{3D}*

3.3.1 BACKGROUND

Nowadays, as mentioned above, numerical analysis are an important part to the achievement of good and more accurate results, depending on how the physical processes are modeled. The numerical code *FLAC^{3D}* (Fast Lagrangian Analysis of Continua) is a three-dimensional finite difference program developed primarily by *Itasca Consulting Group* in 1994, for geotechnical engineering calculations, making it the perfect choice for this study. Particularly, this program is suited to simulate the behaviour of three-dimensional structures of soil, rock or other materials where a continuum analysis is required.

To a better understanding of this program, its main characteristics are as follows:

- Explicit (i.e., uses a time-stepping procedure to solve a problem without forming the stiffness matrix (Neiva 2011)) calculation that provides stable solutions to unstable physical processes and ensures that plastic collapse and flow are modeled accurately;
- Lower processing capacity than the finite element method;
- Models complex behaviours that the finite element method is unable to solve, like unstable systems and large displacements and strains;
- Possesses several constitutive models (Mohr-Coulomb, elastic, plastic, hardening-soil, among others) to different types of materials;
- Provides a correct representation of the geometry of the ground and geological features and large-strain simulation of the continua (such as faults, joints or frictional boundaries);
- Two types of hysteretic damping: Rayleigh damping (used in time-domain programs) and local damping (frequency independent);
- Constitutive elements are represented by semi-regular polyhedron shapes, such as bricks, wedges, tetrahedrons and pyramids;
- Suitable specification of boundary conditions (velocity and displacement or stress and force) and initial conditions (including gravitational loading);
- Possible definition of the water table for effective stress calculations;
- Structural elements that interact with the nearby rock or soil;
- Built-in scripting language, *FISH*, to add user-defined features, that allows the implementation of any constitutive model to be relatively simple;
- Graphical output in a variety of formats;
- Built-in text corrector offers command syntax error checking.

The reason why this program was chosen instead of another three-dimensional geotechnical software, such as *PLAXIS^{3D}* or *PFC^{3D}* (Particle Flow Code) is due to the fact that they operate under the finite element method, and cannot be so thorough regarding the particles geometry and the bender elements modelling, which is a crucial part of this study. For example, *PLAXIS^{3D}* is frequently used to construct and simulate complex soil-structure interaction problems and includes elasto-plastic deformation, advanced soil models, stability analysis, static, consolidation and safety analysis with the option for

global or local mesh refinement for the automatic generation of unstructured of finite element mesh. On the other hand, *PFC*^{3D} was also developed by *Itasca Consulting Group* and is a discontinuum analysis code used in any field where the examination of the dynamic behaviour of a particulate system is required. Besides, *FLAC*^{3D} was the only software freely available.

As can be observed in Figure 26 and having in consideration the simple procedure in Figure 25, after reaching the initial equilibrium state, there is the possibility of changing some properties of the model without affecting the whole project, since the study was made in a time-domain software. Then, the calculation of the resulting response of the model is made, depending on a specific number of steps. The number of steps can be controlled by the user or automatically by the program itself. In the end, it all comes down to the user and his experience, regarding the interpretation of the results.

To perform a simple analysis, the basic commands in order are as shown in the figure.

FLAC^{3D} is robust in the sense that it is especially suited for dynamic calculations in the time-domain, enabling the direct application to the grid points and the consideration in the consecutive calculation cycles, keeping the same computational cost, no matter the alterations made to the properties of the model during calculation. Therefore, this software is capable to simulate everything that varies in time, making it suited for the simulation of bender elements and the dynamic behaviour of the soil, which is exactly the intent of this study.

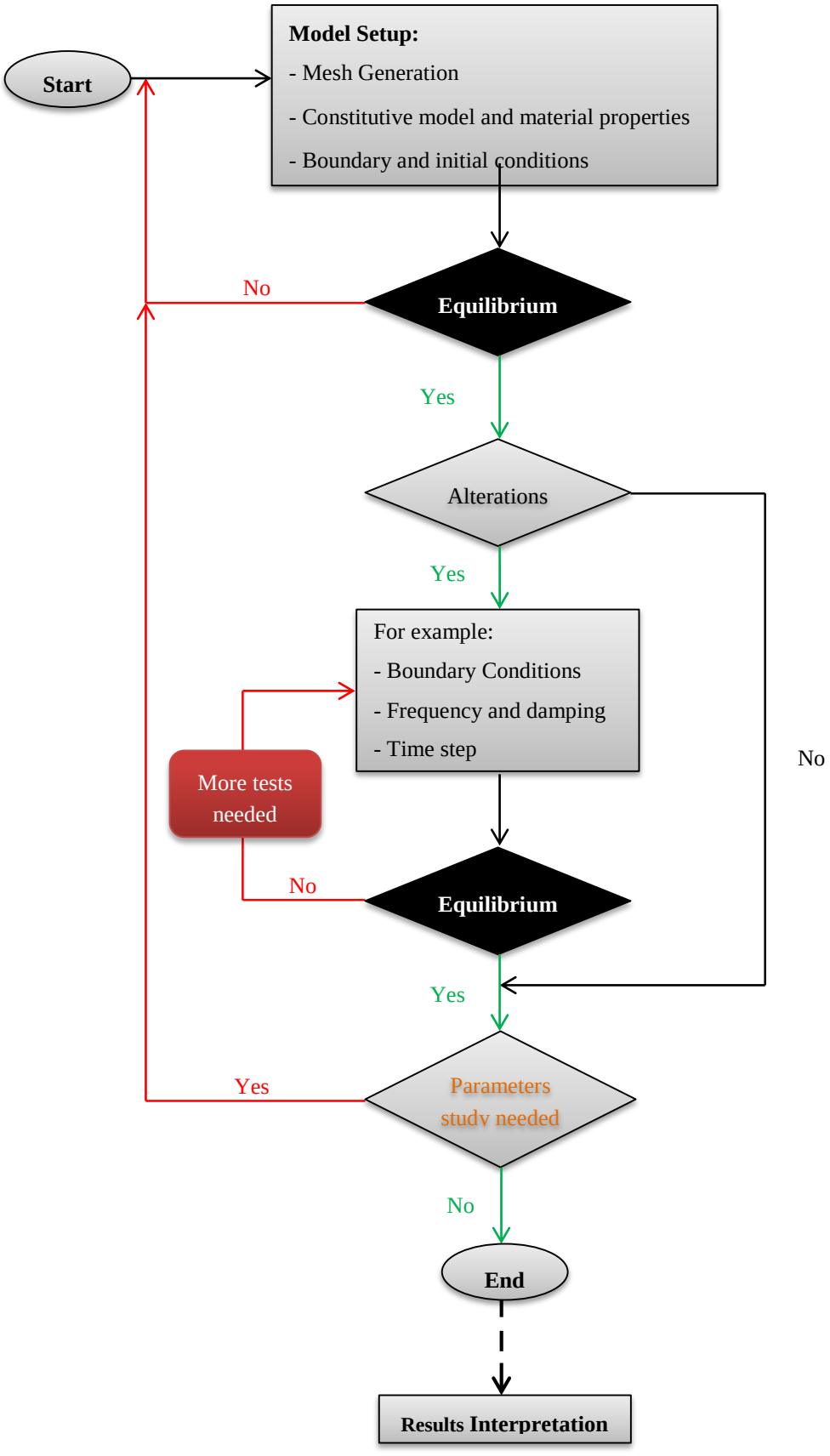

Figure 26 – General solution analysis

3.3.2 OTHER USES OF THE PROGRAM *FLAC^{3D}*

There are many dissertations, dissertation and scientific articles regarding the use of the finite difference and the three-dimensional program *FLAC^{3D}*. Next, it is going to be explained in small detail two of those approaches.

Bearing in mind the dissertation by Eduardo Fortunato (Fortunato 2005), on the topic of renovation of railway platforms and studies related to the ultimate bearing load, it can be considered:

Objectives: The development of a method to approach the renovation of railway platforms in operation, namely in relation to the evaluation of the bearing capacity and reinforcement techniques. The intention is to establish the most suitable procedures to the old and renewed railways substructure description, through tests conducted in situ, in the laboratory and its authentication by numerical modelling.

In situ and Laboratory Tests: Triaxial test with a cylindrical specimen, plate load test (PLT) and stress cell load tests.

Numerical analysis: In the inferior boundary, vertical displacements were prevented and along the vertical boundary, the horizontal displacements were prevented, in order to respect the symmetry of the model. To corroborate the obtained results in the laboratory, a series of models were implemented, such as the Mohr-Coulomb failure criteria, the anisotropy Boyce model to describe the behaviour of granular layers and an elastic model to characterize the foundation soil, having in consideration that the Young's modulus varies linearly in depth.

Results interpretation regarding the use of the numerical analysis: Considering the observed values of the granular layers obtained from plate load tests, it was possible to procure approximate values of both stress from inside the layers and surface deflection through the use of a numerical model, making it possible to represent the results of the tests executed on the physical model. So, in general, the results attained from *FLAC^{3D}* were fairly approximated in comparison with the ones observed. Furthermore, it permitted the stress and strain response assessment of the granular layers and the soil foundation, when subjected to the external loads enforced by trains and to the influence of climate conditions.

On the other hand, the dissertation by João Rio (Rio 2006), regarding the use of bender elements in order to evaluate the advances in laboratory geophysics considers:

Objectives: The development of a study through laboratory and numerical tests, concerning the influence of the dynamic behaviour of an ordinary bender element test system, considering a sample and the geometry of the piezoelectric transducer tests.

Laboratory tests: Triaxial tests.

Numerical analysis: Since an exact solution for this dynamic problem cannot be achieved, this kind of analysis is necessary for a better understanding of all things regarding the use of bender elements. For this reason, two parametric studies were made using simply sinusoidal pulse signals, with the only difference being the sample geometry, namely its diameter, and the use of a load instead of a force displacement in the second parametric study, by means of embedded transmitting bender elements, to assess the influence of the sample on the wave propagation phenomenon. The boundary conditions considered in both models were similar, being fixed in the horizontal direction along the vertical face of the cylindrical symmetry, except the bottom end face, which was fixed in the vertical direction but free

to move in the other one. The top end surface was absorbent in order to avoid any wave reflection back into the system, therefore not allowing any more behaviour complexity.

In short, there were considered a number of samples, each one with some degree of difference regarding the boundary conditions and geometry of the sample.

Monitoring study: It was used a velocimeter, capable of recording the motion of the subject, without any interference. This way, the dynamic responses can be achieved and the obtained mechanical properties confirmed.

Results interpretation regarding the use of the numerical analysis: Considering the obtained results it is possible to conclude that a numerical model can monitor the response of any node of the sample and not only on a single receiving point. It can also be ascertained a clear influence of the sample geometry in the results of the generated wave propagation from bender elements. There is an obvious distinction between exclusively propagated and reflected waves, the latter ones dominating the response at the receiving end. Basically, there can be accomplished a complete control over the properties of the system, when a numerical simulation is taken into account, the only drawback being the need for better calibrations between actual and numerical studies.

4
PARAMETRIC AND SENSITIVITY STUDIES

4.1 INTRODUCTION

The objective of this study is to understand the dynamic behaviour of a residual soil in a true triaxial apparatus embedded with vertical and horizontal bender elements with a numerical model. This is a continuation of a previous study made by Ferreira (2009), regarding the geomechanical characterization of residual soils from Porto granite with various combinations of the three main variables of the stress tensor. The present work aims to further understand and attempts to validate the results of the stiffness parameters derived from the measurement of seismic waves, considering a vast array of aspects, such as inherent and induced anisotropy, degree of saturation and natural structure. For this purpose, it is important to note that the geometry of the equipment along with the boundary conditions used in the tests, in this case, a true triaxial cubical apparatus, are very relevant and can significantly influence the results.

4.2 PREVIOUS LABORATORY TESTING

In order to achieve good results in the software code it is necessary to have a good control and the ability to interpret the results correctly, especially concerning the parallelism with previous laboratory tests. Considering the laboratory testing made by Ferreira (2009), the equipment used was a true triaxial apparatus embedded with bender elements. As already stated (section 2.3.2.5), a true triaxial apparatus can possess several types of boundaries, namely rigid, flexible and mixed boundaries. This device is particularly interesting since its design enables the variation of the principal stresses and its simplicity and uniformity of imposed deformations or stresses allows controlled gradual rotations of the principal axes of stress and strain. Besides, it provides the possibility for the measurement of seismic wave velocities, through the bender elements, not only in the principal orthogonal directions but also in the inclined ones, leading to redundant, but necessary and relevant results nonetheless, given the subjectivity and uncertainty of these measurements.

The true triaxial apparatus considered was a result of the cooperation between the Faculty of Engineering of the University of Porto (FEUP) and the University of Western Australia. The device consists of six square platens assembled in a cubical frame of 250 mm internal side length and made by anodized aluminum, conferring better durability characteristics (Figure 27). In each platen are embedded bender elements and adjacently are made two holes, equipped with porous stones, for pore pressure application and control. The bender elements are in this case, T-shaped (Figure 27c) in order to enable seismic wave measurements in two directions with a single transducer. Although there have been many designs and

calibrations along the years, the model presented by Dyvik and Madshus (1985) is still the basis of the current design of each individual bender element. The choice of this particular shape is associated with the possibility of propagation of the waves in two orthogonal directions, both horizontal (X and Y), and vertical (Z), as well as in the inclined directions, which is beneficial in terms of operation. In other words, with these bender elements it is possible to optimise the wave measurements with the minimal number of transducers.

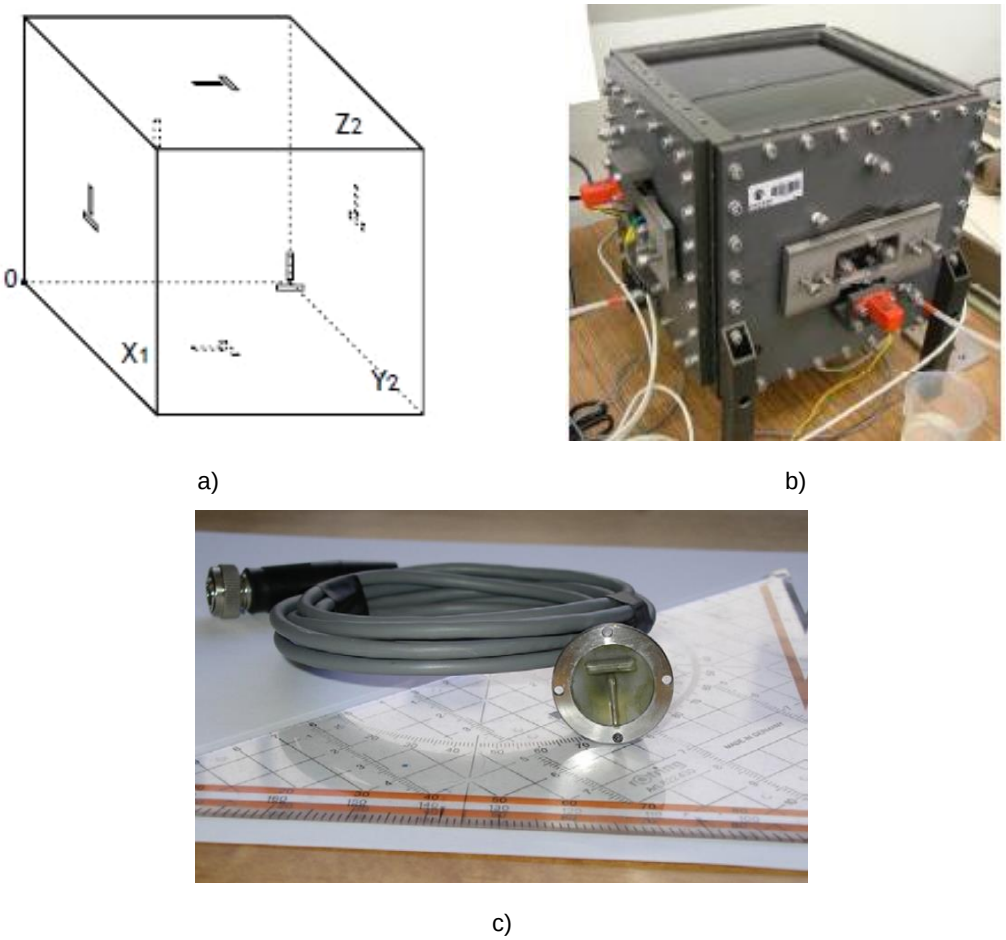

a) b)

c)

Figure 27 – True triaxial apparatus: a) Nomenclature for the platens and shape of the bender elements (Ferreira, 2009); b) FEUP true triaxial apparatus; c) T-shaped pair of bender elements

From the available database of laboratory true triaxial tests results, the preliminary selection of tests considered simple stress-paths, allowing the anticipation of the behaviour and the quick interpretation of the differences between tests, since these could only be attributed to soil conditions, state and stress field parameters. From those tests, the final selection focused on tests with an isotropic or anisotropic (biaxial) loading on reconstituted residual soil samples from Porto granite, with consideration of the inherent and induced anisotropy.

4.3 DESCRIPTION OF THE MODEL SIMULATION PROGRAM

4.3.1 MESH GENERATION

The characteristics of the mesh, namely the number of elements and their distribution, is usually trusted to the judgement of the engineer, considering that its choice will have a major influence on the accuracy of the results (Hardy *et al.* 2002). Since this study regards the numerical modelling of a true triaxial apparatus, the desired shape of the mesh is a cube. In the program *FLAC*^{3D}, the corresponding primitive mesh shape is a brick, as can be observed in Figure 28.

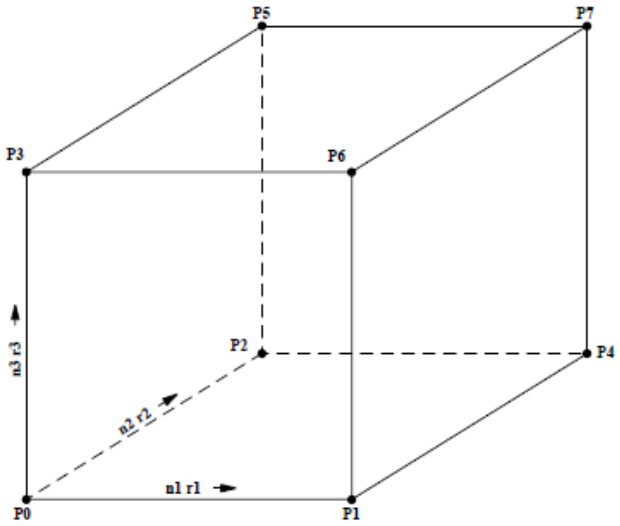

Figure 28 – Brick shaped mesh (Itasca 2002a)

On the other hand, since the true triaxial apparatus is embedded with bender elements, its insertion in the brick is fundamental. Therefore, another shaped mesh is necessary, namely a radbrick, so that the different and stiffer properties of the bender elements are considered, as can be observed in Figure 29. The soil and the bender elements are thereby modelled as two different media.

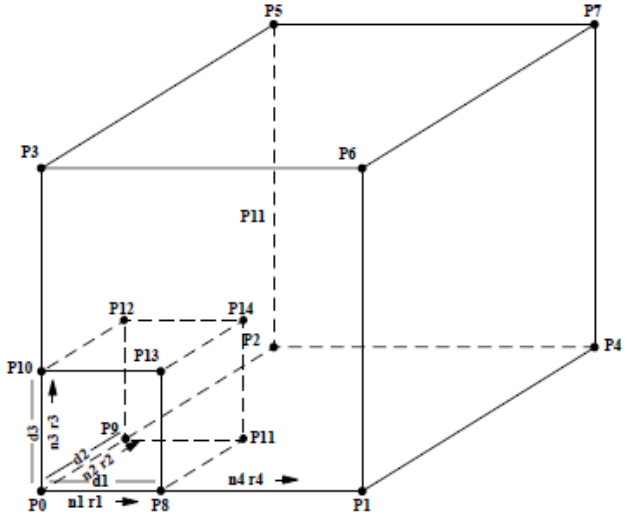

Figure 29 – Radially graded mesh around brick (Itasca 2002a)

However, in order to obtain this desired mesh combination, a series of experiments had to be made. The experiment first made regarded a brick of 10x10x10 m, in other words, the mesh was divided in 10 smaller bricks in the three main directions, x, y and z. Yet, it was not discretized enough, leading to less accurate results. With this information in mind and the usual position of the bender elements in the true triaxial apparatus, which is in the middle of each platen, the decision was to use the combination of the two shapes presented in Figure 29. Since it was not feasible to create T-shaped bender elements in each of the 6 faces of the model (as in the apparatus), it was decided to consider separate vertical and horizontal bender elements in different vertical faces, which would lead to nearly identical results for a much simpler mesh. This hypothesis will also be investigated.

The dimensions used for the brick were 0.15x0.15x0.15 m with five smaller sized square dimensions or zones of the bender elements as illustrated in Figure 30. The number of zones should be carefully selected, since a balance is needed among the accuracy of the model and the calculation time. Nevertheless, when constructing the radbrick, a geometric ratio must be in order, given that a finer mesh with a gradual change in size, from the smallest to the largest, can lead to significantly improved results.

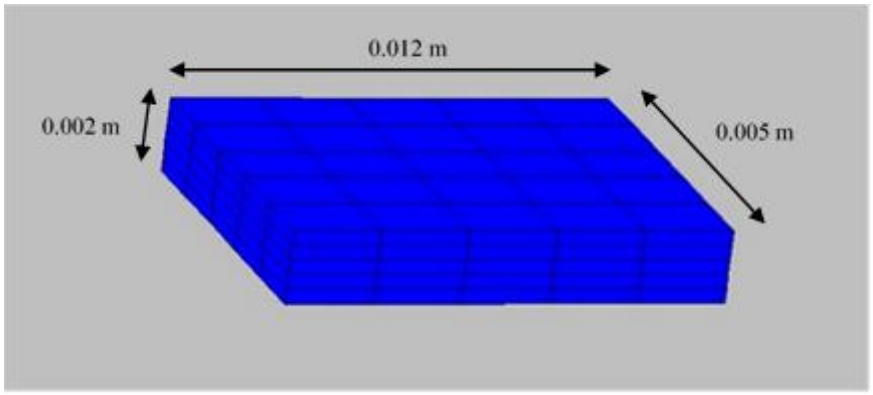

Figure 30 – Dimensions of the bender elements

This was the first step taken since it was not possible to input the coordinates all at once. Yet, it was necessary to “cut” the brick and the radbrick, attaining exactly the mesh in Figure 31.

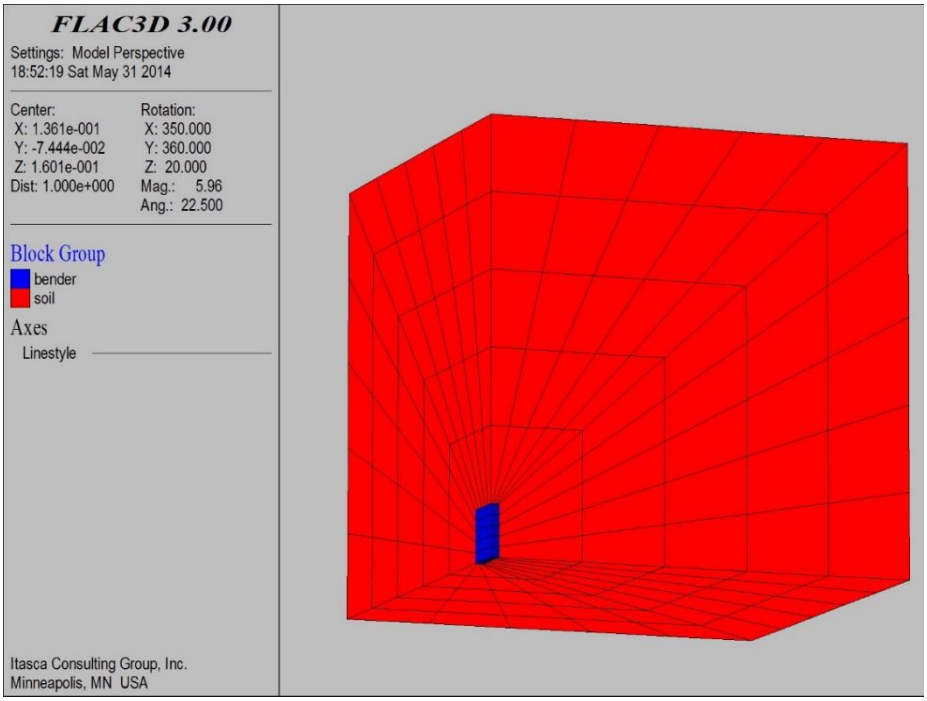

Figure 31 – Brick and radbrick mesh, representing the soil and a vertical bender element, respectively

Then, through simple brick shapes, the rest of the upper half of the cube was made (Figure 32).

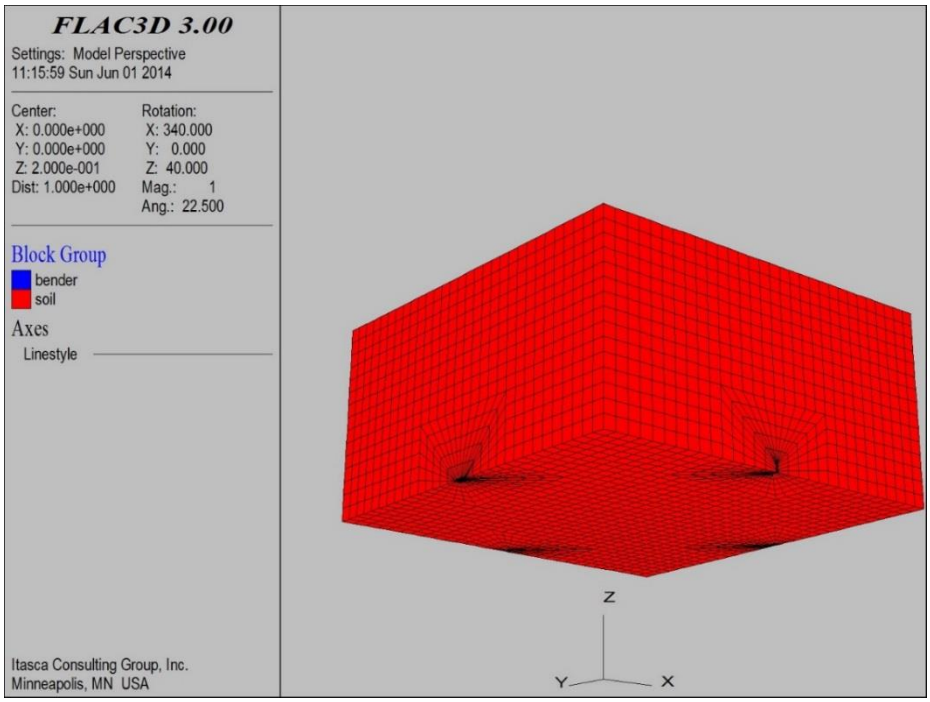

Figure 32 – Upper half of the true triaxial apparatus, with both vertical and horizontal bender elements

The final mesh was thereby achieved by a series of reflections of the planes YZ and XZ, resulting in Figure 33.

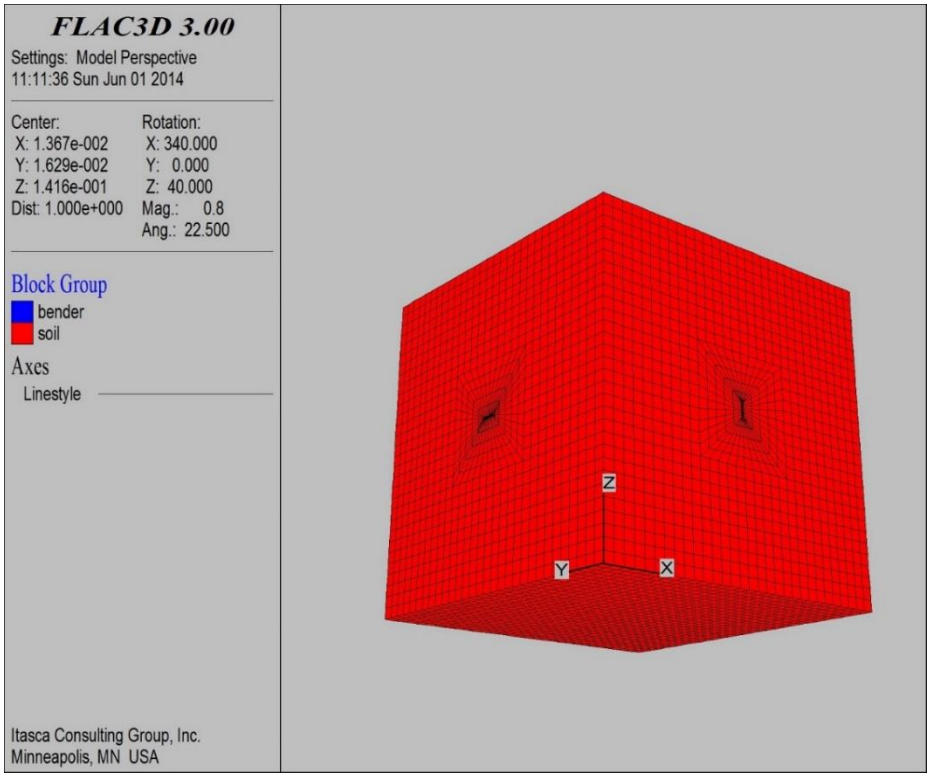

Figure 33 – Full representation of the true triaxial apparatus with embedded bender elements

4.3.2 CONSTITUTIVE MODELS AND PROPERTIES

The geomaterials to be analysed in this study is a residual soil from Porto granite. First of all, residual soils are formed when the physical, chemical and biological processes, associated to weathering, develop faster than the processes of erosion and transport, resulting in the formation of a soil in the same place of origin. The physical weathering is most common in dry and moderate climates and is responsible for the degradation of the parent rock, exposing its surface to potential chemical attacks, while chemical weathering is most common in sub-tropical and tropical climates, since there is a direct relationship with humidity and temperature, and they are responsible for oxidation, dehydration, decomposition, among others. Biological weathering is a combination of both physical and chemical weathering. Its characteristics include heterogeneous masses, as weathering varies with depth; presence of bonding bridges between particles; limited knowledge of the stiffness behaviour and rest stress state and difficulty in attaining undisturbed samples for quality laboratory testing (Viana da Fonseca 1996). Residual soils from Porto granite are leucocratic, alkaline rocks, with two micas and medium-to-coarse grains (Viana da Fonseca 2006). These soils possess very complex characteristics, which are a consequence of the variability and heterogeneity of the parent rock, and of course the distribution and spatial arrangement of the particles and pore spaces. Furthermore, these residual soils are characterized by several weathering processes and parameters such as localization, hydrology, topography, localization, climate, degree of vegetation, among others (Viana da Fonseca 2003). Therefore, the complex behaviour of these residual soils provides the perfect opportunity for research using advanced laboratory and numerical tools.

Once the mesh is generated and the properties decided, it is time to associate them to a constitutive model. Unfortunately, there is not a single and unique constitutive model capable of characterising all the aspects of the real behaviour of a soil. For that reason, it is necessary to make decisions concerning

the wanted features for a specific problem and choose the most suitable constitutive model (Potts and Zdravkovic 1999). For this purpose, a series of constitutive models can be considered, such as: linear elastic, non-linear elastic, anisotropic, cross-anisotropic, Mohr-Coulomb, elasto-plastic, Hoek-Brown, Drucker-Prager, among others.

One of the models chosen for this study was the linear elastic model, given that in dynamic conditions, which is the case of this study, the soil has an elastic behaviour (see section 2.2.2), besides providing a straightforward and approximately accurate response of the model, considering the early stages of this new research. The elastic model can be characterized by its linear stress-strain behaviour with no hysteresis on unloading, leading to a coincidence of the directions of the main incremental stress and strain. Linear elasticity is, contrary to the non-linear elasticity model, the most widely used model in solids and structures. Thomas Young devised a formula which relates stress, strain and elasticity in a simple but most effective way:

$$\sigma = E \times \varepsilon \tag{4.1}$$

This equation was first formulated after Hooke compared this model to a linear spring where deformations could gradually and proportionally increase with the applied forces. In this model, the materials are considered continuous and homogeneous, and its application only extends to stress states that do not produce yielding, not depending on the point of departure for most parameters. This model is thereby characterized by an isotropic behaviour. This description, along with the existence of only two material constants, E, μ, K or G, distances itself from the non-linear elastic constitutive model, simply because in the latter, the elastic parameters (five in this case) vary whether with stress and/or strain level. The non-linear models, can assume an isotropic or anisotropic behaviour and are unable to reproduce the tendency to change volume when sheared (Potts and Zdravkovic 1999). Besides, they strongly depend on the setting of the constitutive formulation, along with its undergoing of large deformations and disability of accurately reproduce failure mechanisms.

Since there is a representation of the true triaxial apparatus, which is ultimately considered a soil sample and the fact that the bender element is far stiffer than the soil, given its constitution (see section 2.3.2.1), both the soil sample and the bender elements will be modelled as two different media, as previously stated. To guarantee the significant stiffness of the bender element, its elastic properties were considered approximately ten times higher than those of the soil (Table 3). The properties of the bender elements were experimentally determined by Rio (2006) and although these values are associated to specific dimensions and materials of a particular bender element, which may be different from the ones in this study, they will not affect significantly the performance of the model.

Table 3 – Elastic properties of the residual soil from Porto granite and the bender elements

Soil	Bender Element
Shear modulus (G)=80.00 MPa	Shear Modulus (G)=1000 MPa
Poisson's ratio (v)=0.10	Poisson's ratio (v)=0.25
Young's modulus (E)=176.00 MPa	Young's modulus (E)=2500 MPa
Bulk modulus (K)=73.33 MPa	Bulk modulus (K)=1700 MPa
Density (ρ)=2000 kg/m^3	Density (ρ)=3000 kg/m^3

The elastic constants were achieved after knowing the shear modulus, *G*, parameter dependent of the stress components, namely the consolidation stress (*p'*), which provides a more accurate estimate of the evolution of stiffness with time. Therefore, the value of 80 MPa for this particular soil was attained, having in consideration a reference value of the consolidation isotropic stress of 100 kPa. Poisson's ratio, *v*, comprehending the ratio between lateral and axial strains, is also known, with most materials within the following range limits:

$$0 \leq \nu \leq 0.5 \tag{4.2}$$

As observed in Table 3, the value considered for Poisson's ratio regarding the soil was 0.10. This is an artificial low value, yet apparently is the most appropriate for this kind of dynamic modelling, despite the fact that the usual value adopted by many authors to characterize residual soils (Viana da Fonseca 1996), which are the ones of the soil sample, is 0.30. This conclusion will be explained in more detail in section 4.4.5. However, the chosen value would not be appropriate for studies where the strain rate is several degrees of magnitude higher.

On the other hand, Young's modulus, *E*, is a stiffness measurement considering an elastic and isotropic material and is given by:

$$E = 2 \times G(1+\nu) \tag{4.3}$$

Furthermore, the bulk modulus, *K*, can be technically defined as the ratio of hydrostatic pressure in relation to the relative volume change. A positive bulk modulus will thereby lead to a positive volume change. This constant was achieved from the following expression:

$$K = \frac{\sigma}{\frac{\Delta V}{V}} = \frac{\sigma}{\varepsilon_{XX} + \varepsilon_{yy} + \varepsilon_{zz}} = \frac{E}{3(1-2\times\nu)} \tag{4 4}$$

Furthermore, the choice of the model regarding the bender elements was the same, in order to recreate a proper response of its behaviour. In other words, the bender elements induce strains in the very small region (see section 2.2.1), which is adequately characterized by a linear elastic model.

The other model relevant to this study, but only as far as the soil is concerned, was the transversely isotropic or cross-anisotropic model. Anisotropy is a property that exists practically all around us. Whether in computer graphics, physics and cosmology, chemistry, medical ultrasound imaging or most importantly in geology and engineering, anisotropy is a significant parameter which varies with direction, providing information about the physical and mechanical properties of a material or soil. There can be distinguished two components of soil anisotropy, first suggested by Casagrande and Carillo (1944), namely inherent and induced anisotropy (see section 2.2.2), which may occur in most field

situations. In short, inherent anisotropy is related to the preferential orientation taken by the particles, caused by the arrangement of soil fabric and associated to over-consolidated soils, aged, structured or compacted soils, whereas induced anisotropy is associated to more recent soils and can be characterized by a random disposition of the particles, due to the stress states to which the soil has been subjected to. In other words, if on one hand, inherent anisotropy is completely independent of stresses and strains and can be defined as a physical characteristic inherent to the material, induced anisotropy is caused by a strain clearly dependent of the stresses and strains applied (Casagrande and Carillo 1944). Nevertheless, anisotropy is closely related to stiffness, given the dependency of the latter with effective stress. This dependency leads to an increase of stiffness with stress and to an expectancy of stress anisotropy due to frictional resistance. Moreover, under isotropic loading, soils can exhibit small-strain stiffness that vary with direction (Stokoe and Santamarina 2000).

Regarding laboratory testing, the use of seismic wave velocities enables the observation of several degrees of anisotropy. The direct measurement, whether propagated (wave direction) or polarised (particle movement direction, see Figure 49) in different directions allows the identification of distinct values of stiffness from which the level of anisotropy can be determined. However, even though the strength and deformation characteristics of residual soils are dependent of the shearing loading direction, due to anisotropy, these direct shear wave measurements are only preliminary, given the limited amount of samples that were carried out (Ferreira 2009).

The assessment of anisotropy, namely the inherent anisotropy was also carried out in *FLAC*^{3D}, by a series of experiments, considering the cross-anisotropic or transversely isotropic properties of the residual soil presented in Table 4. These properties are based in the elastic properties in Table 3, the only differences being the Young's modulus normal to the plane of isotropy, E_3, which is about 70% of the value of the Young's modulus in the plane of isotropy and Poisson's ratio in these different directions too, although they were both considered equal to the one in the previous table. For a better understanding of the influence of these results, observe section 4.4.7, where the parametric studies of anisotropy in *FLAC*^{3D} are taken into account.

Table 4 – Transversely isotropic elastic properties of the residual soil from Porto granite

Soil Properties	
Young's Modulus (E_1) in the plane of isotropy	176.00 MPa
Young's Modulus (E_3) normal to the plane of isotropy (E_3=0.70xE_1)	123.20 MPa
Shear modulus (G_{13}) for any plane normal to the plane of isotropy	80.00 MPa
Poisson's ratio (v_{12}) charactering lateral contraction in the plane of isotropy when tension is applied in the plane	0.10
Poisson's ratio (v_{13}) charactering lateral contraction in the plane of isotropy when tension is applied normal to the plane	0.10

These values are slightly different from those of the actual soil, given its considerably smaller sample size, not reflecting the exact response of a residual soil. They are useful nonetheless, leading to a series of results, approximate to the real ones.

4.4 SIMULATION STUDIES

In order to comprehend the degree of influence of a number of parameters of the numerical model such as geometry, time step, amplitude, frequency, damping, Poisson's ratio, boundary conditions, anisotropy, a series of parametric and sensitivity studies were made, from which the parameters of the final model would be defined. It was considered the use of a simpler model than the one of Figure 33, namely without the representation of the bender elements, so that the decision of the most appropriate features to compose the model could be made as efficiently as possible. Nevertheless, in this simple model the bender elements are in fact simulated, by the application of a velocity starting in the midpoints of the faces A (horizontal bender element) and B (vertical bender element) and finishing in faces C and D, respectively. Moreover, though one of the objectives of this dissertation was to compare both the time and the frequency domain results, the lack of time did not allow it, except for the parametric study of the input frequency. For that reason, they were all considered to be in the time-domain, since it is the most immediate method and given that this study always considers the identification of the first arrival of the wave.

For an easier interpretation of the results presented next, a cube shaped mesh with indication of the axes directions and the nomenclature of each face of the model, is displayed in Figure 34.

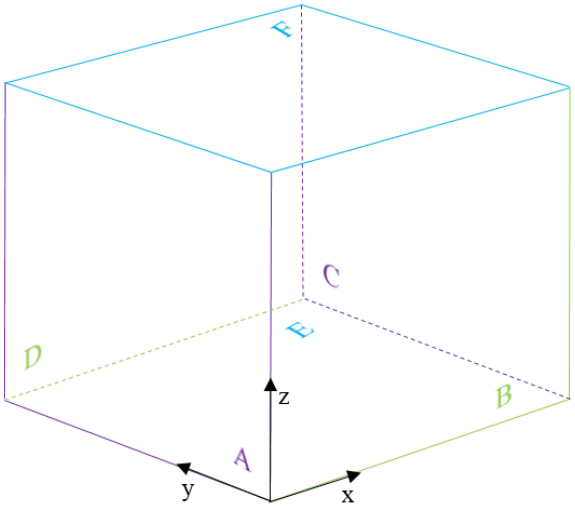

Figure 34 – Simple schematics of the true triaxial apparatus model

4.4.1 FILTER OF THE SIGNAL

For a more accurate sensitivity study and in order to obtain results easier to interpret, a numerical artifice that would not compromise the signal, was introduced. This filter is applied to the original input or output signal, "cleaning" it. Basically, every two wave periods, the average of the points is subtracted by a period before and after that specific point. An example of the high improvement of the visualization of the signal can be observed in Figure 35. As a result of the application of the filter, sinusoidal waves do not tend to infinity as before, but are now tending to zero and therefore, equilibrium. Sometimes, there is a small numerical error, given the manual input of the filter by the user, but it is negligible, since the results are not significantly affected.

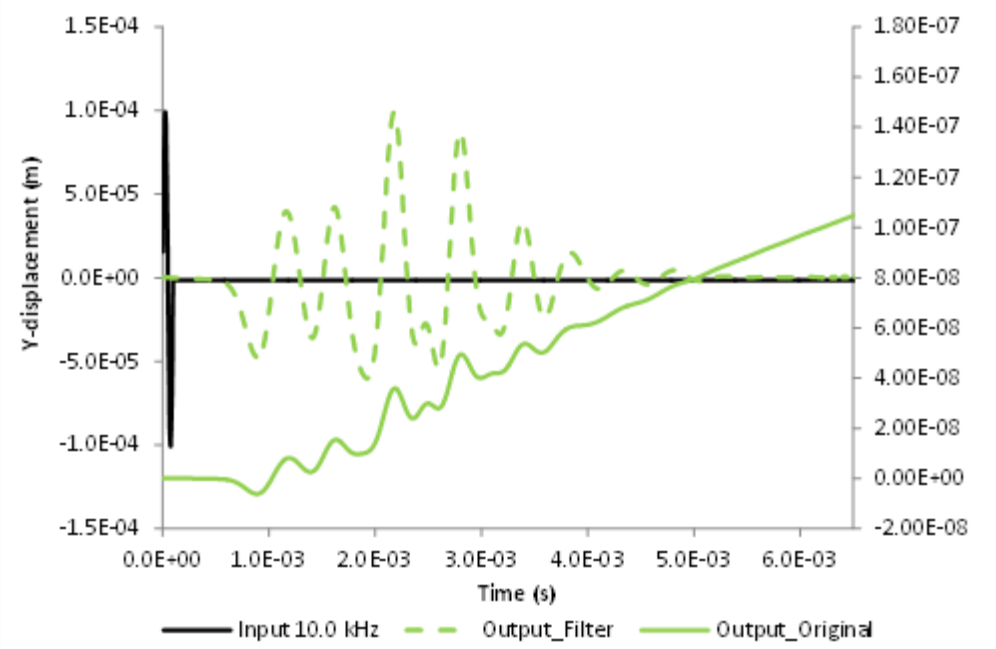

Figure 35 – Example of a sine wave without and with a filter in the output signal

4.4.2 TIME STEP

In reality, all dynamic problems vary with time. When a particular case is time dependent, the inertia effects become significant, since the value of the time period is alike or less than the period of the fundamental frequency. On the contrary, if it is not time dependent, then the time period of its loading event is considerably higher in relation to the time period of the fundamental frequency of the system. In *FLAC*^{3D}, time step adopts an explicit method, where no iterations are needed to find equilibrium between the elements, considering that the time step is small enough to guarantee no variation within it. This way, it is possible for the elements to be evaluated independently, for example, if a change is made inside a single element, namely of the stress value, this would not affect the surrounding elements, nor the calculated displacements, at least until the following step. Furthermore, it can be automatically calculated and there is not a need of manual input. Nevertheless, since information can propagate, depending on the maximum speed characteristic of each material, a series of experiments were made, with different time step values, in order to achieve the appropriate balance between the results obtained and the computer processing capacity (Figure 36). However, when the program is ran, the time steps inputted in the program suffer a change in the degree of magnitude, as can be observed in Table 5.

Table 5 –Comparison between the time step inputted and that of the model

Time Step Inputted	Time Step of the Model
1.0e-4	1.0e-3
1.783e-5 (automatic time step)	1.783e-4
5.0e-6	5.0e-5
2.5e-7 (time step chosen)	2.5e-6

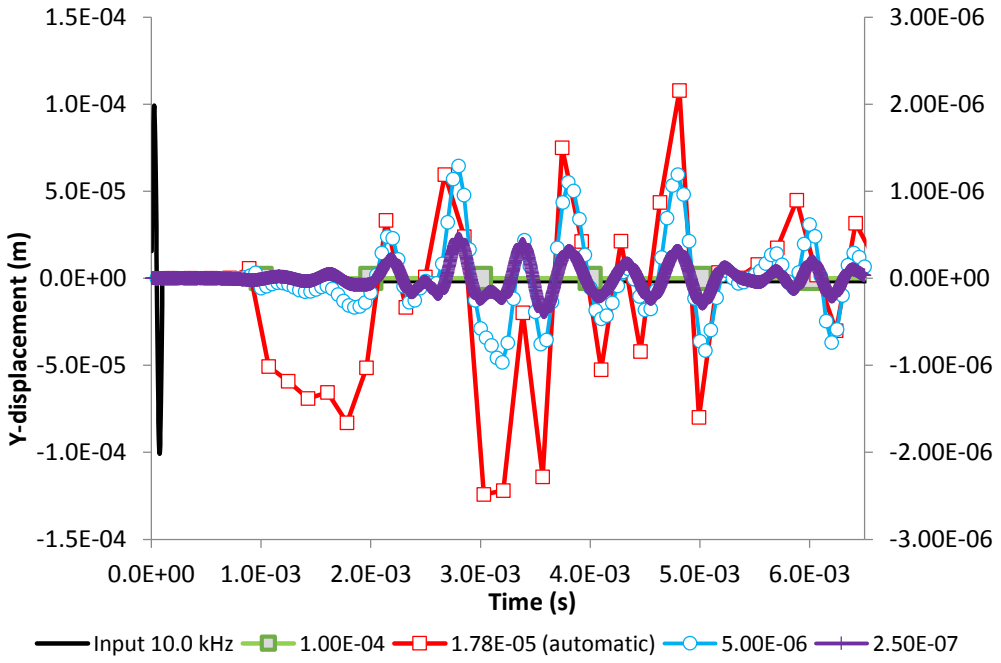

Figure 36 – Time step variation

As stated above, the time step can be automatically calculated by a self-analysis of the program itself, however, the natural time step of 1.783×10^{-5}, is not the most appropriate, given the lack of sufficient data to correctly translate the shape of the output signal. This can be verified by its significant drift in comparison to the higher time steps and the markers in the outputs of the signal, showing the number of points in each one. The value below the automatic time step does not even allow the formation of a clear signal. On the contrary, the values with higher degrees of magnitude provide a more continuous signal and therefore a clearer improvement regarding the quality and number of data of the signal. The value chosen for the model was 2.5×10^{-7}, since there is a perfect balance between the number of data values, quality of the signal and processing capacity of the computer. Besides, it is only from this degree of magnitude that a proper shape of the input signal can be achieved. Studies were made for higher degrees of magnitude, but the processing time was incredibly high and impossible to consider in this dissertation. The secondary axis, in the right side of the graphic was included in order to maintain the real amplitude of the signals for a better visualization of the results.

With this knowledge in mind and as there is not a perfect choice regarding the value of the time step since it varies from model to model, the user should first discover the natural time step and then decide, by trying different value for the time steps, which is the value that better suits each specific model.

4.4.3 AMPLITUDE AND FREQUENCY

Amplitude, *A*, is the measure over a single period of a periodic variable. In other words, it is the magnitude of the difference between extreme values of the oscillation of a certain variable, usually a wave. The amplitude can be translated by the following wave equation:

$$x = A \times \sin(t - K) + b \tag{4.5}$$

Where:

- A represents the amplitude of the wave;
- x represents the oscillating variable;
- t represents time;
- K represents a time arbitrary constant;
- B represents a displacement arbitrary constant.

A parametric study considering local damping, to decide which value would be the best fitted for the problem at hand, was in order.

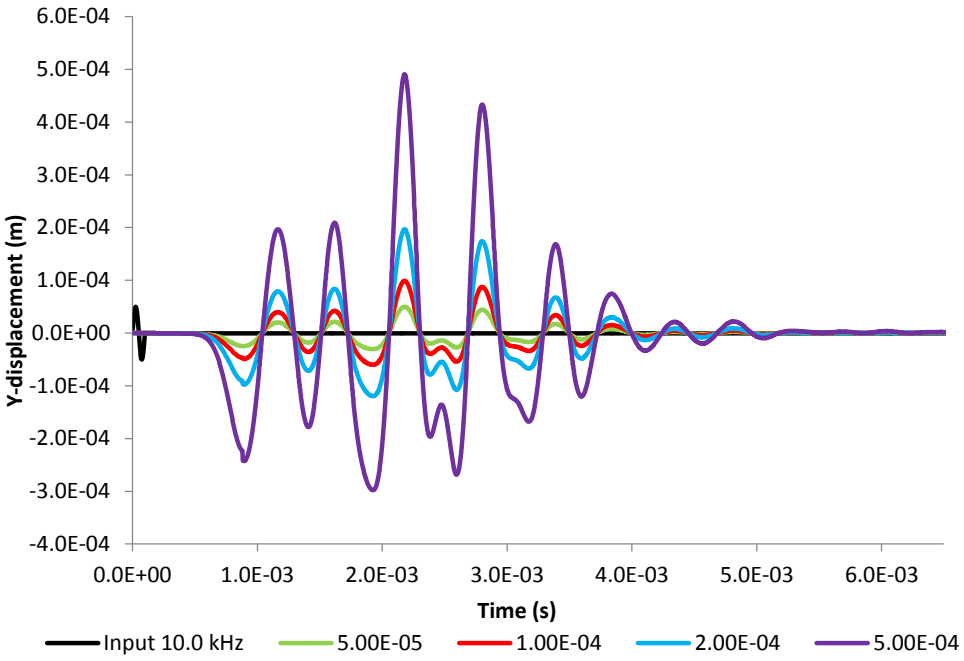

Figure 37 – Linear amplitude variation

These results show an evident linearity between the values of the amplitude of the signal, validating the constitutive model used in this study, namely, the linear elastic.

On the other hand, frequency, *f*, can be defined as the number of cycles per unit time, making this parameter intertwined with the period, *T*, which is the duration of one cycle.

$$T = \frac{1}{f} \tag{4 6}$$

Although this study is in the time domain and not in the frequency domain, the frequency of the system is a relevant parameter to have in consideration.

Regarding the results obtained in *FLAC*^{3D}, the influence of the frequency of the model is significant. First, it was important to understand the behaviour of the model with the variation of the input frequency (Figure 38). Considering local damping, in the frequency that corresponds to 0.4 kHz, it is possible to visualize a discrepancy in the values of the input, leading to a less continuous signal. The output is also characterized by significant discrepancies, as if there were two different signals. In fact, this value corresponds to an induced frequency, being below the natural frequency of the system, given the apparent low velocity of the signal, which leads to a poor representation.

On the other hand, the higher values of frequency show major differences in comparison. The output signal is now independent from the input frequency and both the latter and the output signal are far more fluid and continuous, due to the high velocity of the system, thereby corresponding to the resonant frequency of the system. However, for the value of 8 kHz, it is possible to observe a slight drift on the natural frequency of the system, which most probably corresponds to a numerical error. This drift is confirmed for the frequency of 10.0 kHz, increasing with the frequency. This is due to the undamped free vibration, in other words, the input frequency is higher than the resonant frequency of the system.

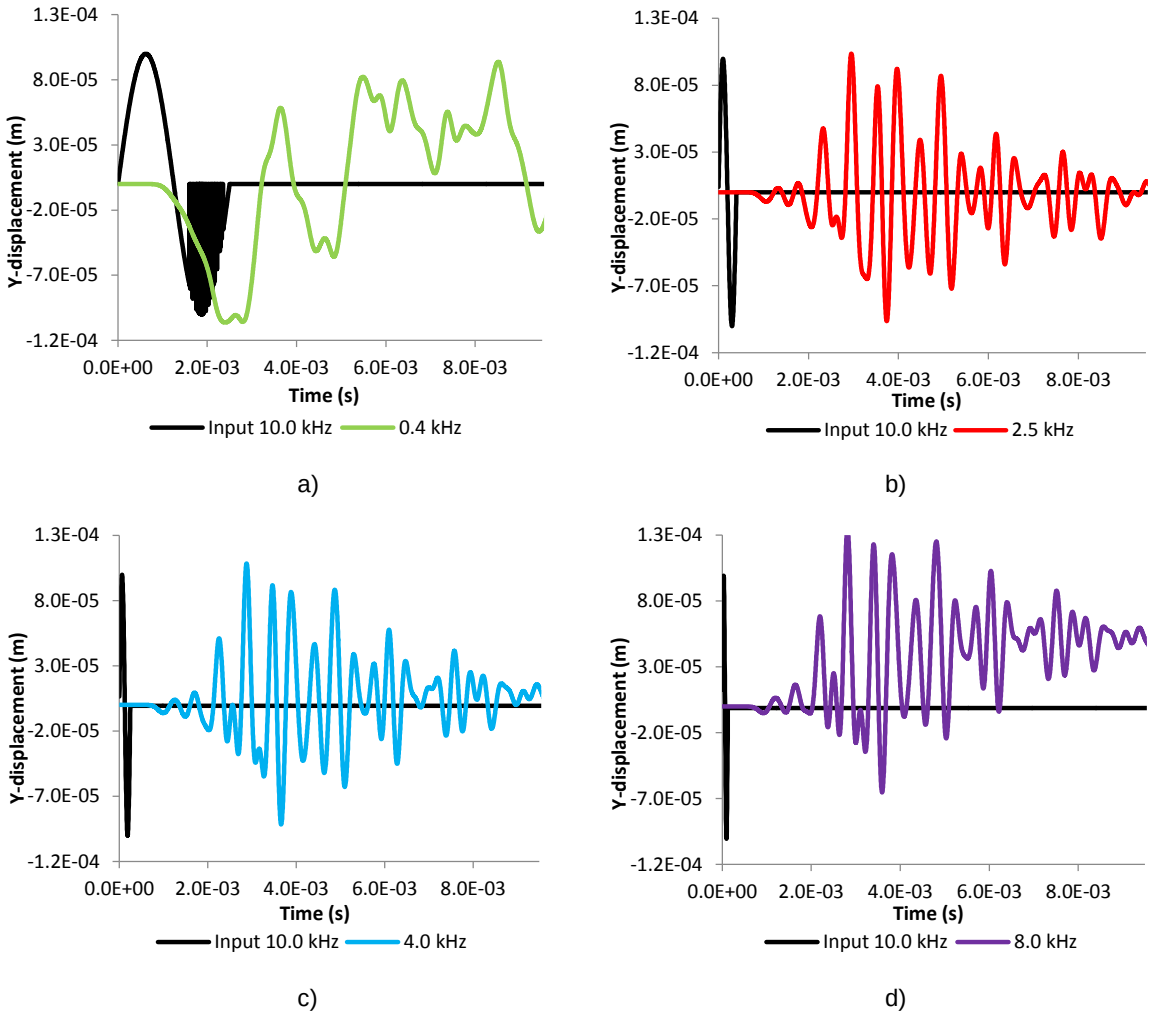

Figure 38 – Variation of input frequency, considering local damping: a) 0.4 kHz; b) 2.5 kHz; c) 4.0 kHz; d) 8.0 kHz

On the topic of frequency variation, considering Rayleigh damping and a constant Poisson's ratio of 0.1, (Figure 39) it is possible to observe an evident change in the input frequency and a similarity of the output signals, excepting the frequency corresponding to 0.5 kHz and the frequencies higher than 5.0 kHz, lower and higher than the resonant frequency of the system, respectively. Truth is, the input frequency does not influence the output, except when the drift starts to appear. Due to this drift, for a better visualization of the results, it was found to be necessary to apply a filter for frequencies equal to or above 10 kHz (section 4.4.1).

These results were obtained considering an input in face A and an output in face C, however, for an output closer to the input location, the results are more likely to be influenced. The results include the first arrival of P and S waves, observed in the same figure. The first arrival of P waves of the model itself and not the theoretical one, can be easily visualized by the plain observation of Figure 39, corresponding to the first inflection of the output signal, contrary to the S wave, which is far more difficult to unravel. The higher the frequency, the more apart are the theoretical values and values of the model, regarding the first arrival of the P waves.

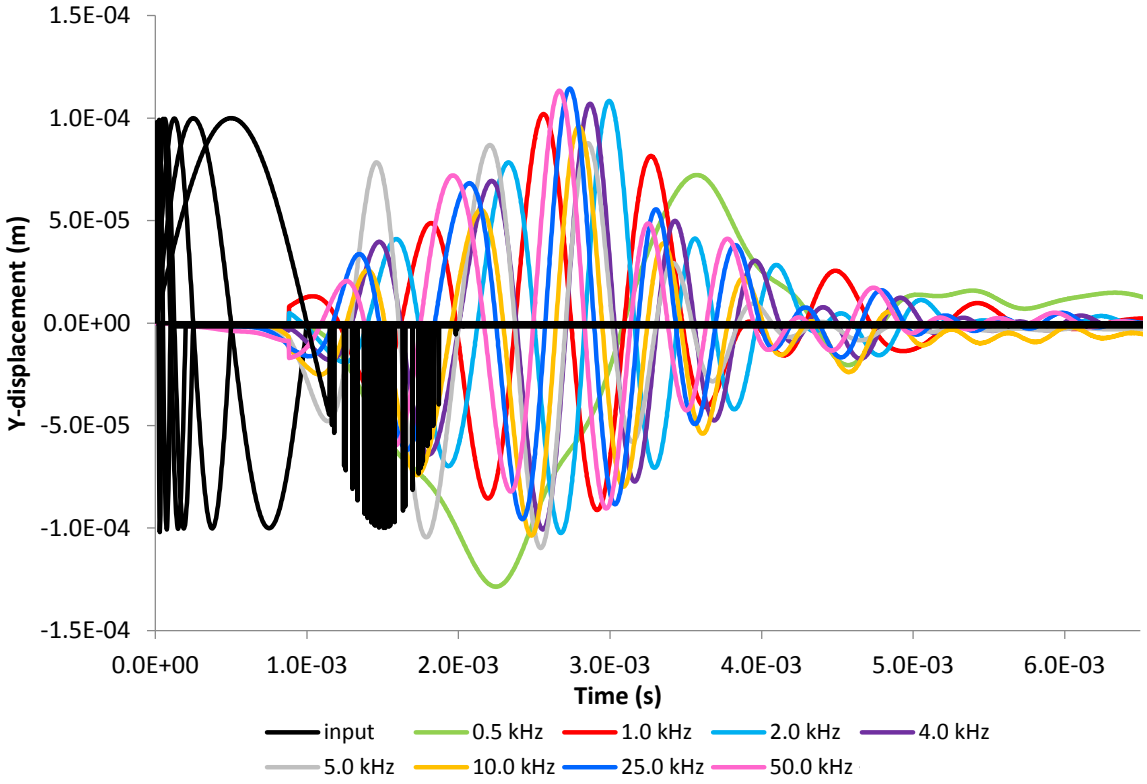

a)

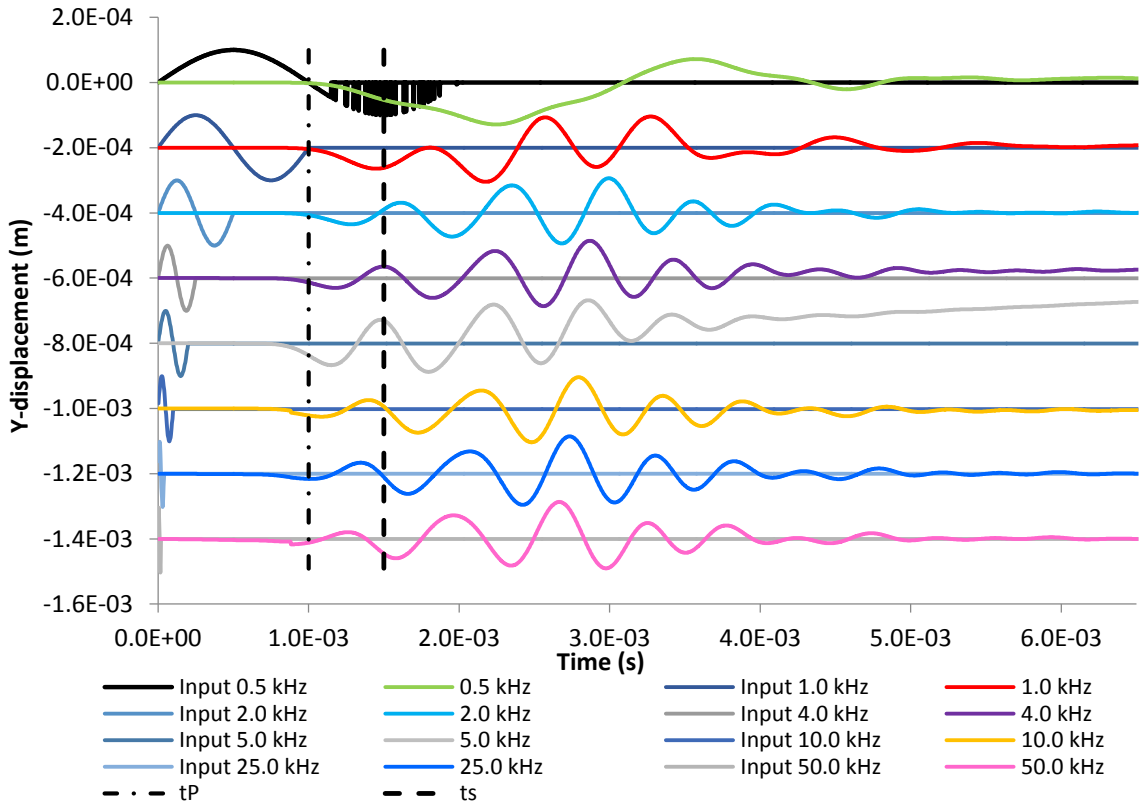

b)

Figure 39 – Variation of frequency, considering Rayleigh damping

In order to validate these results, an analysis was made in the frequency domain regarding the power spectra variation for input frequencies from 0.5 kHz to 50 kHz (Figure 40).

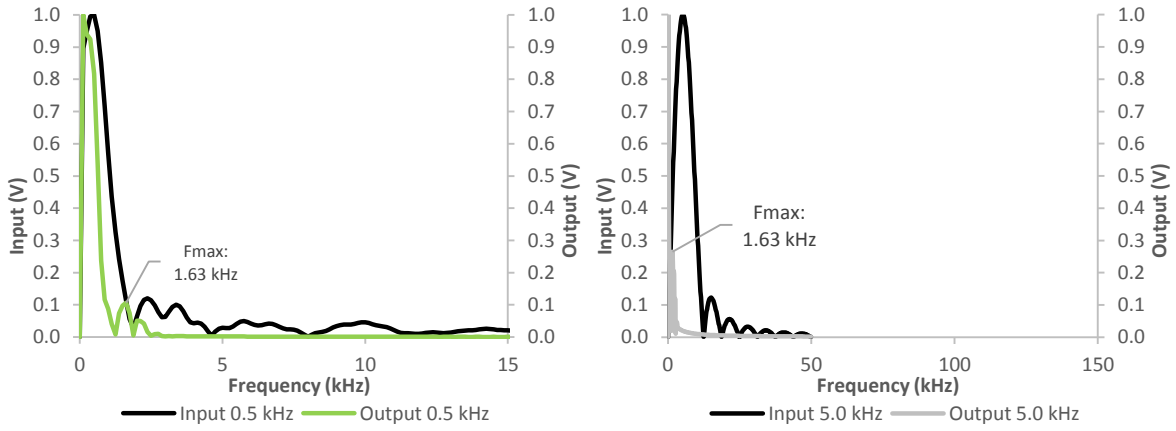

a) d)

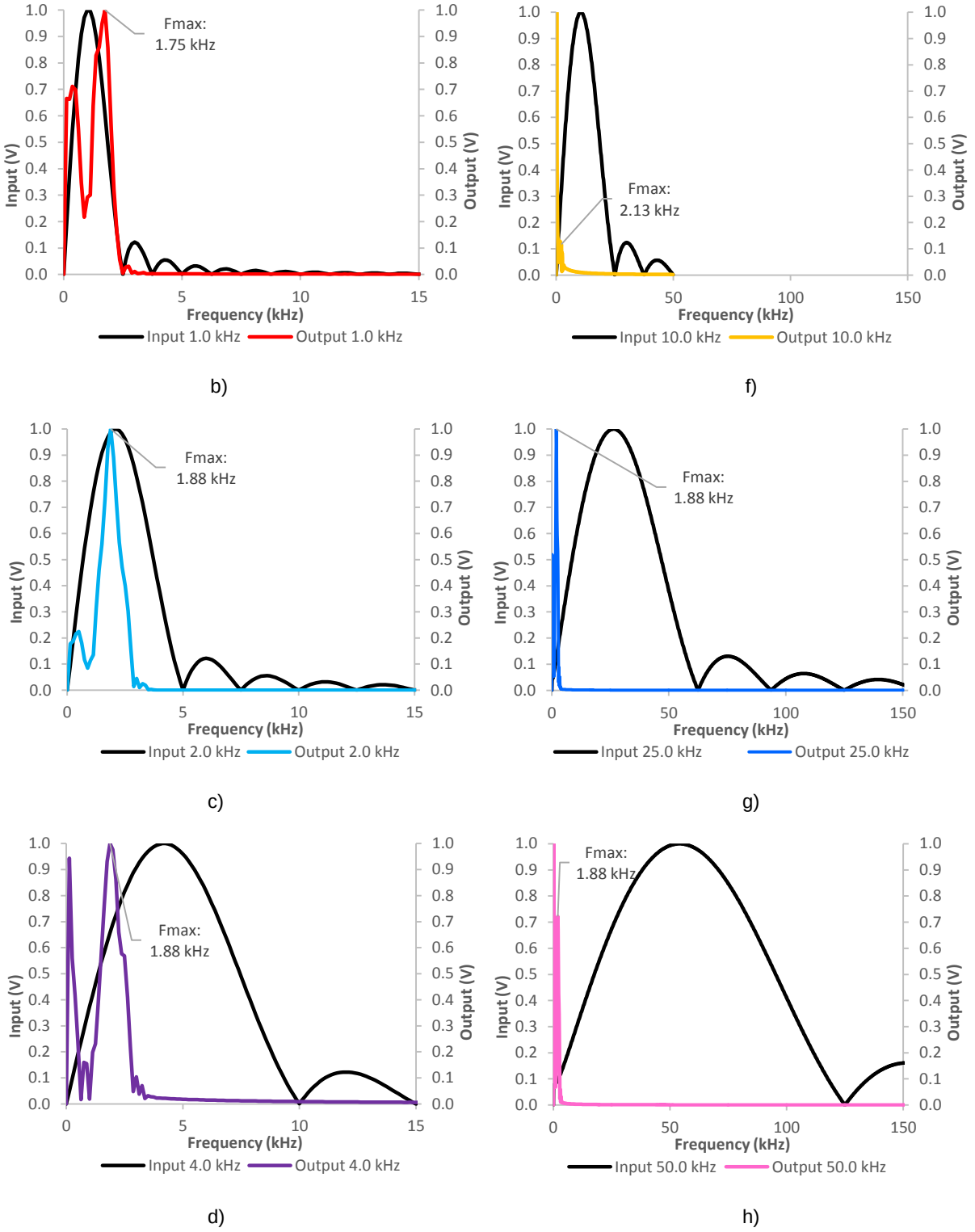

Figure 40 – Frequency spectra for different frequency values, with indication of the central frequency

The graphs in this figure show that, even though a wave is applied with a certain energy and frequency, the soil responds in its own characteristic way, with a dominant natural frequency around 2.0 kHz, as can be seen by the indication of the value of the central frequency below. In other words, the output

signal is not centered with the input frequency. There is a initial high value for all the different frequencies, yet it corresponds to a numerical error. However, this dominant output frequency does not coincide with those of the input in the time domain.

Moreover, since these results correspond to a consolidation stress of 100 kPa, it is up to the user to adjust them, given that the higher the stress, the higher the velocity of the signal and the higher the frequency.

4.4.4 DAMPING

As stated in section 2.1.3, the most common models of damping are the viscous damping, more suitable for analytical problems and the hysteretic damping, which is the one used by *FLAC*^{3D}. The latter can be divided into two forms of damping, namely local and Rayleigh damping. Local damping is frequency dependent for only simpler cases, besides being less expensive and needing less computational processing capacity than Rayleigh damping. Also, its modelling can be done by the addition or removal of mass proportional to both the mass and acceleration of the element in question, hence conserving the total mass of the system, to oscillating elements. On the other hand, Rayleigh damping is frequently used in time-domain programs, and is frequency-independent in a specific range of frequencies, being frequency-dependent outside that range (Wilson and Bathe 1976). However, contrary to the local damping, this kind of damping requires two constants, since it is independently proportional to the stiffness and mass of the system, making its estimate more intuitive (Rio 2006).

Both types of damping were applied in *FLAC*^{3D}, in order to better understand the influence that frequency has in each one.

Considering Figure 41, for the local damping, there is an overlap of the input signals, the only difference being its amplitude. Overall, it is possible to conclude that the higher the fraction of critical damping, the lower the amplitude of the signal and more its approximation to zero and equilibrium. This happens probably because the higher the damping value, the nearer it is to the critical damping coefficient, c_c, which is equal to one. This coefficient represents the reaching of an equilibrium position without the need for the system to oscillate more. Every damping value can eventually reach equilibrium or get nearly there within the time given, except for the damping value of 0.01, which would practically translate to the existence of friction, not allowing for the signal to return to a position of equilibrium, in other words, residual damping. Altogether, all the damping values could be used for this study, however, the value chosen to use in the model was 0.05, given its slow and steady approximation to equilibrium, that is, without large differences between impulses. With this value, it is possible to obtain a high variation of amplitudes and thus more detailed results in the numerical simulations of this type of soil.

On the other hand, Figure 42 represents Rayleigh damping. For this type of damping, two different parameters were needed, namely the fraction of critical damping operating at center frequency and frequency. Considering the same fraction of critical damping, namely 0.05, to different values of frequency from 2.5 kHz to 12.0 kHz, it is possible to verify that the higher the frequency, the lower the amplitude of the overall output wave and the quicker it takes to reach equilibrium.

For example, the output wave of 2.5 kHz has so much energy, that it takes longer to reach equilibrium, despite its low frequency in the beginning. Also, the damping associated to the frequency of 5.0 kHz suffers high amplitude variations, which is not adequate for this performance. Therefore, the most appropriate values would be the ones corresponding to 8.0 kHz or 10.0 kHz, which are the ones closer to the input frequency. Nevertheless, since the input frequency value is 10.0 kHz, it seems only fitting that the chosen value would be the same.

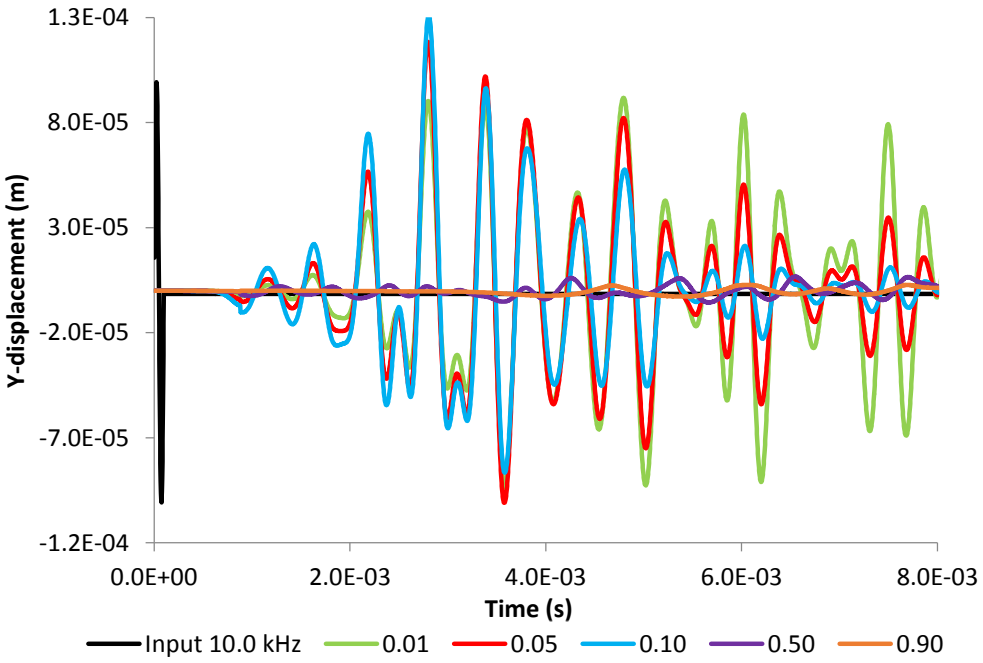

Figure 41 – Local damping, considering several fractions of critical damping

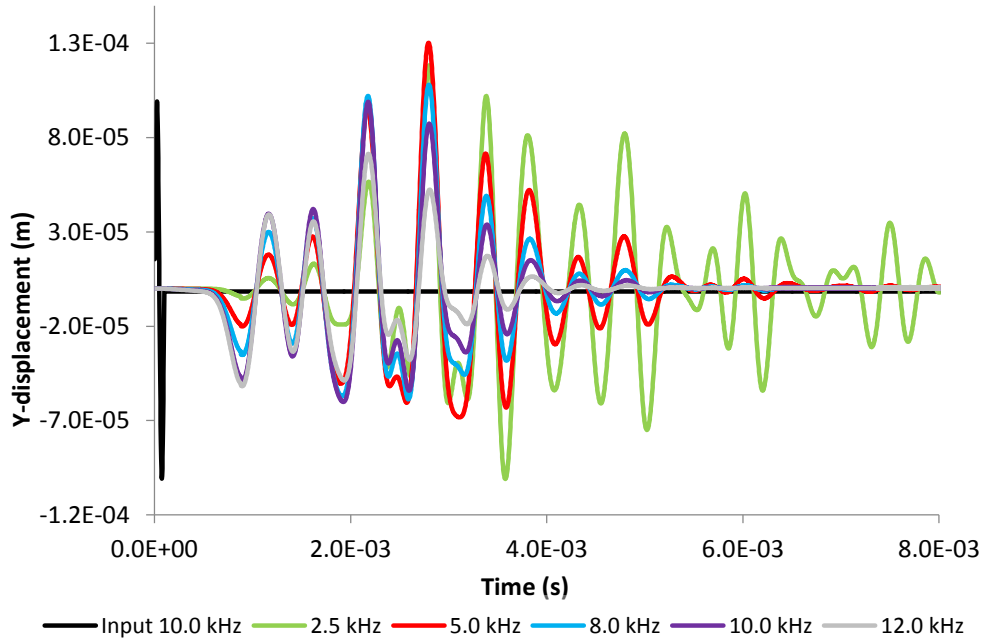

Figure 42 – Rayleigh damping, considering a certain fraction of critical damping, namely 0.05, to several frequency values

Taking these results into account, the only thing missing was to decide which type of damping to use in the consequent studies and in the comparison between numerical and experimental results, to be

presented in Chapter 5. Considering the best results for each type of damping, namely 0.05 for local damping (Figure 43) and 10.0 kHz for Rayleigh damping (Figure 44), the one that was thought best suited was the correspondent to Rayleigh damping, given its similar response to what happens in reality.

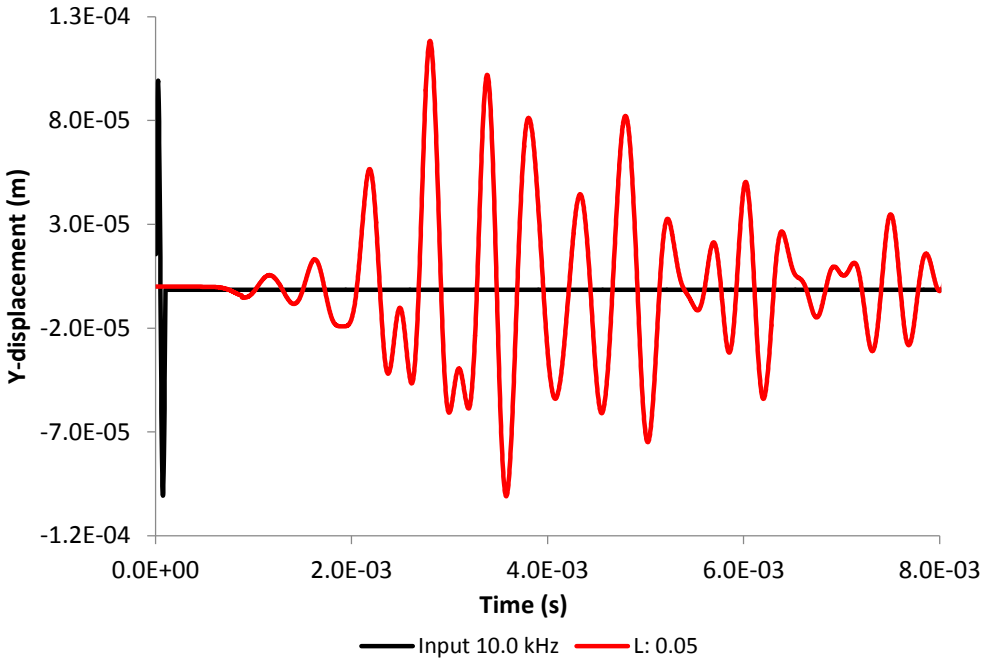

Figure 43 – Local damping (L) regarding a fraction of the critical damping of 0.05

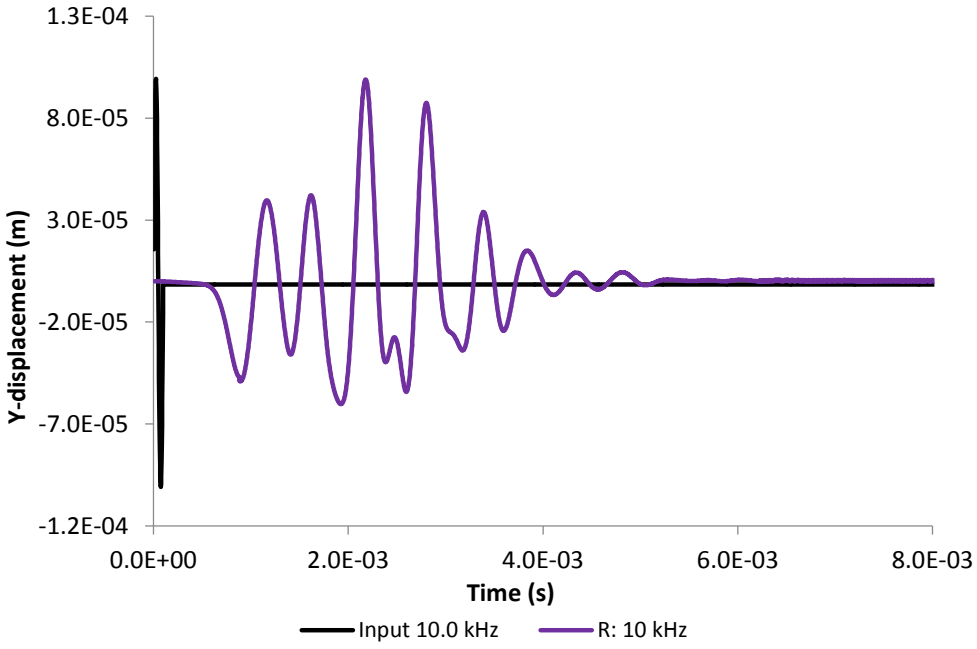

Figure 44 – Rayleigh damping (R), regarding a fraction of critical damping of 0.05 and a frequency of 10 kHz

4.4.5 POISSON'S RATIO

Poisson's ratio, ν, comprehends the ratio between lateral and axial strain, in other words, it is the ratio of relative contraction to relative expansion and is within 0 and 0.5 for most materials, given that the bulk modulus, *K*, the shear modulus, *G* and Young's modulus, *E*, require positive values. Namely, when the soil is loaded in undrained conditions, the Poisson's ratio is around 0.5, which implies that the volumetric deformation equals zero. In other words, in this type of condition, water is the fundamental parameter and since it is incompressible, there is no change in the volume. An example of a material with similar behaviour is rubber. Most steels and rigid polymers have a Poisson's ratio of around 0.3. On the other hand, when the behaviour of the soil is analysed in drained conditions, Poisson's ratio is close to zero, for example, like cork, which exhibits very little expansion when compressed.

The results observed below consider an input frequency of 5.0 kHz and Rayleigh damping. Comparing to what was discussed in section 4.4.3 and 4.4.4, the best value for the input frequency would be between 5.0 and 10 kHz. Nevertheless, given the lack of continuity in the signals the lowest frequencies and the start of a drift in the input frequency of 5.0 kHz when Rayleigh damping is considered (Figure 39), it was thought best to choose the value of 5.0 kHz. Figure 45 a), correspondent to a node in face C and Figure 45 b), correspondent to a node between face A and C, clearly demonstrates the significant influence of Poisson's ratio. The first arrival of both P and S waves is more evident in b), even though in this point there is already some degree of reflection of the output signal, probably due to the near-field effect, which is significantly higher in the boundaries. In other words, the first arrival of the waves is more influenced in the zone near face C, given the higher reflection of the signal, due to the large dimensions of the model, leading to a lower reflection in b). Additionally, comparing a) and b), it is possible to observe a more anticipated damping of the output signal in b), verifying the premise of a more reduced reflected wave in the midpoint node of the specimen.

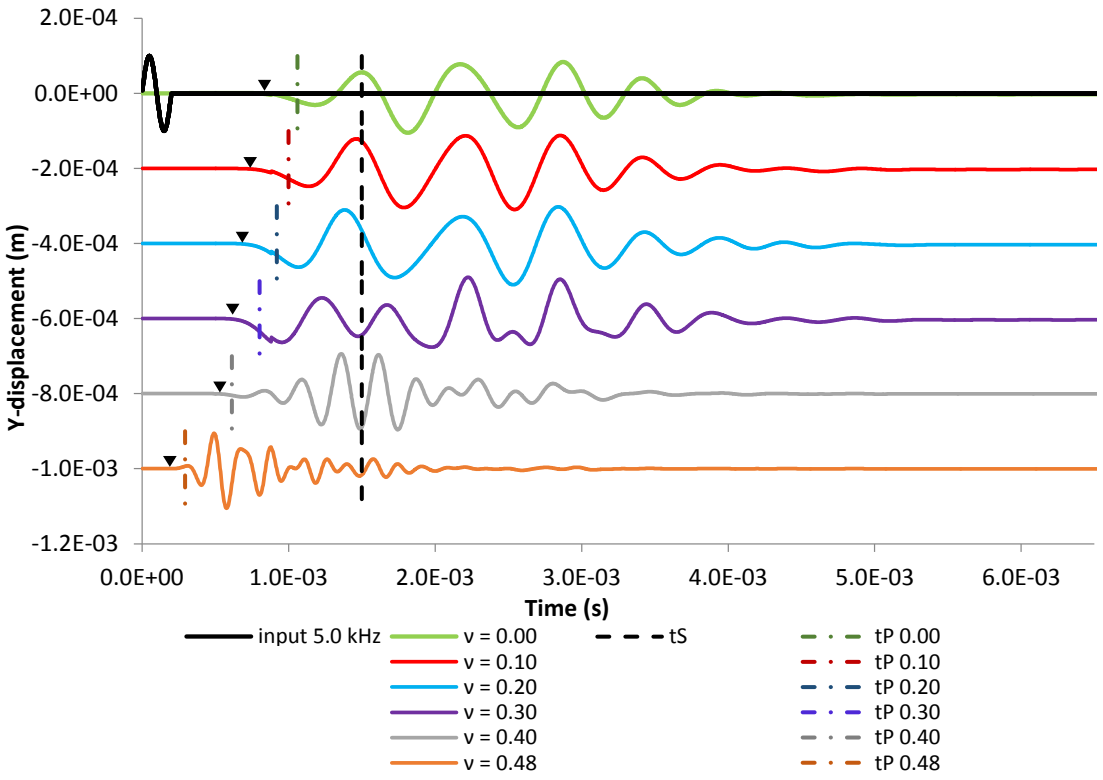

a)

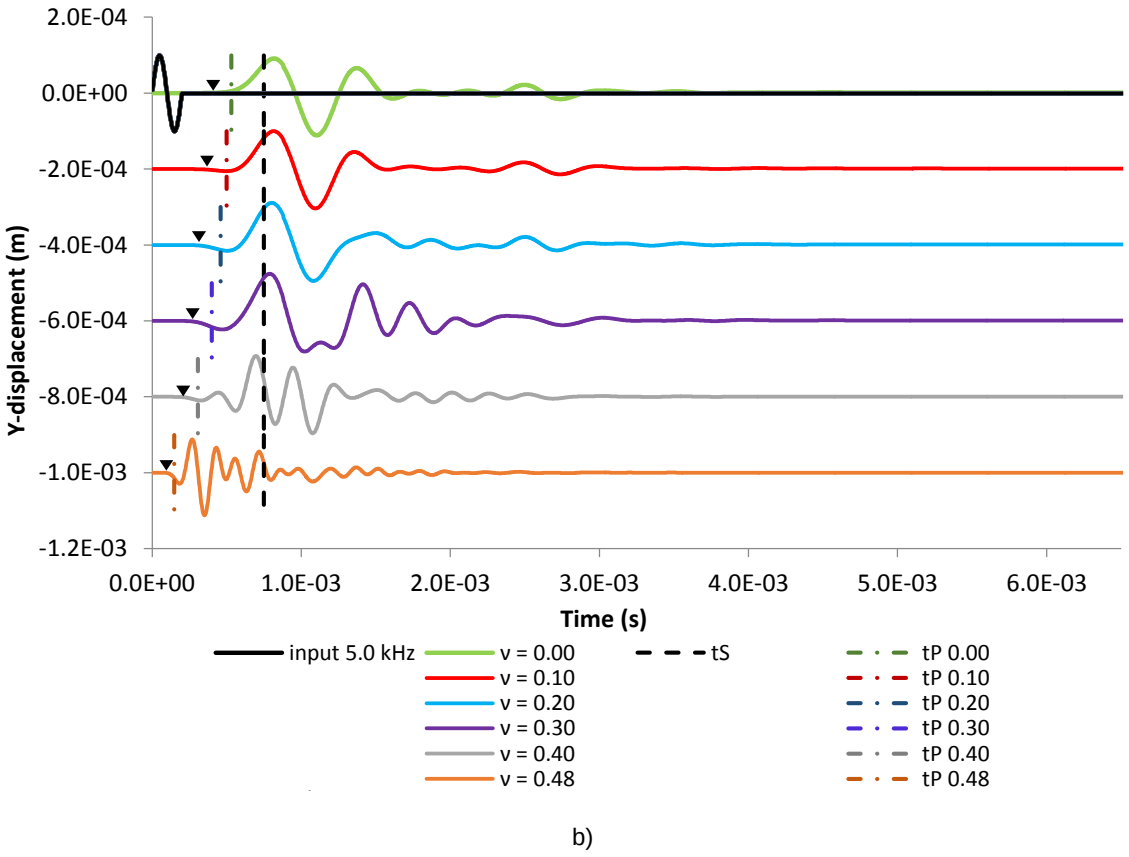

b)

Figure 45 – Variation of Poisson's ratio and the first arrival of both P and S waves in: a) Face C; b) Middle point between face A and C

It is possible to verify what was previously mentioned with the results presented in Table 6. Considering a constant shear modulus, the change in the values of both the Young's modulus and bulk modulus lead to a significant variation between the values of the velocities regarding P waves, clearly proving the significant influence of the different values of Poisson's ratio. This influence is especially large between the values of the Poisson's ratio of 0.40 and 0.48 (the value 0.50 is physically impossible, verified by the value of the bulk modulus and therefore the velocity, which tend to infinity).

In Figure 45 the first arrival of P waves of the model, translated by the first inflection of the output signal is demonstrated with an inverted triangle and the theoretical first arrival by a pointed line segment, which can be observed in the table below. The results of the model refer to manual determinations of travel time, considering the first shear wave arrival, contrary to the theoretical ones, which were calculated from the equations present in section 4.3.2. The results between them, although different, are not that significantly diverse, validating the constitutive model considered and its properties. The values of velocities of the S waves are the same, since they are not influenced by the Poisson's ratio, only by the shear modulus, which is constant. Besides, these values, regarding the model, are difficult to deduce simply by observing the figure. However, it is possible to narrow the time interval of the first arrival, namely in the immediate zone after the first peak or the first trough, which increases with Poisson's ratio.

Table 6 – Variation of P and S wave velocities with Poisson's ratio

Poisson v	Shear Modulus, G (MPa)	Young's Modulus, E (MPa)	Bulk Modulus, K (MPa)	V_S theoretical (m/s)	V_P theoretical (m/s)	$V_{P\ model\ (*)}$ (m/s)	$V_{P\ model\ (**)}$ (m/s)
0.00	80.00	160.00	53.33	200.00	282.40	335.20	337.08
0.10	80.00	176.00	73.33	200.00	300.00	370.37	381.68
0.20	80.00	192.00	106.67	200.00	326.60	414.94	434.78
0.30	80.00	208.00	173.33	200.00	374.17	462.96	491.80
0.40	80.00	224.00	373.33	200.00	489.90	540.54	588.24
0.48	80.00	236.80	1973.33	200.00	1019.80	1176.47	1219.51

(*): P wave velocity corresponding to an output in face C.

(**): P wave velocity corresponding to an output in the midpoint node between faces A and C.

Therefore, taking these results into account, the best suited value to include in the final model is the Poisson's ratio of 0.1, which appears to be the most fitted to provide plausible results in terms of dynamic behaviour. Also, this value stands in agreement with previous studies, namely from Rio (2006).

4.4.6 BOUNDARY CONDITIONS

Having in consideration the true triaxial apparatus used in the laboratory, it is possible to distinguish two types of boundary conditions, namely reflective and absorbent boundaries. Even though it is possible to demonstrate the reflective boundary condition in the true triaxial apparatus, given its metallic platens, which favour the reflection of waves inside the specimen, it is not possible to study a specimen in this apparatus considering an absorbent boundary condition. It would be unrealistic. It is only possible to study an absorbent boundary in a cubical cell, with flexible boundaries, usually made of rubber. Therefore, although the study considers a true triaxial apparatus as the source of the experiments, this study is important to confirm the complexity of the reflective boundary in comparison with the absorbing one.

Boundary conditions have to be present in the system in order to occur an infinite propagation of waves. These can be designed by a series of commands in the program, including a fixed displacement or force or even an impermeable boundary. The constructed model, including the bender elements, have the bottom end vertically fixed, simulating an infinite medium downwards, but with free horizontal movement, along with null initial displacement and velocity conditions in all directions. Due to the existence of a free boundary or reflective boundary in the vertical planes of the model, there is no resistance to the passage of a wave, causing it to be reflected back into the system with the same signal, enabling the existence of a more complex behaviour, as opposed to an absorbent boundary. Nevertheless, even though the absorbent boundary is a particular feature of *FLAC*^{3D}, a completely absorbent surface cannot be guaranteed, and there is the chance of a decrease in the efficiency of the model for wave components, regarding the capacity of reflection at lower angles from the surface. Figure 46 shows an absorbing boundary at the top end surface of the two dimensional model and a load applied both at the left and right boundaries with the vertical displacement restrained in the bottom end surface.

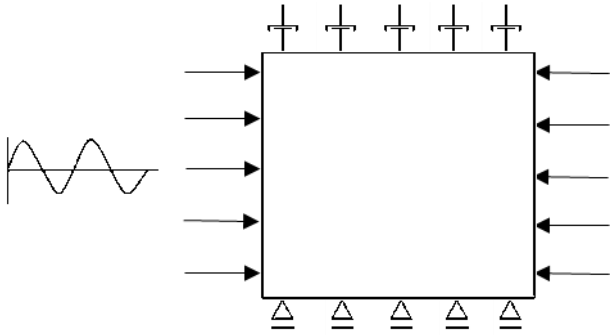

Figure 46 – Two dimensional plane model

However, the program *FLAC*^{3D} considers stress free and unconstrained boundaries by default, obliging the user to input an adequate boundary to this particular study. Additionally, since this program can lead to an underestimation of both stresses and displacements when a fixed boundary is simulated and an overestimation when a stress boundary is applied, a careful interpretation of the results should be in order. For a better understanding of these results, a comparison between reflected and absorbent boundaries was made and can be observed in Figure 47.

This figure shows no difference concerning the input signals or transmitters (face A), contrary to both the output signals or receivers (face C), whether in the midpoint between faces A and C or on face C. The reflective and absorbent boundaries are similar throughout approximately half the time (or half the travel length) considered in the figure. Moreover, the boundaries belonging to the midpoint in between faces A and C, are more similar than the ones belonging to the receiver located in face C, due to the higher reflection present near the limit of the model, enabling to conclude that the higher the reflection, the higher the energy of the wave and the lower the absorbency. Thereby, the midpoint between faces A and C behaves as if it was in an infinite medium. The further from the transmitter, the more the difference among first arrival times of P and S waves, which is in compliance to their real behaviour. Additionally, it is important to mention that the midpoint is more affected by the posterior reflections of the wave signal, than the signal of the receiver, although with far less energy. The reflection velocity of the receiver was calculated considering three times the total length of the cube (3 x 0.30 m = 0.90 m), contrary to the midpoint where it was considered the total length of the cube plus the distance to the middle point (0.15 m), making a total of 0.45 m. These reflections are not usually easily visualised in the output of the waves, however there is a higher approximation between the midpoints and the receivers of the reflected and absorbent boundaries near the values theoretically calculated. Figure 47 shows that, for the midpoint of the model, there is clear evidence of the second passage of the S wave for the case of reflective boundaries, confirming that existence of important reflections at the faces of the model. On the other hand, at the receiver, the differences between reflective and absorbent boundaries are mainly on the longer oscillation of the first arrival wave, which is actually mixed with the second arrival of the wave due to its reflection.

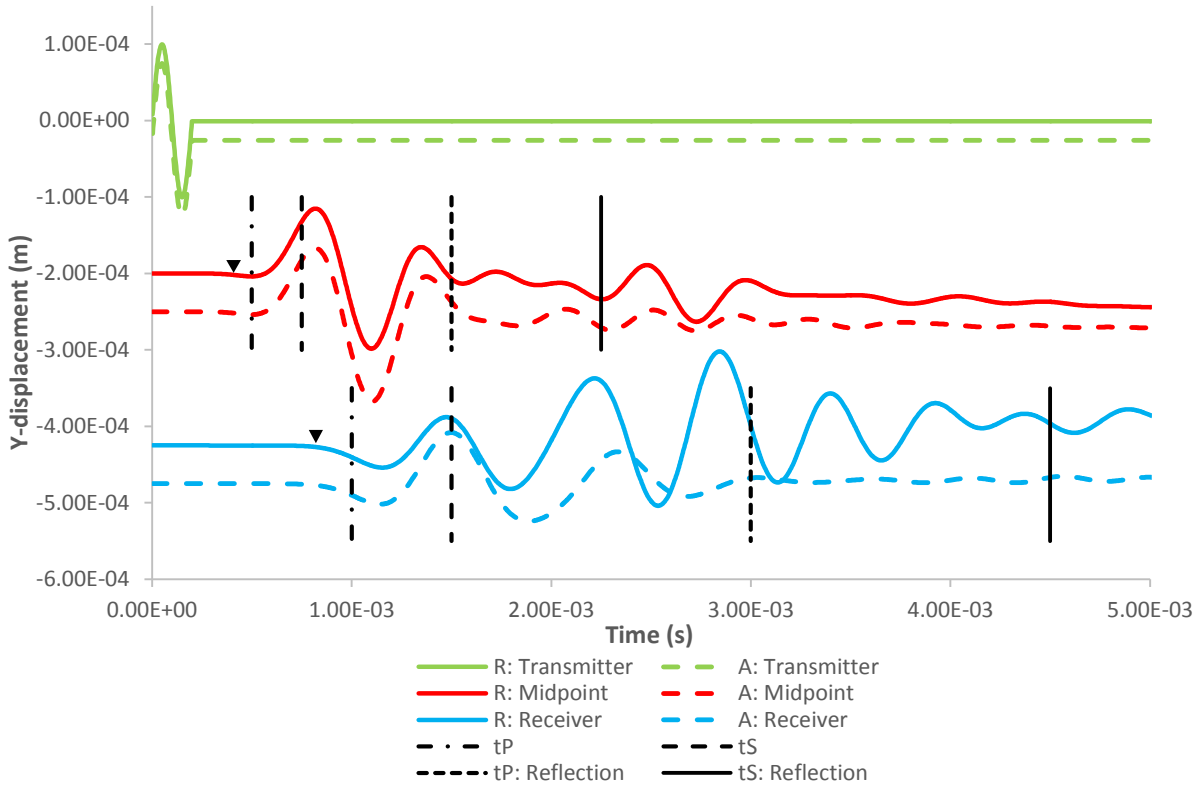

Figure 47 –Reflective (R) and absorbent (A) boundary conditions

There is a correlation between the presence of boundary conditions and the complexity of the behaviour of the propagation of waves. Comparing the reflective and the absorbent boundaries, it is possible to conclude that the absorbent boundaries do not introduce any component regarding reflected waves back to the system, thus reducing the complexity of the signals and easing its interpretation.

Since the present study focuses on a true triaxial apparatus with reflective boundaries, reflected waves are expected to appear, as confirmed by these numerical results.

4.4.7 ANISOTROPY

The assessment of anisotropy, in this particular case, cross-anisotropy, previously explained in section 4.3.2, was developed in *FLAC*^{3D}, considering the residual soil as cross-anisotropic or transversely isotropic, which properties have already been presented in Table 4. These properties include a lower vertical Young's modulus, normal to the plane of isotropy, approximately 70% of the horizontal one, so that the presence of anisotropy would be more easily acknowledged, translating into a lower vertical stiffness of the residual soil.

Having these properties in mind, the results obtained proved the symmetry and the presence of anisotropy in the model. These results include the X (horizontal) and Z (vertical) displacements of the model from the program *FLAC*^{3D} (Figure 48).

Figure 48 and Table 7 show a great similarity between the values of either the horizontal and vertical displacements, regarding the isotropic behaviour. On the other hand, there are slight differences regarding the anisotropic behaviour, namely a higher vertical displacement, just enough to confirm the presence of anisotropy. This is due to the lower Young's modulus normal to the plane of isotropy (Z) and to the vertical polarization, contrary to the Young's modulus in the plane of isotropy (X, in this case), which suffer no variation whatsoever. In Table 7 it was decided to do the horizontal and vertical displacements for both face A to C and B to D, in order to confirm the validity of the model. The values were the same, confirming that the model is behaving properly in mechanical terms.

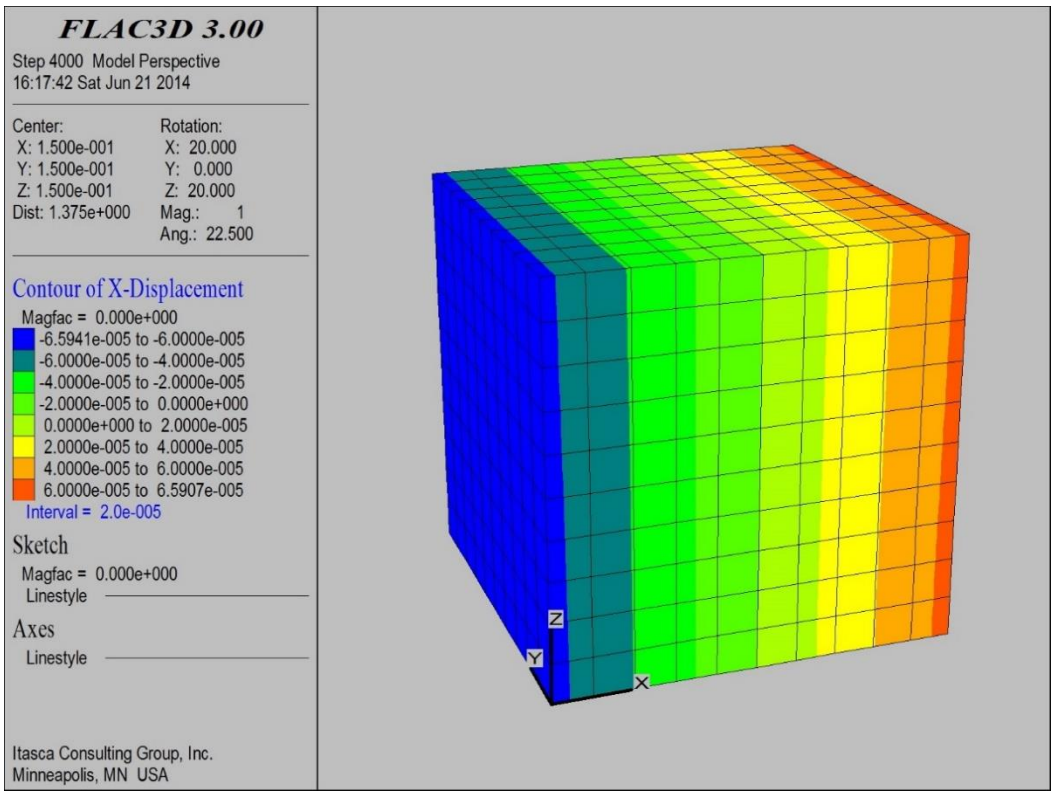

a)

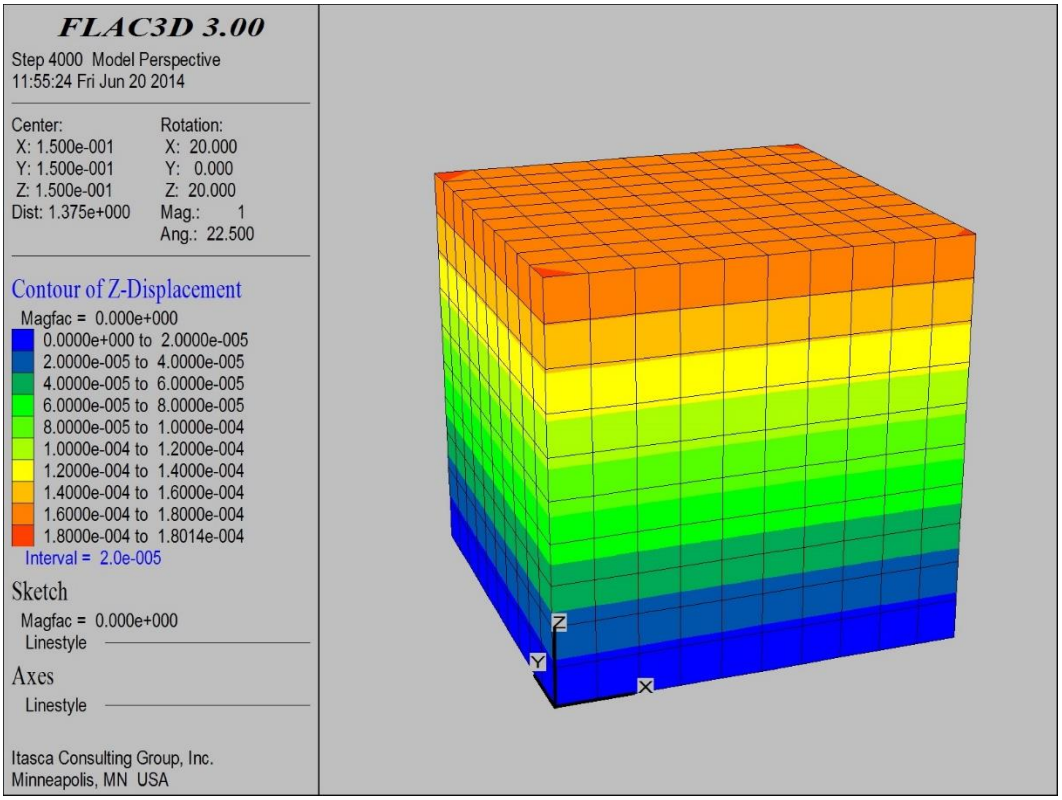

b)

Figure 48 – Displacements, from face A to C, considering an anisotropic constitutive model: a) X-displacement (horizontal); b) Z-displacement (vertical)

Table 7 – Horizontal and vertical displacements of both isotropic and anisotropic models

	Model	$E_1 = E_H$ (MPa)	$E_3 = E_V$ (MPa)	Horizontal-displacement (m)	Vertical displacement (m)
A to C (X)	Isotropic	176.00	176.00	1.38×10^{-4}	1.27×10^{-4}
	Anisotropic	176.00	123.20	1.32×10^{-4}	1.80×10^{-4}
B to D (Y)	Isotropic	176.00	176.00	1.38×10^{-4}	1.27×10^{-4}
	Anisotropic	176.00	123.20	1.32×10^{-4}	1.80×10^{-4}

The difference between the anisotropic and isotropic behaviour can also be perceived from the propagation of seismic waves. To attain these results, it was necessary to take into consideration the propagation and polarization of the waves (Figure 49). For example in case a), whenever a wave is applied in face A , its propagation is in the horizontal direction, namely X, however it is polarised in the vertical direction, Z, since it coincides with the movement of the particle. The same reasoning goes to b), where the wave propagation is horizontal (Y) and its polarisation is also horizontal (X).

Figure 50 confirms that the results vary with the variation of anisotropy.

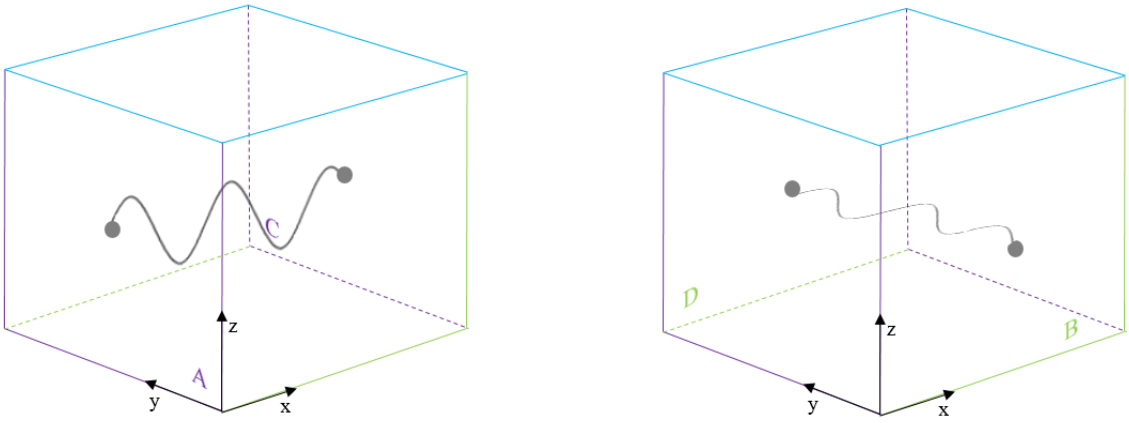

a) b)

Figure 49 – Polarization of the model: a) Vertical; b) Horizontal

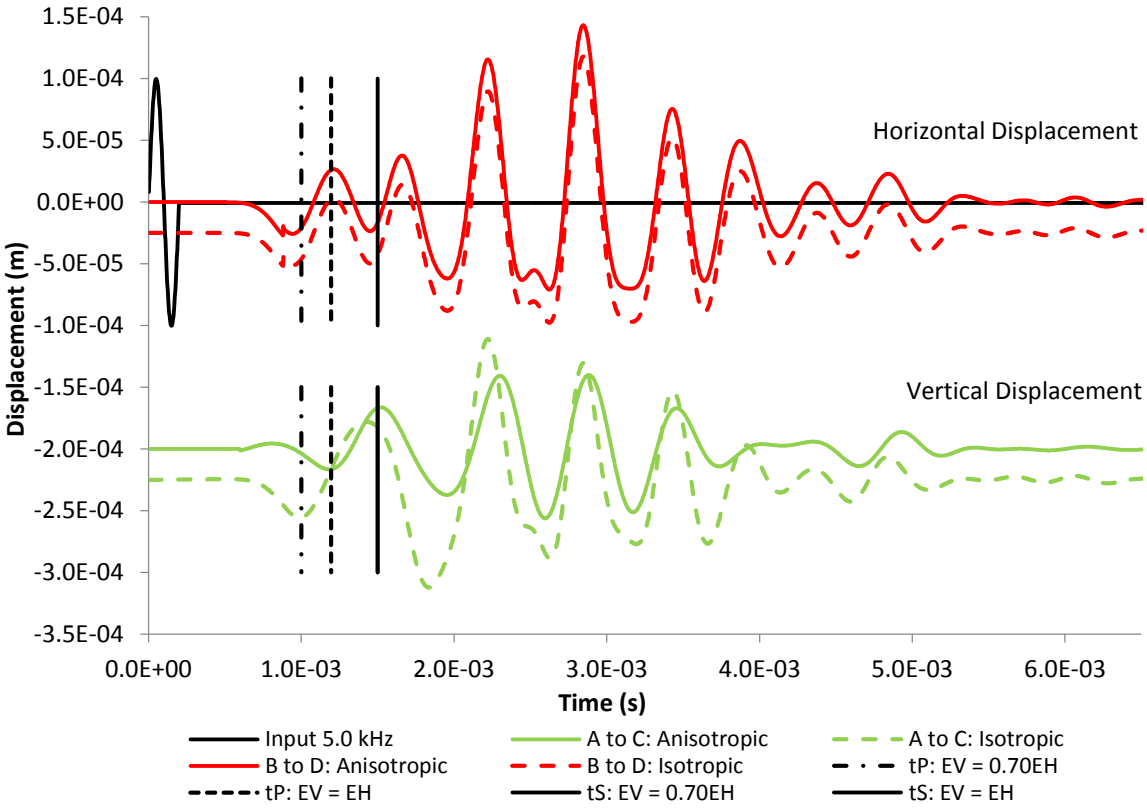

Figure 50 – Anisotropic and Isotropic behaviour from face A to C and B to D

This variation is present in the signal from face A to C, given the late arrival of the signal, related to a low velocity, in agreement with a lower Young's modulus in the plane normal to the plane of isotropy. Moreover, there is no evidence of anisotropy on the signal from face B to D, since the Young's modulus value remains constant, which means that the behaviour of the model in each direction is independent from each other. In truth, there could be some kind of difference between the isotropic and anisotropic models due to the combined effect of the different values of stiffness, which does not seem to occur.

4.5 KEY FINDINGS

In this chapter were presented the parametric and sensitivity studies applied to a simpler version of the developed numerical model, which for such purpose and for simplicity, do not include the bender elements and their different properties in comparison with the ones of the residual soil from Porto granite. Nevertheless, the bender elements were simulated through an applied velocity in the lateral boundaries of the model, namely from face A to C, connecting horizontal bender elements and B to D, connecting vertical bender elements (Figure 49).

However, these studies were neither coordinated with each other, nor performed simultaneously. These studies were developed in order to understand the influence of parameters such as the time step, the amplitude, frequency, damping and Poisson's ratio, boundary conditions and anisotropy in the results. On one hand, there are the parametric studies where only one single parameter varies, in order to facilitate the interpretation of the results and decide which features are best suited for the model. Basically, this process consisted of a trial and error approach. On the other hand, the sensitivity studies are associated to the uncertainty regarding the output of a certain system, being therefore useful to test the relationship between the parameters and the validity of this particular model. Since these studies belong to a numerical model, all the parameters are controlled by the user, contrary to what happens in laboratory testing.

Most was already stated during the chapter, but the main findings are as follows, considering a linear elastic constitutive model. First, it was important to decide which time step and duration of the model would be the most appropriate. This choice however depends exclusively on the user. Regarding the frequency, whether in the time or frequency domain, the main conclusion is that the better suited for any model, should be approximate to the value of the input frequency, also having in mind the proximity between the first inflection of the output wave and the theoretical first arrival of seismic waves. This way, there is no significant drift, due to the deviation from the resonant frequency of the system and no discrepancy in the results. The type of damping used on the other hand is somewhat intuitive and varies from study to study, given the advantages and disadvantages of both the local and Rayleigh damping. Taking into account that the higher the frequency, the lower the amplitude of the signal and the quicker the reach of equilibrium, in the end it is up to the user to decide which one is better suited. In this case, the choice depends on the comparison with the laboratory results achieved by Ferreira (2009), which will be presented in Chapter 5. However, for the following studies, the damping considered was Rayleigh damping, given the perfect balance between amplitude, velocity and quick reach to equilibrium. Poisson's ratio is also a significant parameter and its choice is associated to the proximity of the first arrival of both P and S waves and the first inflection of the signal, as it was the choice of the frequency. Additionally, the fact that the value of the shear modulus remained constant throughout the calculations and given the variations in either bulk and Young's modulus, highly influenced the first arrival of seismic velocities.

The boundary conditions and anisotropy are far more complex studies and it is not possible for the numerical modelling to accurately simulate all the properties of a real system (Rio 2006). Nevertheless, it was possible to achieve some relevant conclusions, regarding the differences between reflective and absorbent boundaries and isotropic and anisotropic constitutive models. Regarding the boundary conditions, the main conclusion is that there is a correlation between the presence of boundary conditions and the complexity of the behaviour of the propagation of waves. Namely, the higher the reflection, the higher the energy of the wave and the lower the absorbency, meaning that the more apart from the receiver, the lower the energy of the signal. When comparing reflective and absorbent boundaries it is possible to conclude that the absorbent boundaries do not introduce any component regarding reflected waves back to the system, avoiding a higher complexity in its behaviour. For these reasons, the boundary

conditions, have significant more influence in the zones nearer to the limits of the specimens. To assess anisotropy in a more effective way, it was considered a lower value of the Young's modulus normal to the plane of isotropy, maintain the same value of the Young's modulus in the plane of isotropy. The results of the model proved the symmetry of the model used, by providing identical results from faces A to C and B to D, as well as the validation of the change in the behaviour of the soil in each direction.

A more detailed analysis of damping, boundary conditions and anisotropy is analysed in the next chapter, as well as a comparison between the results attained and the laboratory results (Ferreira 2009), namely concerning dry reconstituted residual soil specimens.

5
RESULTS AND DISCUSSION

5.1 INTRODUCTION

This chapter was the main objective of this dissertation, namely the comparison between numerical results and laboratory results achieved by Ferreira (2009). However, the previous numerical results did not consider different properties regarding the bender elements. These were actually simulated by the application of a wave velocity, taking into account both its direction of propagation and polarization (Figure 49). Basically, this chapter comprises the conclusion of two main objectives, the validation of the model and the analysis of specific tests.

5.2 SIMULATION MODEL

In order to compare the numerical with the experimental results, it was important to first verify if the complex mesh with included the bender elements functions properly. Considering the mesh in Figure 33, namely the horizontal bender element, a local damping of 0.05 and the soil properties chosen in Chapter 4, the signal response of the model can be observed in Figure 51.

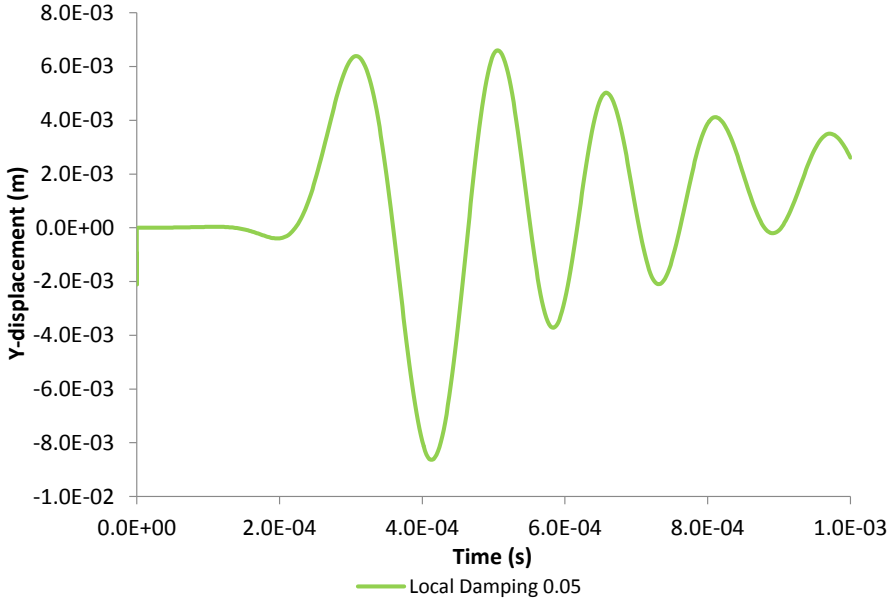

Figure 51 – Output signal response of the complex model

Given the results, t is possible to assume the validity of this model and its similarity to the simpler model used throughout this dissertation. Therefore, the simpler model can be continuously used, since the results would be approximate, but with considerably less running time.

5.3 PRELIMINARY COMPARISONS

Among the true triaxial tests made by Ferreira (2009), a number of tests consisted of dry ($w \approx 0\%$) and wet ($w \approx 30\%$) reconstituted residual soil specimens, intended to reproduce the behaviour of a non-structured soil. The dry condition allows a complete elimination of suction effects, despite its difficult preparation and reconstitution process, causing an unwanted but inevitable heterogeneity and layering. On the contrary, the wet condition, is far easier to prepare at a very high void ratio, leading to a much more homogeneous sample. Nevertheless, given the probability of entrapment of air bubbles among the soil particles, there is a possibility of an unmeasured quantity of capillary negative pressure (Ferreira 2009).

Table 8 – Physical properties of the reconstituted specimens tested in the true triaxial apparatus

Specimen	γ [kN/m^3]	w_0 [%]	e_0
R2W-TT	19.1	28.4	0.770
R3W-K_0TT	18.8	30.7	0.850
R4D-K_0TT	14.1	1.2	0.883
R8D-TT	12.7	1.0	1.067

These extreme conditions are intended to isolate and separately analyse the effects of structure in this non-structured soil, when testing intact soil specimens. Additionally, this equipment is not appropriate to study shear strength, since it is not capable of supporting large strains to achieve failure. Therefore, the true triaxial apparatus is ideal to study the dynamic behaviour of the soil and its stress-strain response in the elastic domain.

Next, a comparison will be presented between the study of some of the parameters in Chapter 4, namely in terms of the shape and configuration of the signals, regarding damping, boundary conditions and anisotropy, and actual examples of the experimental results performed by Ferreira (2009), in order to validate the achieved results.

5.3.1 DAMPING

In order to validate the numerical model and the soil properties considered in Chapter 4, a comparison was made between the best chosen values of damping, whether from local damping or Rayleigh damping and an example was selected from a true triaxial test on specimen R2W-TT, at an isotropic loading stage of 400 kPa. The selection of this example, which evidences the typical damping observed in the laboratory, was made solely based on the quality and clarity of the output signal.

Considering Figure 44, where the results of the parametric study on damping are illustrated, and comparing it with the graph in Figure 52, a certain similarity is clear. Previously, Rayleigh damping was

selected as the type of damping to be applied in the numerical simulations, between local and Rayleigh damping, given its greater proximity to reality. Comparing the mentioned figures, it is possible to visualise that both neither have a signal with many cycles, quickly reaching a position of equilibrium, demonstrating a rapid damping, which does not correspond to local damping, where the opposite is dominant. For this reason, it is confirmed that Rayleigh damping has been correctly selected as the one closer to experimental results.

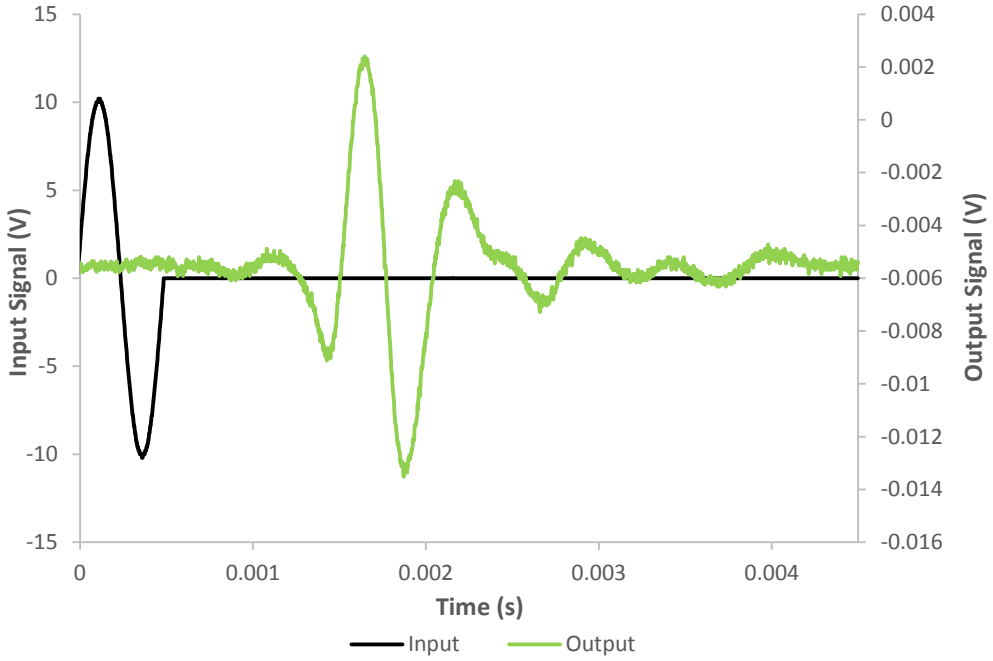

Figure 52 – Example of a typical damped signal on specimen R2W-TT

5.3.2 BOUNDARY CONDITIONS

On the topic of boundary conditions, namely reflective and absorbent ones and considering Figure 53, an example of a reflective boundary, with anisotropic properties and an isotropic loading of 50.0 kPa, and the results on Figure 47, it is possible to establish a relation between them. However, this correlation is only amid reflective boundaries and the experimentally measured signal reaching the receiver.

Having in mind that the experimental specimen to which the previous results are compared, R8D-TT, is a dry specimen, thereby possessing more capability of reflection, their signal shapes are approximate, with a weaker signal in the beginning, followed by a rise in the amplitude of the signal, and then a slower damping, until the eventual reach of equilibrium. This comparison regards the somewhat difference regarding the amplitude of the signals, and the presence of near-field effects in Figure 53 before the first arrival of the S wave.

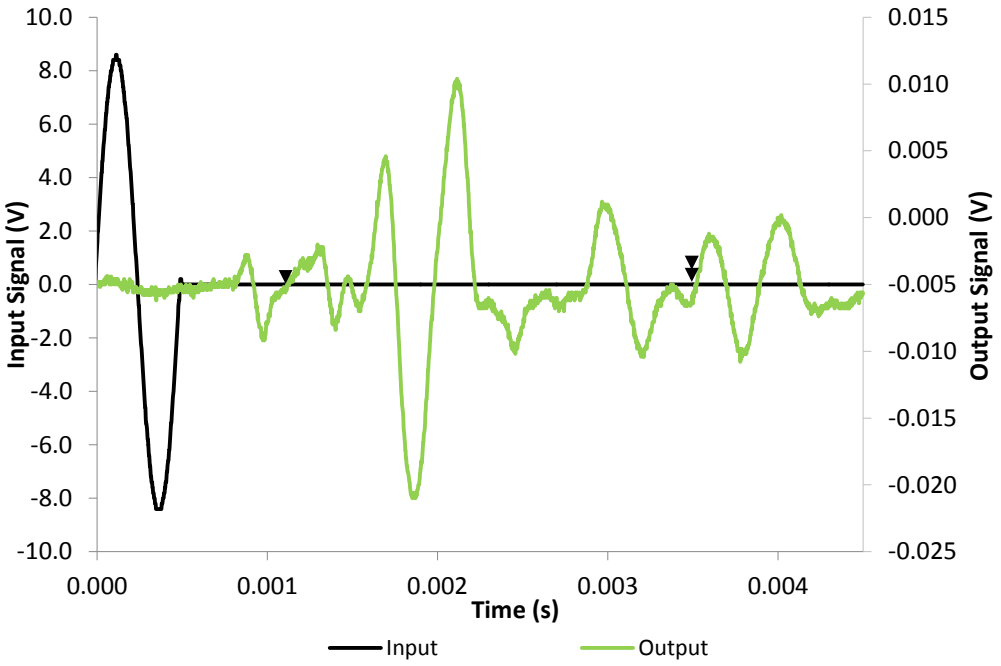

Figure 53 – Example of a reflective boundary of the specimen R8D-TT

5.3.3 ANISOTROPY

Anisotropy on the other hand, requires a more extensive comparison, in terms of the displacements and of the seismic wave propagation response.

The assessment of anisotropy has also been a field study for many researchers, in order to better understand the behaviour of soils. One of the means of detecting this parameter is through the direct measurement of shear wave velocities or S waves either propagated or polarised in different directions, which are able to detect different stiffnesses, from which the level of anisotropy can be achieved. For that objective, Graham and Houlsby (1983) proposed an anisotropy ratio, α_G, which comprises the relation between both the horizontal and vertical shear modulus:

$$\alpha_G = \frac{G_{hh}}{G_{vh}} \tag{5.1}$$

The results of the anisotropy ratios of both experimental and numerical tests, respectively, are presented in Table 9 and Table 10.

Table 9 – Anisotropy ratios, α_G, considering residual soil specimens from Porto granite

Specimens	Types of test	hh/hv X	hh/hv Y
R2W-TT	TT (iso)	1.06	---
R4D-K_0TT	TT (K)	0.80	0.81
R8D-TT	TT (iso)	1.20	1.31

Table 10 – Anisotropy ratios, α_G for numerical results and comparison to experimental results

Model	E_V (MPa)	E_H (MPa)	G_{hh} (MPa)	G_{vh} (MPa)	$\alpha_{G\ numerical}$	$\alpha_{G\ laboratory}$
Isotropic: $E_V = E_H$	176.00	176.00	80.00	80.00	1.00	1.00
Anisotropic: $E_V = 1.4xE_H$	123.20	176.00	80.00	56.00	1.42	1.25 (R8D-TT)
Anisotropic: $E_V = 0.7xE_H$	246.40	176.00	80.00	112.00	0.71	0.80 (R4D-K_0TT)

First of all, it is important to apprehend that while the experimental tests measure anisotropy, in these numerical simulations, a certain value of anisotropy is imposed. It is for this reason that in the previous chapter, the study of anisotropy assumed a particular value to relate both shear stiffnesses. These ratio values, defined as 1.4 and 0.7, were intentionally chosen in order to enhance the difference between the two modulus and ease the visualization of anisotropy in terms of behaviour. Regarding the comparison of both methods, the results are approximate, validating the model in mechanical terms.

Given the validation of the simulation model, it is possible to compare the horizontal and vertical displacement values from Table 7, considering the properties of the soil anisotropic and an isotropic loading of 100 kPa.

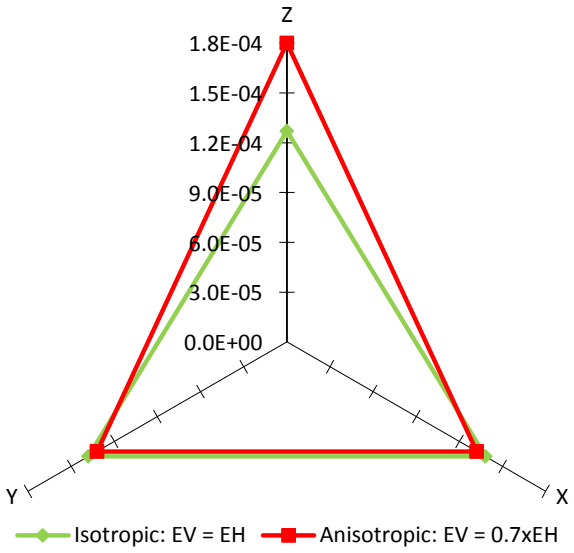

Figure 54 – Displacements for both isotropic and anisotropic constitutive models

5.4 COMPARISON WITH LABORATORY TESTS

In this sub-chapter, it is established a comparison between the results from specific laboratory tests (Table 8), already considering the validity of the simulation model. Unfortunately, due to time conflicting issues, the comparison between the two types of results is only going to regard the dry residual soil specimens, namely, R8D-TT and R4D-K_0TT.

5.4.1 R8D-TT

Considering the laboratory tests undertaken, this particular test, R8D-TT, included an array of unload-reload cycles, which provided the chance to measure shear wave velocities repeatedly at the same stress levels. However, this measurement led to a significant soil deformation during isotropic loading, varying the values of the void ratio. After these isotropic cycles were finalized, a series of three-dimensional stress conditions were imposed, taking into account the same mean effective stress, *p'* (Ferreira 2009). For this comparison, only the isotropic stages will be analysed, which are presented in Figure 55.

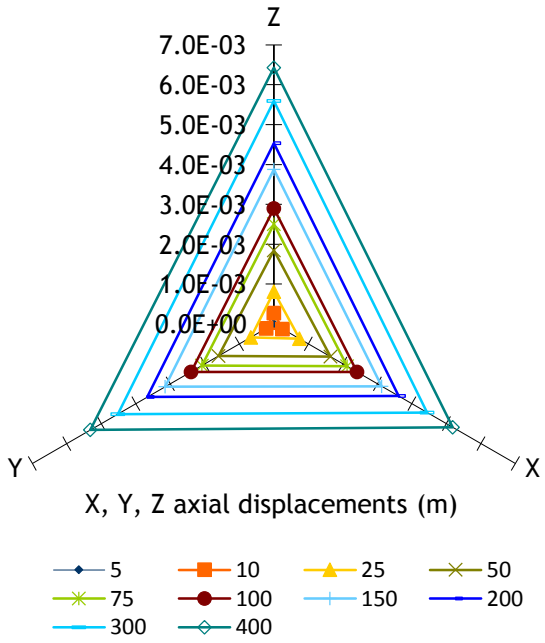

Figure 55 – Three-dimensional view of the strains measured in the experimental test for isotropic loading

For a realistic comparison, several values of stresses were considered in the numerical model, namely 100 kPa, 200 kPa and 500 kPa, under isotropic conditions. Considering these stresses, a study of the displacements that occurred during the loading process were made and can be observed in Table 11, as well as three-dimensionally in Figure 56.

Table 11 – Vertical displacements, considering several stress values

Stress (kPa)	Shear modulus, G (MPa)	Young's modulus, E (MPa)	Bulk modulus, K (MPa)	Poisson's ratio, v	Displacement (m)
100	80.00	176.00	73.33	0.10	1.27×10^{-4}
200	80.00	176.00	73.33	0.10	2.63×10^{-4}
500	80.00	176.00	73.33	0.10	6.71×10^{-4}

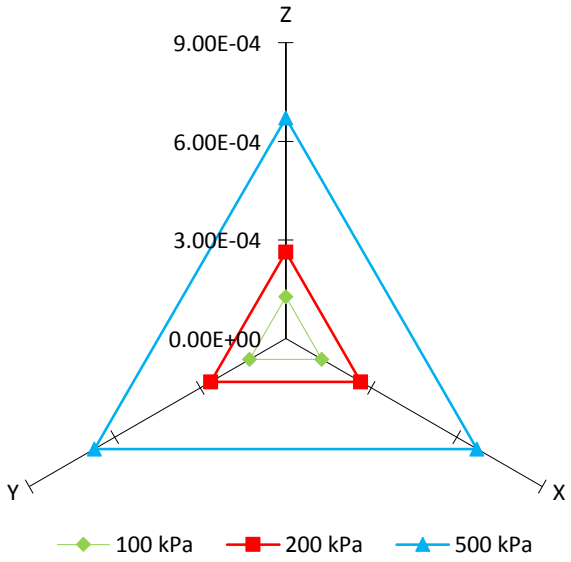

Figure 56 – Three-dimensional view of the strains associated with each isotropic stress stage

By observing the values presented in Table 11 and Figure 56 it can be verified that the deformation of the model is concomitant with the applied stresses. Comparing these results with those from the laboratory, it is important to realize that, even though the degrees of magnitude of the displacements in the laboratory test are significantly higher than the ones of the model, the comparison is valid. The main reason why these values are so different is associated with the compliance and bedding errors of the laboratory equipment. Since the platens of the true triaxial apparatus are rigid and the measurement is made on its outside, it is not possible to accurately measure such small displacements. Given that, the displacement values are not independent from the stresses applied, allowing the volumetric variation of the soils. Additionally, the capacity of the true triaxial apparatus to measure these values comes with a slight margin of error, given its compliance. Therefore, it was expected that the degree of magnitude of the displacement values of the experimental tests were higher than the numerical.

Finally, it is worth understanding how the seismic waves behaved by varying the stress applied, as illustrated in Figure 57. It is possible to realize that the shape and configuration of the waves is not considerably affected by the different stresses, what leads to conclude that these are independent from the loadings applied. This result can be justified by the characteristics of the constitutive model, which is linear elastic, with imposed stiffness moduli.

On the other hand, the soil responds with volumetric deformations, thus increase the stiffness and necessarily the seismic wave velocities of the specimen with increasing loads. This non-linearity is naturally included in the laboratory results, since the tests were developed in residual soil specimens that incorporate such behaviour.

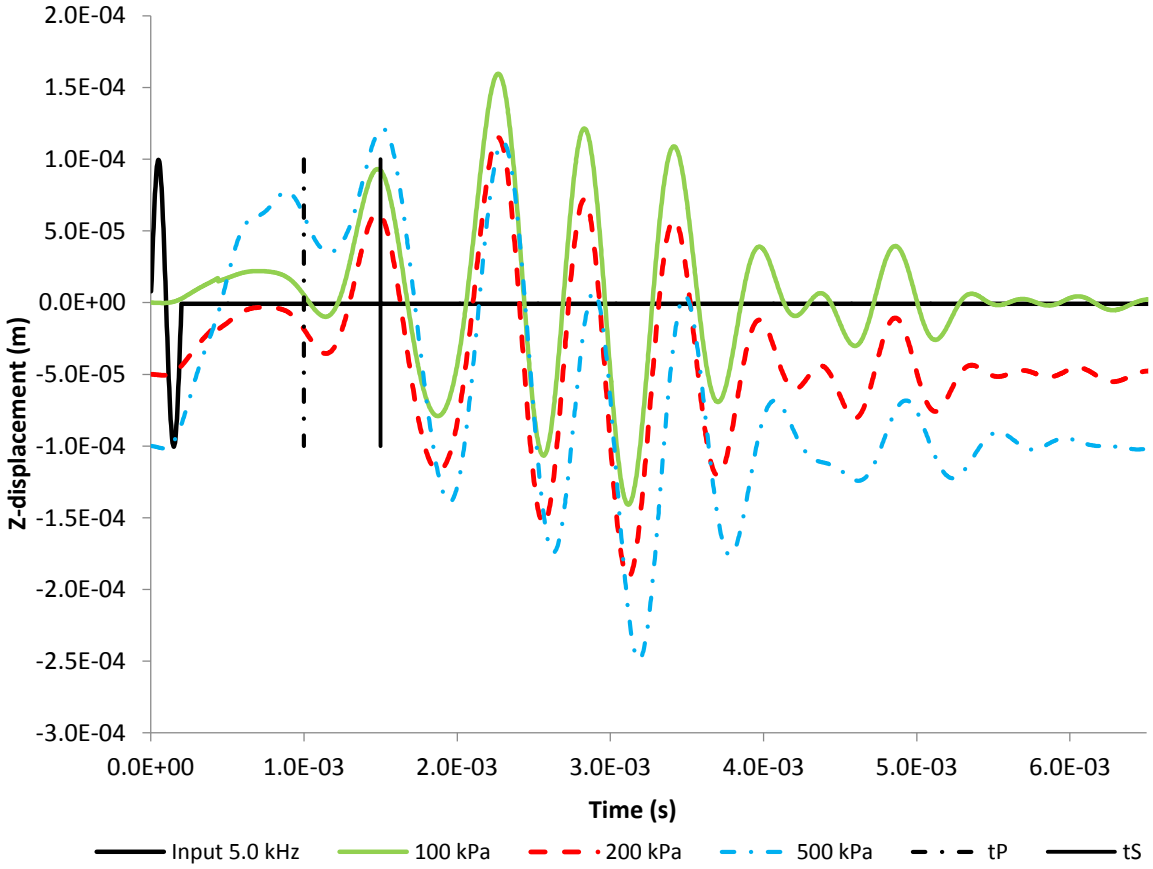

Figure 57 – Simulations of seismic wave propagation for several stress values

5.4.2 R4D-K_0TT

Since there was only a slight distinction among the shear wave velocities regarding the different stress components applied, in the previous specimen, it was necessary to try a different approach and contrary to the specimen R8D-TT, this specimen was tested under anisotropic conditions. This test was also carried out in order to investigate if the true triaxial apparatus would be able to impose a K_0 stress state condition. If this was possible, the at rest stress parameters could be achieved (Ferreira 2009). There were considered two different loadings, one with the horizontal stress equal to 35 kPa and the vertical stress to 100 kPa and another with the double, that is, a horizontal stress of 70 kPa and a vertical stress of 200 kPa. Moreover, not only was a comparison made between isotropic and anisotropic constitutive models, but there were also considered two different values of anisotropic ratio, in order to evaluate the anisotropic behaviour of the model.

Considering the results from Table 12 and Table 13 it is possible to conclude that the higher the stress applied the higher the displacement, which is logical. Nonetheless, taking into account an isotropic material, it can be verified that the vertical displacements are higher than the horizontal displacements, in agreement with the loading conditions. When considering an anisotropic material, namely the anisotropic model with the higher vertical Young's modulus, it can be observed that the differences between horizontal and vertical displacements are also in agreement with loading conditions and even though the soil is more rigid in the vertical direction, it exhibits a higher strain in that direction, due to the higher vertical stress. Additionally, it can be observed that by comparing both tables and Figure 58

a) and b), that there is a more accentuated vertical displacement when the horizontal stress is 70 kPa and the vertical stress is 200 kPa.

Table 12 – Horizontal and vertical displacements of a horizontal stress of 35 kPa and a vertical stress of 100 kPa

Model	$E_1 = E_H$ (MPa)	$E_3 = E_V$ (MPa)	Horizontal displacement (m)	Vertical displacement (m)
Isotropic $E_V=E_H$	176.00	176.00	$3.85x10^{-5}$	$2.70x10^{-5}$
Anisotropic $E_V=1.4\ E_H$	176.00	246.40	$3.96x10^{-5}$	$1.92x10^{-5}$
Anisotropic $E_V=0.7\ E_H$	176.00	123.20	$3.68x10^{-5}$	$3.84x10^{-5}$

Table 13 – Horizontal and vertical displacements of a horizontal stress of 70 kPa and a vertical stress of 200 kPa

Model	$E_1 = E_H$ (MPa)	$E_3 = E_V$ (MPa)	Horizontal displacement (m)	Vertical displacement (m)
Isotropic $E_V=E_H$	176.00	176.00	$7.52x10^{-5}$	$6.36x10^{-5}$
Anisotropic $E_V=1.4\ E_H$	176.00	246.40	$7.80x10^{-5}$	$4.54x10^{-5}$
Anisotropic $E_V=0.7\ E_H$	176.00	123.20	$7.10x10^{-5}$	$9.06x10^{-5}$

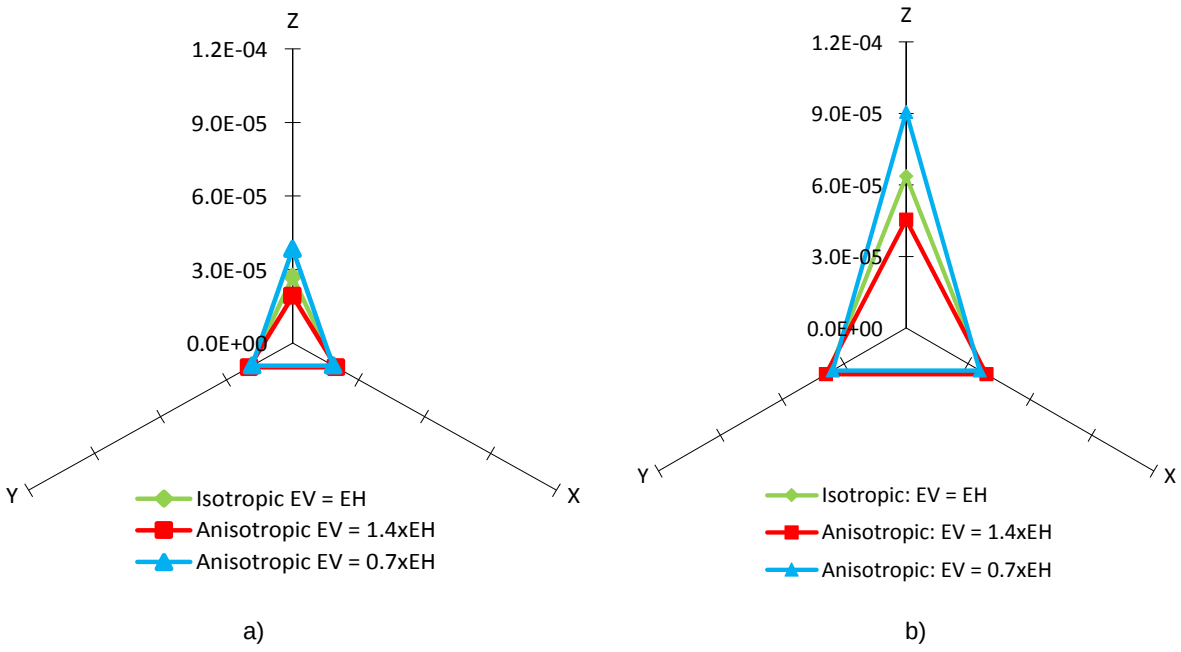

a) b)

Figure 58 –Horizontal and vertical displacements, correspondent to horizontal and vertical stresses of: a) 35 kPa and 100 kPa; b) 70 kPa and 200 kPa

Taking into account the signal variation and considering significantly higher stresses (Figure 59) than the previous ones, it is possible to verify that there is virtually no change between both types of constitutive models. This validates what was said in section 5.3.3, regarding the use of a linear elastic constitutive model instead of the highly non-linear behaviour experienced by most soils, as well as the compliance effect characteristic of this apparatus. This provides clear evidence that the value of stiffness is the one that commands the behaviour of the model.

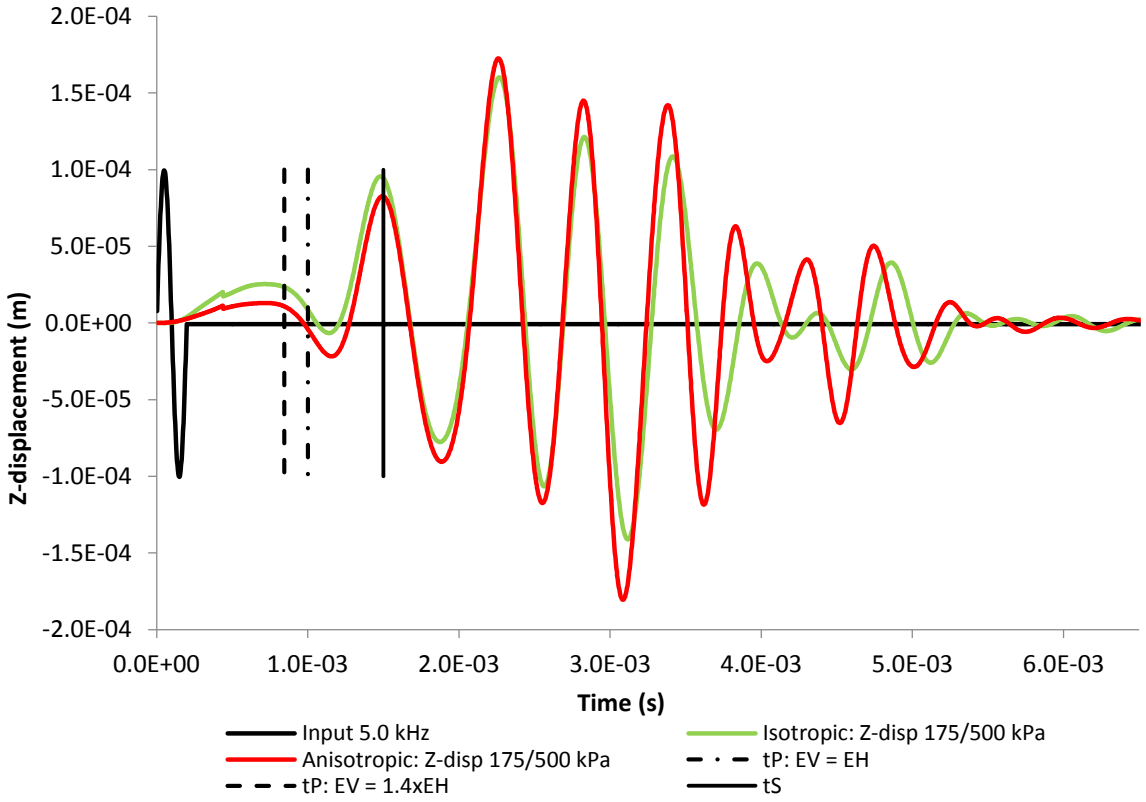

Figure 59 – Signal variation, considering a horizontal stress of 175 kPa and 500 kPa

With the results achieved in this chapter, it is possible to understand that, by the comparison with experimental results, the proposed simulation model developed in this work to evaluate the various parameters of the residual soil from Porto granite is appropriate. And even though it does not consider actual bender elements embedded in the platens of the true triaxial apparatus model, it behaves as expected and has proven to be capable of simulating both the stress-strain relationship and the propagation of seismic waves.

6
CONCLUSIONS

6.1 KEY FINDINGS

The use of seismic wave velocities is by far one of the best methods to analyse the behaviour of the soil and the evolution of the stiffness moduli.

The true triaxial apparatus is vital for this study, as one of its capabilities is the measurement of seismic wave velocities, through the embedded bender elements, not only in the principal orthogonal directions but also in the inclined ones, which may be redundant, but relevant and important nonetheless, since it leads to a more robust and reliable characterization (Ferreira 2009). Given this advantages, the major objectives were to study the dynamic behavior of a residual soil from Porto granite, by developing a numerical model of the true triaxial apparatus, capable of simulating the measurement of seismic wave velocities through bender elements and by comparing it to previously developed experimental results.

However, even though a correctly designed model was achieved, a simplified model was used instead, with benefits in terms of simplicity of the program itself and computation time, without affecting the quality and representativeness of the results. The model used to assess the various parameters that could influence the behavior of the soil and thereby the results, was a much simpler model with a cubical shape and applied velocities in the lateral boundaries in order to simulate the existence of both vertical and horizontal bender elements. This way, even though there were no different properties of the bender elements included in the model, a wave signal could still be created and evaluated, in considerably less amount of time. The parametric and sensitivity studies proved that this model was more than enough to correctly characterize the soil.

After the validation of the simulated model by these studies, a comparison between numerical and experimental tests had to be made, in order to have a more realistic view of the results. Due to time conflicting issues, it was only possible to compare the numerical results with the dry reconstituted residual soil specimens, one under isotropic loading conditions and other under anisotropic stresses. Having in consideration the differences between a numerical analysis and an experimental one, namely the linear elastic behaviour of the first versus the highly non-linear behaviour present in the soil specimens, it is possible to conclude that the comparison was successful and the measurement of the stiffness parameters achieved in the laboratory was verified.

Since this dissertation was the first numerical modelling approach to study a true triaxial apparatus, it was necessary to develop an extensive preliminary study, mostly presented in Chapter 4. Therefore, a greater effort was made in the implementation and improvement of the model, as well as in the study of

the finite difference program *FLAC*^{3D}, than in the comparison with the laboratory results. Parameters such as time step, amplitude, frequency, damping and Poisson's ratio were all important to characterize, in order to evaluate their influence in the response of the model and to correctly assess the results regarding boundary conditions and anisotropy, which are clearly more elaborate studies.

Additionally, even though the constitutive model used was the linear elastic, under isotropic conditions, and given the fact that soils, including residual soils are highly non-linear, this simulated model behaved as expected, providing comparative results.

Altogether, this was a pioneer work, whether regarding the software program *FLAC*^{3D}, the numerical modelling of this particular apparatus or even the quantity of parameters involved for such a short period of time, truth is it was a learning experience for all involved.

6.2 FURTHER WORKS

Concluding this research work, it is clear that much was left to investigate. Since this was a first approach to this subject, in such a specific field, and for a highly complex apparatus, only the surface has been "scratched" so to speak and much remains to be developed in the future.

The most important and obvious future developments to be made are as follows.

Regarding the sensitivity studies:

- the study of the influence of the water level, considering an isotropic loading and imposing a K_0 stress state condition, in order to validate and compare the work previously developed by Ferreira (2009);
- a multi-parametric study regarding the relationship between the input frequency and the Rayleigh damping;
- include in the study a qualitative processing of the signal.

Regarding the numerical modelling in *FLAC*^{3D}:

- investigation of all parametric and sensitivity studies in the frequency domain, not only the variation of frequency, for a more accurate comparison between the results and a better comprehension of the influence of the different parameters;
- the simulation of a cubical cell, in order to compare with more accuracy the influence of flexible or absorbent boundaries with the rigid or reflective boundaries of the true triaxial apparatus;
- the use of a different constitutive model that would be able to consider the evolution of stiffness;
- the evaluation of all the comparisons between numerical and experimental results with the more complex model that includes the properties of the bender elements, in order to achieve an even more approximate response to the real behaviour of the soil.

"We must be willing to get rid of the life we planned so as to have the life that is waiting for us."

Joseph Campbell

REFERENCES

Airey, D. W. and Wood, D. M. 1988. "The Cambridge true triaxial apparatus." *ASTM special technical publication* (977):796-805.

Arroyo, M., Medina, L. and Muir Wood, D. 2002. "Numerical modelling of scale effects in bender-based pulse tests." *NUMOG VIII, Pande, GN & Pietruszczak, S.(eds)*:589-594.

Arthur, J. 1988. "Cubical devices: versatility and constraints." *ASTM special technical publication* (977):743-765.

Arulnathan, R., Boulanger, R. W. and Riemer, M. F. 1998. "Analysis of bender element tests." *ASTM geotechnical testing journal* no. 21 (2):120-131.

Atkinson, J. 2000. "Non-linear soil stiffness in routine design." *Geotechnique* no. 50 (5):487-508.

Blewett, J., Blewett, I. and Woodward, P. 2000. "Phase and amplitude responses associated with the measurement of shear-wave velocity in sand by bender elements." *Canadian Geotechnical Journal* no. 37 (6):1348-1357.

Bolt, B. A. 1976. "Nuclear explosions and earthquakes. The parted vail."

Braja, M. 1993. "Principles of Soil Dynamics " *PWS-KENT Publishing Company*.

Brignoli, E., Gotti, M. and Stokoe, K. H. 1996. "Measurement of shear waves in laboratory specimens by means of piezoelectric transducers." *ASTM geotechnical testing journal* no. 19 (4):384-397.

Burland, J. 1989. "Ninth Laurits Bjerrum Memorial Lecture:" Small is beautiful"-the stiffness of soils at small strains." *Canadian Geotechnical Journal* no. 26 (4):499-516.

Campanella, R., Robertson, P. and Gillespie, D. 1986. "Seismic cone penetration test". Comunicação apresentada em Use of In Situ Tests in Geotechnical Engineering.

Casagrande, A. and Carillo, N. 1944. "Shear failure of anisotropic materials." *Journal of Boston Society of Civil Engineers* no. 31 (4):74-81.

Cascante, G. and Santamarina, C. 1997. "Low strain measurements using random noise excitation." *Geotechnical Testing Journal* no. 20:29-39.

Crampin, S. 1981. "A review of wave motion in anisotropic and cracked elastic-media." *Wave motion* no. 3 (4):343-391.

Di Benedetto, H., Geoffroy, H., Sauzéat, C. and Cazacliu, B. 1999. "Sand behaviour in very small to medium strain domains." *See Jamiolkowski (1999)*:89-96.

Dyvik, R. and Madshus, C. 1985. "Lab Measurements of Gmax using bender elements". Comunicação apresentada em Advances in the art of testing soils under cyclic conditions.

Fam, M. and Santamarina, C. 1995. "Study of geoprocesses with complementary mechanical and electromagnetic wave measurements in an oedometer." *Geotechnical Testing Journal* no. 18 (3).

Ferreira, C. M. d. F. 2003. *Implementação e aplicação de transdutores piezoeléctricos na determinação de velocidades de ondas sísmicas em provetes Avaliação da qualidade de amostragem em solos residuais*. Porto: FEUP.

Ferreira, C. M. d. F. 2009. *The use of seismic wave velocities in the measurement of stiffness of a residual soil*. Porto: [s. n.].

Ferreira, C. V. d. F., A. and Santos, J.A. 2007. "Comparison of simultaneous bender elements and resonant column tests on Porto residual soil, Soil Stress-Strain Behavior: Measurement, Modeling and Analysis." *A Collection of Papers of the Geotechnical Symposium in Rome, , 2006, Ling, Callisto, Leshchinsky & Koseki (Eds.)*:535.

Fortunato, E. M. C. 2005. *Renovação de plataformas ferroviárias estudos relativos à capacidade de carga*. Porto: [s.n.].

Geoffroy, H., Di Benedetto, H., Duttine, A. and Sauzéat, C. 2003. "Dynamic and cyclic loadings on sands: results and modelling for general stress-strain conditions". Comunicação apresentada em Proc. 3rd Int. Symp. on Deformation Characteristics of Geomaterials, IS Lyon.

Graham, J. and Houlsby, G. 1983. "Anisotropic elasticity of a natural clay." *Geotechnique* no. 33 (2):165-180.

Green, G. E. 1972. "Stress Strain Behaviour of Soils." *Proceedings, Roscoe Memorial Symposium, G.T. Foulis, Henley on Thames*:324.

Hambly, E. 1969. "A new true triaxial apparatus." *Geotechnique* no. 19 (2):307-309.

Hardy, S., Zdravkovic, L. and Potts, D. 2002. *Numerical interpretation of continuously cycled bender element tests. Numerical Models in Geomechanics (NUMOG VII). Pande & Pietruszczak*. Swets & Zeitlinger, Lisse.

Hirakawa, D., Kongkitkul, W., Tatsuoka, F. and Uchimura, T. 2003. "Time-dependent stress–strain behaviour due to viscous properties of geogrid reinforcement." *Geosynthetics International* no. 10 (6):176-199.

Hryciw, R. D. and Thomann, T. G. 1993. "Stress-history-based model for G e of cohesionless soils." *Journal of geotechnical engineering* no. 119 (7):1073-1093.

Ibraim, E., Christiaens, P & Pope, M. 2011. "Development Of A Hollow Cylinder Torsional Apparatus For Pre-failure Deformation And Large Strains Behaviour Of Sand." *Geotechnical Engineering Journal of the SEAGS & AGSSEA, Special Issue on Soil Behaviour* no. 42:68.

Ishimoto, M. and Iida, K. 1937. "7. Determination of Elastic Constants of Soils by means of Vibration Methods.: Part 2. Modulus of Rigidity and Poisson's Ratio."

Itasca. 2002a. FLAC3D, Online Manual.

Itasca, H. 2002b. FLAC3, Fast Lagrangian Analysis of Continua in 3 dimentions. Computer Program.

Jardine, R., Fourie, A., Maswoswe, J. and Burland, J. 1985. "Field and laboratory measurements of soil stiffness." *Proc., 11th Int. Conf. on Soil Mechanics and Foundation Engineering* no. 2:511-514.

Jovicic, V. and Coop, M. 1998. "Stiffness of coarse-grained soils at small strains." *Pre-failure Deformation Behaviour of Geomaterials*:159.

Jovicic, V., Coop, M. and Simić, M. 1996. "Objective criteria for determining Gmax from bender element tests." *Geotechnique* no. 46 (2):357-362.

Ko, H.-Y. and Scott, R. F. 1967. "A new soil testing apparatus." *Geotechnique* no. 17 (1):40-57.

Kumar, P. and Foufoula-Georgiou, E. 1997. "Wavelet analysis for geophysical applications." *Reviews of Geophysics* no. 35 (4):385-412.

Lade, P. V. and Duncan, J. M. 1975. "Cubical triaxial tests on cohesionless soil." *Journal of Geotechnical and Geoenvironmental Engineering* no. 101 (ASCE# 11269 Proceeding).

Lee, J.-S. and Santamarina, J. C. 2005. "Bender elements: performance and signal interpretation." *Journal of Geotechnical and Geoenvironmental Engineering* no. 131 (9):1063-1070.

Lings, M. 2001. "Drained and undrained anisotropic elastic stiffness parameters." *Geotechnique* no. 51 (6):555-565.

Lomize, G. M. a. K., A. L. 1967. "On the Strength of Sand." *Proceedings, Geotechnical Conference, Norwegian Geotechnical Institute, Oslo* no. 1:219.

Love, A. E. H. 1927. "A treatise on the mathematical theory of elasticity." *Dover Editions*:309.

Marchetti, S., Monaco, P., Totani, G. and Marchetti, D. 2008. "In situ tests by seismic dilatometer (SDMT)." *From research to practice in geotechnical engineering* no. 180:292-311.

Matsuoka, H., Sun, D. a., Kogane, A., Fukuzawa, N. and Ichihara, W. 2002. "Stress-strain behaviour of unsaturated soil in true triaxial tests." *Canadian Geotechnical Journal* no. 39 (3):608-619.

Muscolino, G., Palmeri, A. and Ricciardelli, F. 2005. "Time-domain response of linear hysteretic systems to deterministic and random excitations." *Earthquake engineering & structural dynamics* no. 34 (9):1129-1147.

Neiva, A. A. S. 2011. *Considerations of Wave-transmission from soil into structure based on numerical calculations*. Porto: [s. n.].

NicollHighwaycollapse. http://en.wikipedia.org/wiki/Nicoll_Highway_collapse.

Piezo Systems, I. 1994. History of Piezoelectricity. www.piezo.com.

Porovic, E. 1995. "Investigations of soil behaviour using a resonant-column torsional-shear hollow-cylinder apparatus", Imperial College London (University of London).

Potts, D. M. and Zdravkovic, L. 1999. *Finite element analysis in geotechnical engineering*. London: Thomas Telford.

Raposo, N. C. d. S. C. 2012. *Propagação de vibrações num complexo subterrâneo em rocha*. Porto: FEUP.

Rayleigh, J. and Lindsay, R. 1945. "The Theory of Sound, vols. 1 and 2Dover." *New York*.

Redwood, M. 1960. *Mechanical waveguides*. Pergamon Press.

Rio, J. F. M. E. 2006. "Advances in laboratory geophysics using bender elements", University of London.

Roesler, S. K. 1979. "Anisotropic shear modulus due to stress anisotropy." *Journal of the Geotechnical Engineering Division* no. 105 (7):871-880.

Sá, J. M. d. A. C. d. 2004. "Métodos de Aproximação em Engenharia", FEUP.

Saada, A. and Townsend, F. 1981. "State of the art: laboratory strength testing of soils." *Laboratory shear strength of soil, ASTM STP* no. 740:7-77.

Sadek, T. 2006. "The multiaxial behaviour and elastic stiffness of Hostun sand", University of Bristol.

Sanchez-Salinero, I., Roesset, J. M., Stokoe, I. and Kenneth, H. 1986. *Analytical studies of body wave propagation and attenuation*. DTIC Document.

Santamarina, J. C., Klein, A. and Fam, M. 2001. "Soils and waves:Particulate materials behavior, characterization and process monitoring." *Journal of Soils and Sediments* no. 1 (2):130-130. http://dx.doi.org/10.1007/BF02987719. doi: 10.1007/BF02987719.

Santos, J., Camacho-Tauta, J., Parodi, M., Viana Da Fonseca, A. and Ferreira, C. 2007. "Use of random vibrations to measure stiffness of soils." *Experimental Vibration Analysis for Civil Engineering Structures (EVACES'07), Porto*:1169-78.

Shirley, D. J. and Hampton, L. D. 1978. "Shear-wave measurements in laboratory sediments." *The Journal of the Acoustical Society of America* no. 63 (2):607-613.

Stokoe, K. H., Joh, S.-H. and Woods, R. 2004. "Some contributions of in situ geophysical measurements to solving geotechnical engineering problems". Comunicação apresentada em Proceedings.

Stokoe, K. H. and Santamarina, J. C. 2000. "Seismic-wave-based testing in geotechnical engineering". Comunicação apresentada em ISRM International Symposium.

Teachavorasinskun, S., Shibuya, S. and Tatsuoka, F. 1991. "Stiffness of sands in monotonic and cyclic torsional simple shear". Comunicação apresentada em Geotechnical Engineering Congress—1991.

Timoshenko, S. and Goodier, J. 1971. "Theory of Elasticity, McGraw-Hill, New York, 1970." *Fok-Ching Chong received the BS degree from the Department of Electrical Engineering, National Taiwan University, Taipei, Taiwan, in*.

Viana da Fonseca, A. 1996. "Geomechanics in Residual Soils from Porto Granite. Criteria for the Design of Shallow Foundations", Thesis (PhD), University of Porto.

Viana da Fonseca, A. 2003. "Characterising and deriving engineering properties of a saprolitic soil from granite." *Porto.'Characterisation and Engineering Properties of Natural Soils'. Swets & Zeitlinger, Lisse*:1341-1378.

Viana da Fonseca, A. C., J.; Ferreira, C.; Santos, J. A.; Almeida, F., Pereira, E., Feliciano, J., Grade, J., and Oliveira, A. 2006. "Characterization of a profile of residual soil from granite combining geological, geophysical and mechanical testing techniques." *Geotechnical and Geological Engineering* no. 24, No. 5:1348.

Viggiani, G. and Atkinson, J. 1995. "Interpretation of bender element tests". Comunicação apresentada em International Journal of Rock Mechanics and Mining Sciences and Geomechanics Abstracts.

Wilson, E. L. and Bathe, K.-J. 1976. "Numerical methods in finite element analysis."

Wood, D. M. 1974. "Some Aspects of the Mechanical Behaviour of Kaolin under Truly Triaxial Conditions of Stress and Strain", University of Cambridge.